ADVANCED REDUCTION PROCESSES-A NEW CLASS OF TREATMENT PROCESSES

A Dissertation

by

BHANU PRAKASH VELLANKI

Submitted to the Office of Graduate Studies of
Texas A&M University
in partial fulfillment of the requirements for the degree of

DOCTOR OF PHILOSOPHY

August 2012

Major Subject: Civil Engineering

Advanced Reduction Processes - A New Class of Treatment Processes

ADVANCED REDUCTION PROCESSES-A NEW CLASS OF TREATMENT PROCESSES

A Dissertation

by

BHANU PRAKASH VELLANKI

Submitted to the Office of Graduate Studies of
Texas A&M University
in partial fulfillment of the requirements for the degree of

DOCTOR OF PHILOSOPHY

Approved by:

Chair of Committee,	Bill Batchelor
Committee Members,	Ahmed Abdel-Wahab
	Bryan Boulanger
	Qi Ying
Head of Department,	John Niedzwecki

August 2012

Major Subject: Civil Engineering

ABSTRACT

Advanced Reduction Processes - A New Class of Treatment Processes.

(August 2012)

Bhanu Prakash Vellanki, B. Tech., Acharya Nagarjuna University, India;

M.En., Texas A&M University

Chair of Advisory Committee: Dr. Bill Batchelor

A new class of treatment processes called Advanced Reduction Processes (ARP) has been proposed. The ARPs combine activation methods and reducing agents to form highly reactive reducing radicals that degrade oxidized contaminants.

Batch screening experiments were conducted to identify effective ARP by applying several combinations of activation methods (ultraviolet light, ultrasound, electron beam, microwaves) and reducing agents (dithionite, sulfite, ferrous iron, sulfide) to degradation of five target contaminants (perchlorate, nitrate, perfluorooctanoic acid, 2,4 dichlorophenol, 1,2 dichloroethane) at 3 pH levels (2.4, 7.0, 11.2). These experiments identified the combination of sulfite activated by ultraviolet light produced by a low pressure mercury vapor lamp as an effective ARP.

More detailed kinetic experiments were conducted with nitrate and perchlorate as target compounds and nitrate was found to degrade more rapidly than perchlorate. The effects of pH, sulfite concentration, and light intensity on perchlorate and nitrate

degradation were investigated. The effectiveness of the sulfite/UV-L treatment process improved with increasing pH for both perchlorate and nitrate.

TABLE OF CONTENTS

Page

Page

Page

LIST OF FIGURES

Page

Page

Page

Page

Page

Page

LIST OF TABLES

Page

Page

Page

Page

1 INTRODUCTION

1.1 Introduction

A new class of water treatment processes, called the Advanced Reduction Processes (ARPs) has been proposed. The ARPs will produce highly reactive reducing radicals to destroy oxidized contaminants. A similar kind of existing treatment processes, the Advanced Oxidation Processes (AOPs), combines oxidizing agents with activation methods to produce oxidizing radicals. The ARPs will combine reducing agents and activation methods to produce reducing radicals.

A free radical can be defined as any species having an odd number of electrons and thus having an unpaired electron. A free radical normally has a strong tendency to either give up the unpaired electron or accept another electron to form a pair. Therefore, they act as effective reductants (donate electron), or oxidants (accept electron). The hydrogen radical ($H^{\bullet}$) and aqueous electron (e_{aq}^{-}) are examples of reducing free radicals and the hydroxyl radical ($OH^{\bullet}$) an example of an oxidizing free radical.

This dissertation follows the style of *Environmental Science and Technology*.

Oxidation-reduction reactions are the primary method that treatment processes have to destroy environmental contaminants. In general, the kinetics of the redox reactions involved in the degradation of a target compound is the crucial factor in deciding the feasibility of a treatment process that destroys contaminants. The formation of the highly reactive reducing radicals will make the kinetics of the concerned reactions feasible. The radicals are not selective and are thus well suited for use as effective reductants in water/waste water treatment.

Many of the current water treatment techniques for contaminated water only concentrate the contaminant without degrading or eliminating it. Employing ARPs, which make use of such highly reactive and minimally selective radicals, will lead to transformation of the target contaminants into more innocuous products. Also, the partial decomposition of non-biodegradable organic pollutants can lead to formation of biodegradable intermediates.

Advanced Oxidation Processes (AOP) is the name for a group of treatment methods that have been developed to be used when a contaminant can be destroyed by being oxidized. There are many different types of AOP, but they all share a common mechanism – production of hydroxyl radicals ($OH^{\bullet}$) that are very reactive oxidants. Production of oxidizing free radicals by AOP is often accomplished by combining a reagent (e.g. hydrogen peroxide) with an activation mechanism that could apply external energy (e.g. ultraviolet light) or catalysts (e.g. metal ions). The hydroxyl radical is an oxidizing free radical, i.e. a compound that contains an unpaired electron and has a strong tendency to take an electron from another compound to make a pair. There are

also free radicals that are effective reductants, because they have a strong tendency to donate the unpaired electron to the compound being reduced.

A new group of treatment methods is proposed for destroying oxidized contaminants that applies the strategy of combining a reagent with an activating method to produce highly reactive reductant radicals. This group of treatment processes will be called Advanced Reduction Processes (ARP) and will have similar mechanisms to AOP; however, the free radicals being produced will be reducing radicals and the result will be reduction of target contaminants.

A number of reagents are attractive candidates for use in ARP, including dithionite, sulfite, sulfide and ferrous iron. All have been used to some extent in treatment processes and all have chemistries that indicate they will produce highly reactive radicals when properly activated. A variety of activating methods (low-pressure ultraviolet light, narrowband ultraviolet light, electron beam, ultrasound, microwave) will be examined for their ability to generate highly reactive, reducing free radicals.

ARP could be applied to treat a wide range of oxidized contaminants that are problems now and others that are emerging as potential treatment challenges in the future. Chlorinated organics are a continuing problem in groundwater, surface water and contaminated soils. In many cases, they can be removed from a contaminated media by processes based on phase change, but their destruction relies on redox chemistry. Nitrate is another conventional contaminant that is a problem both in drinking water and in surface water, where it is responsible for eutrophication and resulting problems such as the hypoxic zone in the Gulf of Mexico. An emerging oxidized contaminant of concern

is perchlorate, which is a major problem at some government sites where it was used as a component of rocket fuels. It has also been found to be widely distributed in arid regions by natural processes. Fluorinated organics are another class of emerging contaminants of concern and perfluorooctanoic acid (PFOA) is a specific example. Also, endocrine disrupting compounds are receiving increasing attention due to their environmental impacts at low concentrations. A wide variety of compounds have been identified with impacts on the endocrine systems of aquatic animals, but substituted phenolic compounds such as 2,4-dichlorophenol (2,4-DCP) are one type of endocrine disruptor. These oxidized contaminants (nitrate, perchlorate, PFOA, 2,4-DCP, 1,2-DCA) are the targets for this study.

1.2 Research Objectives

The goal of this research is to validate the proposed new class of treatment processes, ARPs, and characterize the degradation of perchlorate and nitrate by the most effective ARP.

Successfully achieving this goal will provide data that supports the theory of ARPs and forms the basis for further research involving formation of reducing radicals to degrade oxidized contaminants. Ultimate development and demonstration of a perchlorate and nitrate treatment process based on formation of reducing free radicals has the potential to provide a lower cost method of destroying perchlorate and nitrate in contaminated ground and surface waters, ion exchange regenerant solutions and other contaminated media.

The objectives are described as follows.

1.2.1 Objective 1: Screen reagents and activating methods for effectiveness against representative targets

This task consisted of batch experiments with all combinations of reagents (4) and activating methods (5), resulting in 20 potential ARP being evaluated against 4 target compounds at 3 pH levels. The experiments covered time periods found appropriate for the activating agent with samples being taken from the reactors over a wide time frame to allow estimating of first-order rate constants that might vary over several orders of magnitude. The purpose of these experiments was not to characterize the degradation reactions, but only to identify conditions where those reactions occur at rates that are possibly high enough to be applicable to a treatment process. Results of these experiments are presented in Chapter 2.

1.2.2 Objective 2: Characterize Perchlorate degradation by Sulfite/UV-L ARP

Batch kinetic experiments were conducted in the UV-L reactor to characterize the kinetics of perchlorate destruction by sulfite/UV-L ARP. Extent of degradation of perchlorate was measured by the decrease in perchlorate concentration. Experimental variables were pH (3 levels), sulfite concentration (3 levels), and UV-L intensity (3 levels). Sulfite concentrations ranged from zero to several times stoichiometric. These results are presented in Chapter 3.

1.2.3 Objective 3: Characterize Nitrate degradation by Sulfite/UV-L ARP

Batch kinetic experiments were conducted in the UV-L reactor to characterize the kinetics of nitrate destruction by sulfite/UV-L ARP. Extent of degradation of nitrate was measured by the decrease in nitrate concentration. Experimental variables were pH

(4 levels), sulfite concentration (4 levels), and UV-L intensity (3 levels). Sulfite concentrations ranged from zero to several times stoichiometric. These results are presented in Chapter 4.

1.2.4 Objective 4: Develop kinetic model

A kinetic model will be developed and applied to characterize results of the batch reactor experiments. The model will include a description of the production of reactive species ($SO_3^{\bullet-}$, e_{aq}^-) from sulfite as functions of intensity of UV-L and concentrations of sulfite. Reactions for these species with other compounds that are often found in water will be included. Reactions for the reactive species and the target compound will be included and coefficients for these reactions will be obtained by conducting non-linear regressions on data produced by the kinetic experiments. Reactions of reactive reductants with the degradation products (chlorate, chlorite, and nitrite) will also be included in general terms, but it is not anticipated that sufficient data on concentrations of products will be obtained to fully describe their reactions. These results are presented in Chapter 5.

2 DISCOVERY INVESTIGATION OF ADVANCED REDUCTION PROCESSES

2.1 Introduction

A new class of water treatment processes, called the Advanced Reduction Processes (ARPs) is proposed and results of preliminary experiments are reported. An ARP degrades oxidized contaminants by producing highly reactive reducing radicals by combining reagents and activation methods. This mode of operation is similar to that employed by Advanced Oxidation Processes (AOPs), but differs in that reducing radicals are produced rather than the hydroxyl radical, which is an oxidizing radical.

A free radical can be defined as any species having an odd number of electrons and thus having an unpaired electron. A free radical normally has a strong tendency to either give up the unpaired electron or accept another electron to form a pair. Therefore, they act as effective reductants (donate electron), or oxidants (accept electron).

In general, the kinetics of the redox reactions involved in the degradation of a target compound is the crucial factor in deciding the feasibility of a treatment process. The formation of the highly reactive reducing radicals will make the kinetics of the desired reactions feasible, when they might be too slow with typical reductants. Many radicals are not selective and are thus well suited for use as effective reductants in water/waste water treatment.

Many of the current water treatment techniques for contaminated water only concentrate the contaminant without degrading or eliminating it. Employing ARPs, which make use of such highly reactive and minimally selective radicals, will lead to

either mineralization of the target contaminants or at least transformation into more innocuous products. Also, the partial decomposition of non-biodegradable organic pollutants can lead to biodegradable intermediates.

Prospective reducing agents and activation methods were chosen for initial experiments testing the concept of ARPs based on their ability to either produce or promote formation of reducing radicals. The target contaminants in these experiments included organics, inorganics and emerging contaminants.

2.2 Background

2.2.1 Activation methods

ARPs use a variety of activation methods to promote production of reductive free radicals from various reagents. In some cases, the activation method might directly degrade a target compound (e.g. photolysis by UV light) or it might produce radicals itself (e.g. production of hydroxyl radical by ultrasound). In these cases, performance of the ARP (activating method plus reagent) should be compared to performance of the activation method itself.

Ultraviolet light

UV light of a variety of wavelengths could be used in ARP and the desired wavelength would depend on the absorption spectra of the reagent to be activated. One type of lamp that is currently used in water and wastewater treatment is the low-pressure mercury vapor lamp (UV-L) and this lamp produces light that is almost entirely at 254 nm. It is also one of the more extensively used activation methods in AOPs *(1)*. Another type of lamp is a narrowband ultraviolet (UV-N) lamp that primarily emits light at 313

nm. These bulbs are marketed for testing the sun-resistance of materials such as paints and plastics *(2)* as well as for treatment of skin disorders *(3)*. Although this UV-N lamp is not currently used in water treatment, it produces light of a wavelength that is more effectively absorbed by reagents such as dithionite.

Ultrasound

When a liquid is irradiated with ultrasound, the ultrasound waves pass through the medium in a series of alternate compression and expansion cycles leading to creation of micro bubbles. Extreme conditions of up to 5000 K temperature and 1000 atm pressure exist at the bubble/water interface upon bubble collapse. The extreme conditions generated during cavitation cause thermal decomposition of water to create both oxidizing ($OH^{\bullet}$) and reducing ($H^{\bullet}$) radical species *(4, 5)*.

Electron Beam

An electron beam (E-beam) is made by accelerating electrons to about 99.9% the speed of light and passing them through the water to be treated. The energy level of radiation (0.01 to 10 eV) is sufficiently high to produce changes in the molecular structure of water, but is too low to induce radioactivity *(6)*. In E-beam treatment, ionizing radiation from an electron beam source is used to produce free radicals that can degrade aqueous contaminants. The oxidizing free radical ($OH^{\bullet}$) and the reducing species ($H^{\bullet}$ and e_{aq}^{-}) are the most reactive products of this reaction and generally control the rate of degradation observed during E-beam treatment.

$$6.9\ H_2O \xrightarrow{\text{(e-beam irradiation)}} 2.8OH^{\bullet} + 0.6H^{\bullet} + 2.7e_{aq}^{-} + 0.47H_2 + 0.7H_2O_2 + 2.7H_3O^{+} \quad (2\text{-}1)$$

The values in parenthesis are called G values and they represent the efficiency of the ionizing radiation in producing reactive species. A G value is defined as the moles of radicals, excited species or other products, formed (or lost) due to absorption of 10^7 J of energy (or approximately the number of radicals, excited species or other products, formed or lost due to absorption of 100 eV) *(7)*.

Microwaves

Microwave energy is a non-ionizing electromagnetic radiation with frequencies in the range of 300 MHz to 300 GHz *(8)*. The most commonly used frequency for home microwave ovens is 2450 MHz and this is also the frequency employed by the majority of the water treatment processes that use microwave irradiation *(9)*. Degradation or enhanced degradation of target compounds by these treatment processes is brought about by the rapid heating caused by microwave irradiation, or by direct microwave action or by both *(8, 10)*.

2.2.2 Reducing agents

Different reductants can be chosen for ARPs based upon their ability to be activated by one or more activation methods and produce reducing radicals or effective reducing agents. Some reductants that could be used in ARP include: dithionite, sulfite, ferrous iron, and sulfide.

Dithionite

Dithionite is known to have a long, weak S-S bond that can be broken to produce two sulfur dioxide radical anions ($SO_2^{\cdot -}$) *(11)*.

$$S_2O_4^{-2} = 2\ SO_2^{\bullet -} \qquad (2\text{-}2)$$

The sulfur dioxide radical anion exists in aqueous dithionite solutions at very low concentrations, as evidenced by the low equilibrium constant for this reaction of 1.4 x 10^{-9} M *(12, 13)*. This free radical anion is a strong reductant with a reported standard reduction potential of -0.66 v *(12)*.

A number of activation methods could potentially increase production of sulfur dioxide radical anions. Dithionite has an absorption peak in the ultraviolet near 315 nm *(14-16)*, so irradiation near this wavelength can provide energy to break the weak S-S bond. Effectiveness of this activation method is indicated by the report that hydrogen was produced by irradiation of dithionite solutions with a high-pressure mercury lamp *(17)*. Possible effectiveness of microwave irradiation as an activation method is shown in reports of improved the reactivity of dithionite in pulp bleaching *(18)*, thionation reactions *(19)*, and reduction of anilines *(20)* following microwave irradiation. Gamma irradiation has been shown to promote formation of the radical anion from dithionite *(21)*.

Sulfite

Sulfite is another possible reagent for use in an ARP. Although sulfite (SO_3^{2-}) is a particular anion, the term "sulfite" will be used here as a general term to describe the group that includes sulfurous acid (H_2SO_3), bisulfite (HSO_3^-) and sulfite (SO_3^{2-}). The UV absorption spectrum of sulfite solutions depends on the pH and concentration of the solutions *(22)*. UV irradiation of sulfite solutions has been generally reported to produce

both oxidizing and reducing radicals. Both the hydrated electron *(23)* and the sulfite radical anion ($SO_3^{\bullet-}$) *(24-27)* are formed in irradiated sulfite solutions.

$$SO_3^{2-} + h\nu = SO_3^{\bullet-} + e_{aq} \qquad (2\text{-}3)$$

The hydrated electron would be a strong reductant and the sulfite radical anion could act as an oxidant or reductant, because it can accept an electron to return to sulfite or it can donate an electron and react with water to form sulfate. Furthermore, it can act as a reductant by reacting directly with molecular oxygen to ultimately form sulfuric acid, which is an important reaction in acid rain production *(28)*.

Although the mechanisms have not been reported, irradiation of sulfite solutions by UV light has promoted their ability to form hydrogen *(17)*, their ability to react with oxygen *(29)* and their ability to dechlorinate *(30, 31)*. Microwave irradiation has also been used to promote the ability of sulfite to bleach pulp *(18)* and promote thionation reactions *(19)*. Sonication has been found to promote the reaction of sulfite solutions with oxygen *(32)*. These reports indicate that addition of these activation methods is likely to promote formation of reducing free radicals.

Sulfide

The potential for sulfide as a reagent in ARP is supported by several studies with different activating methods. Sulfide solutions absorb UV light with a maximum at 230 nm *(33-35)* and irradiation with UV has promoted formation of hydrogen *(17, 33)*. Hydrogen production has also been reported when sulfide solutions are sonicated *(34, 36)* and the mechanism is believed to be primarily through formation and reaction of radicals *(34)*.

Ferrous Iron

Solutions of ferrous iron absorb UV light with a maximum at 220 nm and UV irradiation promotes formation of hydrogen *(37)*. This could occur through reaction of hydrated electrons with hydrogen ions, because hydrated electrons have been shown to be formed in ferrous iron solutions irradiated with UV light *(38)*.

2.2.3 Target contaminants

Five target compounds were investigated in this study. Perchlorate is a highly oxidized form of chlorine that is difficult to reduce. Perchlorate is both a man made and naturally occurring compound. Perchlorate is of concern as it can disturb the functioning of the thyroid gland by interfering with its iodide uptake *(39)*.

Nitrate is one of the most widespread contaminants of ground water in the US, due to its use as a fertilizer and its formation from other nitrogen forms in human and animal wastes. Nitrate adversely affects human health by causing methemoglobinemia in infants as well as inhibiting iodine uptake by the thyroid gland, leading to thyroid dysfunction *(40)*. Active metals, ammonia, borohydride, formate, hydrazine, hydroxylamine, hydrogen and ferrous iron are some of the chemical reducing agents that have been used to chemically reduce nitrate in the presence of catalysts, or high temperatures and pressures. Electrochemical and photochemical techniques are some of the nitrate reduction mechanisms that employ energy sources *(41)*.

PFOA is a synthetic, completely fluorinated organic acid that does not occur naturally in the environment. PFOA is used to make fluoropolymers and can also be released by the transformation of some fluorinated telomers. The physiochemical

stability of PFOA makes it difficult to treat using most conventional treatment methods *(42)*.

2,4-DCP is a chlorinated derivative of phenol. 2,4 DCP is used primarily as intermediate in the preparation of the herbicide 2,4 dichlorophenoxyacetic acid (2,4-D). It is a high volume chemical, which is highly toxic to aquatic organisms *(43)*.

1,2 DCA is a highly toxic and persistent contaminant that is generated from the production and manufacture of polyvinyl chloride and from other industrial facilities. 1,2 DCA is a continuing problem in groundwater, surface water and contaminated soils worldwide. It is difficult to destroy using conventional chemical dechlorination processes *(44)*.

2.3 Materials and Methods

2.3.1 Materials

Chemical reagents and samples were prepared in an anaerobic chamber (Coy Laboratory Products Inc.) containing an atmosphere of 95% N_2 and 5% H_2. Deaerated deionized water (ddw) was used to make all solutions and was prepared by deoxygenating ultra-pure water (18 MΩ cm) with 99.99% nitrogen for 2 h and then with the atmosphere in anaerobic chamber for 12 h.. Aqueous solutions and chemicals sensitive to redox reaction were deoxygenated in an airlock (Coy Laboratory Products Inc.) and kept in the anaerobic chamber. Target compounds and reductants for this research were ACS (American Chemical Society) grade or higher and were used as received.

2.3.2 Analytical procedures

Perchlorate and nitrate anions were measured to monitor degradation of perchlorate and nitrate, respectively. Perfluorooctanoic acid (PFOA) degradation was measured by monitoring the concentration of fluoride produced. 2,4-dichlorophenol (2,4 DCP) degradation was measured by monitoring the concentration of chloride produced. All of the analytes (ClO_4^-, NO_3^-, Cl^-, F^-) were analyzed by ion chromatography on a Dionex 500 ion chromatograph equipped with a 4-mm Dionex AS–16 analytical and guard column. Analysis of perchlorate was conducted with 40 mM sodium hydroxide eluent at 1 mL/min flow rate with a 250 µL sample loop. Analysis of fluoride, chloride and nitrate was conducted with 10 mM sodium hydroxide eluent at 1.25 mL/min flow rate with a 250 µL sample.

1,2-DCA was measured using an OI Eclipse 4660 purge-and-trap concentrator coupled to an Agilent 6890 GC with a 30 m DB-5 column and FID detector. Samples were purged for 11 minutes with desorption time of 2 minutes and bake time of 10 minutes. The GC was operated with the following conditions: 225 °C inlet temperature; 50:1 split ratio; 1.2 mL/min column flow rate (He); 60 °C oven temperature for 2 min, 20 °C/min rate of temperature increase to 200 °C, hold at 200 °C for 2 min; 250 °C detector temperature; 40 mL/min H2 flow rate; 450 mL/min air flow rate. The procedure was shown to have a method detection limit of 0.0063 mg/L with average recovery of 91% and relative standard deviation of replicates (reproducibility) of 6%.

The summary of the analytical procedures for the analytes is presented in Table 2-1.

Table 2-1: Analytical procedure data.

	MDL (μg/L)	Accuracy (% recovery)	Precision (RSD%)
Nitrate	7.3	94.7	1.56
Perchlorate	6.1	95.8	1.46
Chloride	11.7	97.1	1.80
Fluoride	300	94.6	4.37
1,2 DCA	6.3	91.0	6.0

2.3.3 Reactor systems

Two sources of ultraviolet (UV) radiation were used. Ultraviolet light from low pressure bulbs (UV-L) was provided by a Phillips TUV PL-L36W/4P lamp positioned 11 cm above the target solution within an enclosure. UV light from a narrow band source (UV-N) was provided by a Phillips PL-L36W/01/4P lamp in the same enclosure. The UV-L source produced UV light with a wavelength of 253.7 nm and the UV-N source produced UV light in a narrow band centered at 311 nm. The ultrasound reactor system consisted of the target solutions in plastic centrifuge vials, sonicated using a Hielscher ultrasonic processor, UP50H (50 watts, 30 kHz). A commercial microwave was used with plastic bottles as the microwave reactor system. The electron beam at the National Center for Electron Beam Research at Texas A&M University was used as the e-beam irradiation source. It consists of 2 vertically mounted opposing 10 MeV (Million Electron Volt), 18 Kilowatt Electron Beam Linear Accelerators (LINAC). Samples irradiated by the electron beam were placed in 7”x7” plastic bags wrapped in Saran wrap

and the combination was placed within a 10”x10” plastic bag. The Saran wrap was used to reduce oxygen transport into the samples.

Kinetic experiments on degradation of perchlorate and nitrate were conducted using cylindrical quartz reactors. The quartz reactors were obtained from Starna cells (Atascadero, CA, USA). The reactors have an interior diameter of 47 mm and depth of 10 mm. The UV512C Digital UV C Meter obtained from General Tools (New York City, NY, USA) was used to measure the light intensity at the top of the reactor.

2.4 Results and Discussion

A series of screening experiments were conducted to determine what ARP (combination of reagent and activating method) were most effective. Batch experiments were conducted with all combinations of reagents (4) and activating methods (5) (20 potential ARP) with 4 target compounds at 3 pH levels (2.4, 7.0 and 11.2). The experiments cover time periods or energy doses that were found appropriate for the activating agent/reagent pair. Samples were taken from the reactors over a wide range of times to allow estimation of first-order rate constants that might vary over several orders of magnitude. The experiment time periods or energy doses are summarized in Table 2-2.

Table 2-2: Summary of experiment time periods/energy doses.

Activation method	Experiment time or Energy Dose
UV-L and UV-N	20 hours
Ultrasonics	5 hours
Microwaves	1 minute
Electron beam dose	10 KGy*

*1 Gy = 1 J/kg

Results of the screening experiments are summarized semi-quantitatively in Table 2-3. These results indicate that the E-beam and UV-L generally were successful in activating different reagents to degrade the target contaminants. 1,2 DCA, 2,4 DCP and nitrate were more readily degraded compared to perchlorate and PFOA. These results demonstrate that a wide range of ARP can degrade a wide variety of contaminants. Degradation of the target contaminant was observed in some of the control experiments that were conducted with an activation method in the absence of a reductant. In all such cases, more extensive degradation was observed when a reagent was present during application of the activation method.

Table 2-3: Summary of screening experiments.

Activation Method					
Nitrate					
	UV-L	UV-N	Ebeam	Ultrasound	Microwave
Dithionite	+++	0	+++	0	0
Sulfite	+++	0	+++	0	0
Sulfide	+++	0	n.a.	0	0
Ferrous	+++	+	++	0	0
Perchlorate					
	UV-L	UV-N	Ebeam	Ultrasound	Microwave
Dithionite	0	0	0	0	0
Sulfite	+	0	0	0	0
Sulfide	0	0	n.a.	0	0
Ferrous	0	0	0	0	0
DCP					
	UV-L	UV-N	Ebeam	Ultrasound	Microwave
Dithionite	++		+	0	0
Sulfite	+++	++	++	0	0
Sulfide	+++	+++	n.a.	0	0
Ferrous	+++	++	++	0	0
PFOA					
	UV-L	UV-N	Ebeam	Ultrasound	Microwave
Dithionite	+	+	n.a.	0	0
Sulfite	+	0	n.a.	0	0
Sulfide	0	0	n.a.	0	0
Ferrous	0	0	n.a.	0	0
1,2 DCA					
	UV-L	UV-N	Ebeam	Ultrasound	Microwave
Dithionite	+++	n.a.	n.a.	n.a.	n.a.
Sulfite	+++	n.a.	n.a.	n.a.	n.a.
Sulfide	+++	n.a.	n.a.	n.a.	n.a.
Ferrous	+++	n.a.	n.a.	n.a.	n.a.

n.a. = not available, experiment has not yet been conducted
0 negligible removal (0-10%)
+ low removal (10-40%)
++ moderate removal (40-70%)
+++ good removal (>70%)

The ARP that combines sulfite with UV-L provided the most consistently high levels of removal across all contaminants. In particular, it is the only combination tested that was able to achieve destruction of perchlorate. Therefore, this ARP was the first one chosen for further tests. Perchlorate kinetic experiments were conducted with initial concentrations of 0.1 mM perchlorate and 11 mM sulfite and a light intensity of 8 mW/cm^2 measured at the top of the reactor. Nitrate kinetic experiments were conducted with initial concentrations of 0.16 mM nitrate and 2.8 mM sulfite and a light intensity of 4 mW/cm^2 measured at the top of the reactor. The results of the perchlorate and nitrate kinetic experiments are presented in figures 2-1 and 2-2, respectively. No removal of perchlorate was observed in the control experiments that were conducted with either sulfite or UV-L, but not both. However, some removal of nitrate was observed in the control experiment with only UV-L (figure 2-3).

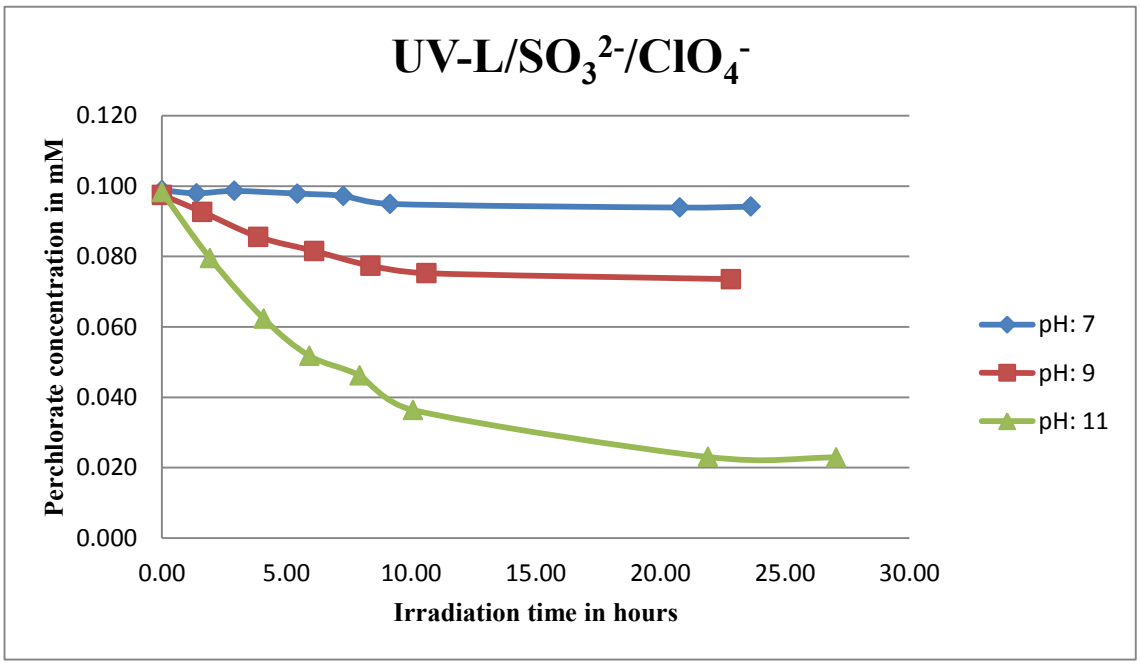

Figure 2-1: Summary of perchlorate kinetic experiments.

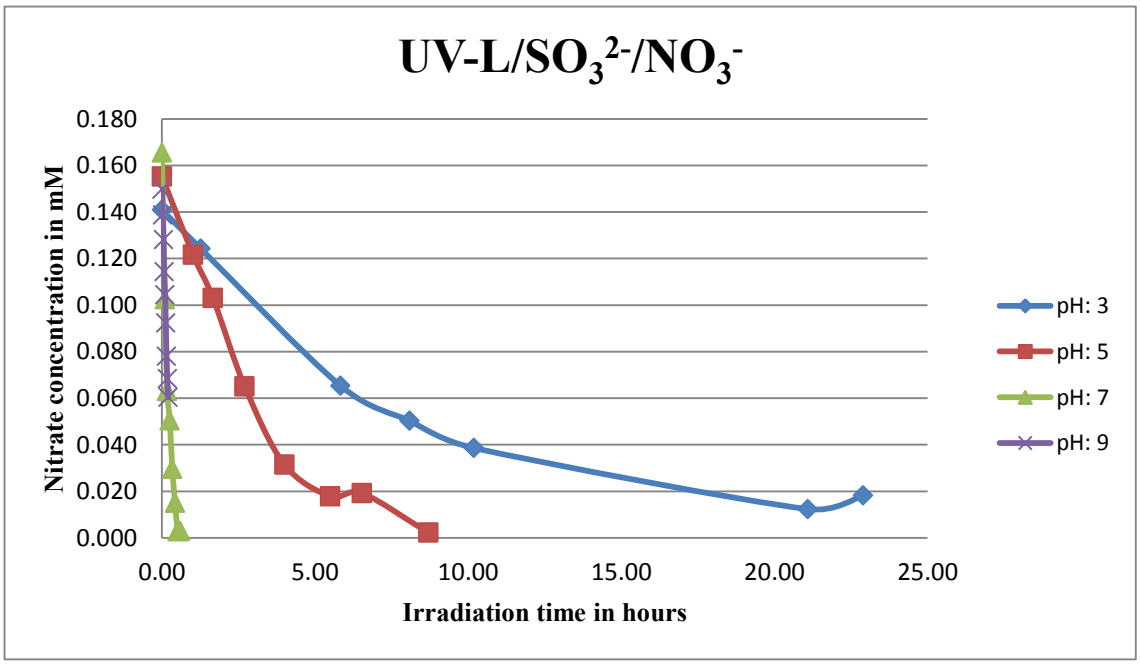

Figure 2-2: Summary of nitrate kinetic experiments.

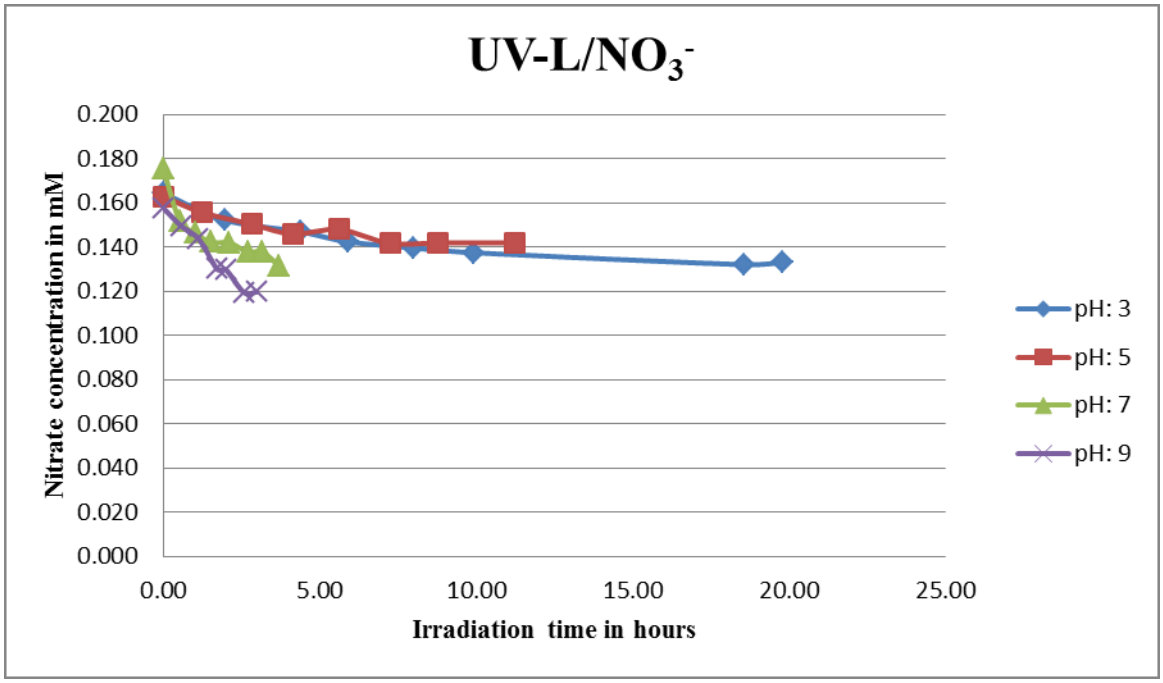

Figure 2-3: Summary of nitrate control experiments.

Figure 2-1 shows that perchlorate removal is incomplete, even at the highest pH. The concentration-time plots show some tendency to be linear early in the experiment (constant rate), but flat (zero rate) later. The zero rate of removal at long time is believed to be caused by consumption of sulfite by photochemical reaction *(24, 25, 45)*. The actual degradation reaction is believed to be the result of reaction between radicals produced by photolysis of sulfite, so as the concentration of sulfite decreases, the rate of degradation of perchlorate decreases.

Figure 2-2 shows that nitrate was removed more rapidly than perchlorate, but that the same behavior was observed (linear degradation early, slow or no degradation later), although nearly complete nitrate removal was observed in all experiments.

The effectiveness of UV-L in stimulating contaminant degradation was measured for each experiment by calculating the quantum yield for removal of perchlorate or nitrate using Equation 2-4. This quantum yield is the ratio of molecules of target compound degraded per photon absorbed by sulfite. The molar absorptivity of sulfite is needed for these calculations and the values used are given in Table 2-4. UV-L was more strongly absorbed at low pH where sulfurous acid (pK_{a1} =1.8, pK_{a2} = 7.2 *(46)*) dominates and at high pH where sulfite predominates.

$$\phi = \frac{r_0 N_A lhc}{I_0 \left(1 - 10^{-\varepsilon C_s l}\right) \lambda_{254}} \qquad (2\text{-}4)$$

where I_0 = irradiance entering reactor (J/m^2-s), ε = molar absorptivity of sulfite (m^2/mole), C_s=concentration of sulfite (mole/m^3), l = depth of reactor (m), λ_{254} = wavelength of UV light (m), r_0 = initial rate of removal of target compound (mole/m^3-s), N_A = Avogadro's number (1/mole), h = Planck's constant (J-s), c = speed of light (m/s).

Table 2-4: Sulfite molar absorptivity at 254 nm.

pH	Molar absorptivity ($M^{-1}cm^{-1}$)
2.5	25.5
5.2	7.6
7.5	15.2
9.0	17.4
10.9	18.2

The results of the calculations for quantum yield are tabulated in Table 2-5 for perchlorate and in Table 2-6 for nitrate.

Table 2-5: Initial degradation rates and quantum yields for perchlorate degradation.

pH	Initial ClO_4^- degradation rate (mM/hour)	Quantum Yield for ClO_4^- degradation
7	0.0003	0.13 E-4
9	0.0031	1.2 E-4
11	0.0088	3.6 E-4

Table 2-6: Initial degradation rates and quantum yields for nitrate degradation.

pH	Initial NO_3^- degradation rate (mM/hour)	Quantum Yields for NO_3^- degradation
3	0.013	0.0027
5	0.033	0.02
7	0.59	0.20
9	0. 48	0.14

The effectiveness of the sulfite/UV-L treatment process improved with increasing pH for both perchlorate and nitrate. This is believed due to the higher concentration of SO_3^{2-}, which absorbs more ultraviolet light and therefore produces more

reactive species (aqueous electrons and the sulfite radical anion). However, SO_3^{2-} will be the dominant species at both pH 9 and pH 11, but perchlorate reduction is much more rapid at the higher pH. Also, the concentration of SO_3^{2-} would be higher at pH 9 than at pH 7, but the initial rate of nitrate removal was observed to be higher at pH 7. Therefore, there are other effects of pH on degradation of target compounds beyond speciation of sulfite/bisulfite/sulfurous acid. Nitrate is much more rapidly degraded than perchlorate and has more efficient use of photons at the higher pH.

Slow degradation of perchlorate is expected, because it has been reported to be a very difficult compound to chemically reduce at room temperature (Table 2-7).

Table 2-7: Summary of chemical reduction of perchlorate and calculated half lives.

Reductant	Typical Half-life[a]	Conditions	Reference
CH_3ReO_2	0.26 hr	25°C, pH 0	*(47, 48)*
Fe(0)	252 day	25°C, $[HClO_4]$=1M, [Fe(0)]=.037 M	*(47, 49)*
Ru(II)	12.5 day	25°C, $[H^+]$ = 0.09-0.30 M	*(50, 51)*
Sn(II)/Mo	890 day	25°C, $[H_2SO_4]$ = 2.5 M, [Mo] (catalyst) = 10^{-5}M	*(52)*
Ti(III)	53 day	50°C, $[H^+]$ = 0.2-1.0 M	*(48, 53)*
Ti(III)	668 day	25°C, $[H^+]$ = 0.1 M	*(54)*
Ti(III)-Hedta	2000 day	25°C, $[H^+]$ = 0.1 M	*(54)*
V(II)	4400 day	49.95°C, $[H^+]$ = 0.11 M	*(55)*
V(III)	14,000 day	49.95°C, $[H^+]$ = 0.11 M	*(55)*

[a] initial concentrations of reductant and perchlorate assumed to be 10^{-4} M and 10^{-5} M.

One hypothesis to explain the mechanism by which the sulfite/UV-L ARP is able to degrade perchlorate is that the sulfite radical ion reacts directly with perchlorate to extract an oxygen atom. This hypothesis is based on literature reports that sulfite acts through an oxygen abstraction mechanism to reduce chorite/chlorate *(56, 57)* and perbromate, the bromine analog of perchlorate *(58)*. Sulfite radical anions also react directly with oxygen as the first step in formation of sulfuric acid *(28, 59, 60)*. If perchlorate were reduced by oxygen abstraction, one mechanism by which it could occur is shown in Equations 2-5 to 2-8. Chlorate would be produced (Equation 2-6), which is easily reduced by sulfite to chloride *(58)*. The sulfate radical anion that is produced

(Equation 2-6) could be reduced by the aqueous electron produced by photochemical decay of sulfite (Equation 2-8). This mechanism is a chain reaction in which Equation 2-5 is the chain initiation reaction, Equations 2-6 and 2-7 are chain propagation reactions and Equation 2-8 is the chain termination reaction.

$$SO_3^{2-} + h\nu = SO_3^{\bullet-} + e_{aq}^- \quad (2\text{-}5)$$

$$SO_3^{\bullet-} + ClO_4^- = SO_4^{\bullet-} + ClO_3^- \quad (2\text{-}6)$$

$$SO_4^{\bullet-} + SO_3^{2-} = SO_4^{2-} + SO_3^{\bullet-} \quad (2\text{-}7)$$

$$SO_4^{\bullet-} + e_{aq}^- = SO_4^{2-} \quad (2\text{-}8)$$

A similar oxygen abstraction mechanism is possible for nitrate reduction. Additionally, the aqueous electron could also play a direct role in the degradation of nitrate.

A second hypothesis to explain the mechanism by which the sulfite/UV-L ARP is able to degrade perchlorate is that perchlorate reduction is due to catalytic effects of trace metals that were present in experimental solution. Taube (1982) has proposed a mechanism for reduction of perchlorate that is based on transfer of an oxygen atom to metals such as V, Mo, Ti, Ru, Os, and U. Other possible catalysts (W, Re) could work through a two-electron transfer mechanism. Complexes of Re have been reported to be effective in perchlorate reduction under some conditions *(47, 48)*. Another potential catalytic mechanism would be for metal ions such as Fe, Ti, Cu and Ni to be reduced to nanoscale, zero-valent metal particles that could achieve two-electron transfers to perchlorate, converting it to chlorate.

The results of the screening experiments are presented in Appendix A.

2.5 Summary

The results of the screening experiments validate the theory motivating ARP, i.e. that combining activation methods and reducing agents to produce reducing radicals can degrade oxidized contaminants. The sulfite/UV-L ARP is an effective ARP and shows the ability to destroy perchlorate and PFOA, which are both compounds that are very difficult to degrade chemically at room temperature. The effectiveness of the sulfite/UV-L treatment process improved with increasing pH for both perchlorate and nitrate.

3 PERCHLORATE REDUCTION BY THE SULFITE/UV-L ARP

3.1 Introduction

The perchlorate anion is both a naturally occurring and manmade compound, which has been detected in ground and surface water, soil and vegetation. It is a highly oxidized form of chlorine and it is difficult to reduce at room temperature. The tetrahedral shape of the perchlorate anion does not allow easy access of electrons to the chlorine atom and a considerable amount of energy is needed to disturb the oxygen atoms in order to allow the electrons access to the chlorine atom. However, it has been used extensively since World War II as an oxidizer in rocket fuels and propellants, because it is a strong and reactive oxidant at higher temperature. Most of the environmental problems caused by perchlorate are due to manmade perchlorate, though there are instances of contamination by naturally occurring perchlorate. Perchlorate is highly soluble, mobile and stable in water. It thus forms large and persistent contaminant plumes when introduced into ground or surface waters. Its release has been reported in at least 25 states in the USA *(61, 62)*.

Perchlorate can cause adverse health effects by interfering with iodide uptake by the thyroid gland. Deficiency of iodide in the thyroid gland affects the production of thyroid hormones, which play an important role in regulating the metabolic processes of the human body. People with thyroid disorders, pregnant women, infants and fetuses are at a greater risk of being affected by perchlorate. The U.S. Environmental Protection Agency has set the human reference dose (RfD) for perchlorate at 0.0007

milligrams/kilogram/day and has decided to regulate perchlorate under the Safe Drinking Water Act *(61, 62)*.

In addition to being highly soluble and resistant to chemical reduction, perchlorate also resists forming complexes with metals and being adsorbed to most surfaces *(62)*. Most chemical processes that degrade perchlorate are slow and require high temperatures or high pressures, or both. Physical treatment processes like ion exchange, reverse osmosis, nanofiltration/ultrafiltration, electrodialysis, and capacitive deionization, are some of the commercially available technologies. Although they remove perchlorate from impacted media, they do not degrade it. Biological processes also have been employed to treat contaminated ground and surface water, soil and wetlands *(62, 63)*.

Advanced reduction processes (ARP) are a new set of water treatment processes that employ a source of activation energy to activate reductants to produce reducing radicals that can effectively degrade oxidized contaminants. The results of the preliminary experiments presented in Chapter 2 demonstrate that the theory behind ARP is valid. The preliminary experiments provide data that show the sulfite/UV-L ARP to be one of the successful ARP tested and the only ARP tested to date that is successful in reducing perchlorate. The sulfite/UV-L ARP involves irradiating target contaminant solutions that contain the reductant sulfite with ultraviolet light of 253.7 nm wavelength. The data from the preliminary experiments indicate that the rate of perchlorate degradation increases with an increase in pH.

Two hypotheses were presented in Chapter 2 to explain the observed ability of the sulfite/UV-L ARP to degrade perchlorate. The first hypothesis was that the sulfite radical ion is effective by itself in reducing perchlorate. This hypothesis was based on literature reports that sulfite reduces perbromate, the bromine analog of perchlorate, through an oxygen abstraction mechanism *(58)*. The second hypothesis was that perchlorate reduction is due to catalytic effects of trace metals that were present in experimental solution.

In this study, the effects of pH and sulfite concentration on sulfite absorption were studied. The effects of sulfite concentration, light intensity, pH and temperature on the ability of the sulfite/UV-L ARP to degrade perchlorate were studied. The products of perchlorate degradation by the sulfite/UV-L ARP were investigated. The hypothesis that perchlorate reduction is due to catalytic effects of trace metals present in the experimental solution was tested.

The degradation of perchlorate to simple compounds by the sulfite/UV-L ARP indicates that it holds promise of being developed into a commercially viable alternative to the present perchlorate treatment technologies.

3.2 Materials and Methods

3.2.1 Materials

Chemical reagents and samples were prepared in an anaerobic chamber (Coy Laboratory Products Inc.) containing an atmosphere of 95% N_2 and 5% H_2. Deaerated deionized water (ddw) was used to make all solutions and was prepared by deoxygenating ultra-pure water (18 MΩ cm) with 99.99% nitrogen for 2 h and then with

the atmosphere in anaerobic chamber for 12 h. Aqueous solutions and chemicals sensitive to redox reaction were deoxygenated in an airlock (Coy Laboratory Products Inc.) and kept in the anaerobic chamber. Target compounds and reductant for this research were ACS (American Chemical Society) grade or higher and were used as received.

3.2.2 Analytical procedures

Perchlorate, chlorate and chloride anions were measured to monitor and identify the products of perchlorate degradation. All of the analytes (ClO_4^-, ClO_3^-, Cl^-) were analyzed by ion chromatography on a Dionex 500 ion chromatograph equipped with a 4-mm Dionex AS–16 analytical and guard column. Analysis of perchlorate was conducted with 40 mM sodium hydroxide eluent at 1 mL/min flow rate with a 250 µL sample loop. Analysis of chlorate and chloride was conducted with 10 mM sodium hydroxide eluent at 1.25 mL/min flow rate with a 250 µL sample. The absorption spectra of sulfite solutions were measured by a Thermo Spectronic Helios Gamma UV-Vis Spectrophotometer using Starna Cells, which are rectangular UV quartz cells with a stopper and a 10-mm light path length.

3.2.3 Reactor systems

Ultraviolet light from low pressure bulbs (UV-L) was provided by a Phillips TUV PL-L36W/4P lamp positioned above the reactors, with both lamp and reactors contained within an enclosure. The UV-L source produced UV light with a wavelength of 253.7 nm. Kinetic experiments on degradation of perchlorate were conducted using

cylindrical quartz reactors obtained from Starna cells (Atascadero, CA, USA). The reactors have an interior diameter of 47 mm and depth of 10 mm. A UV512C Digital UV C Meter obtained from General Tools (New York City, NY, USA) was used to measure the light intensity at the point where light entered the reactor. A fan was used for some of the UV irradiation experiments in order to reduce the extent of the temperature increase.

3.3 Results and Discussion

3.3.1 Effects of pH and sulfite concentration on sulfite absorption spectra

The speciation of sulfurous acid (pK_{a1} =1.8, pK_{a2} = 7.2 *(64)*) among metabisulfite ($S_2O_4^{2-}$), sulfurous acid (H_2SO_3), bisulfite (HSO_3^-) and sulfite (SO_3^{-2}) at different pH is presented in Figure 3-1. Bisulfite is predominant at the acidic pH tested and sulfite is predominant at the basic pH tested. The data were obtained by running simulations using Visual MINTEQ, a free equilibrium speciation model.

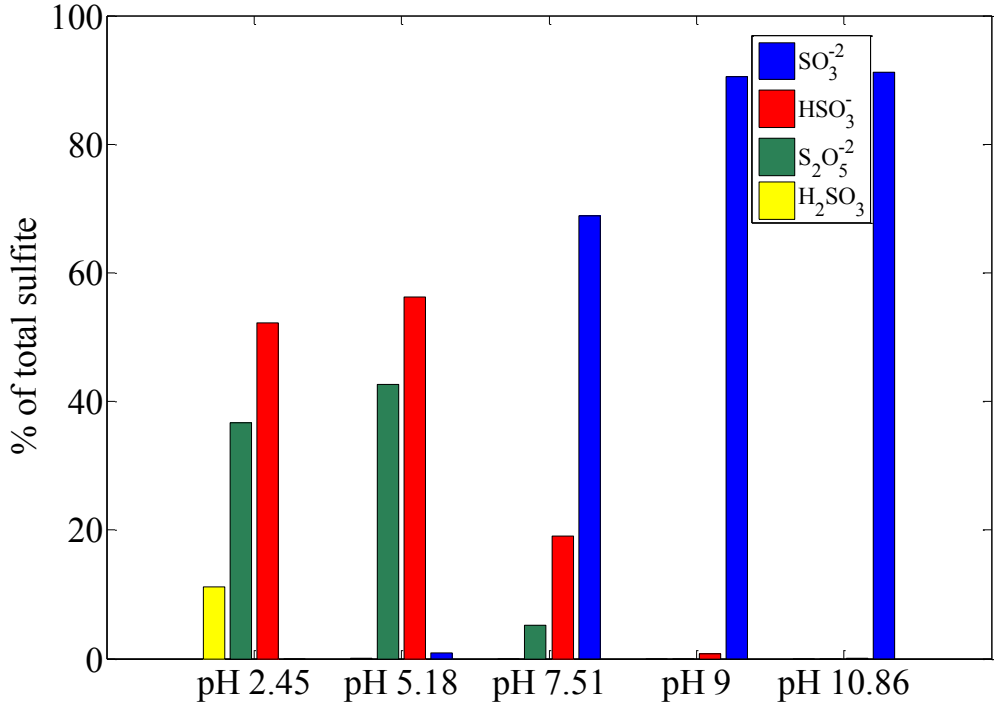

Figure 3-1: Speciation of 0.0159 M sulfite at different pH.

Sulfite absorption spectra at various concentrations and at different pH were measured and are presented in Figures 3-2–3.7.

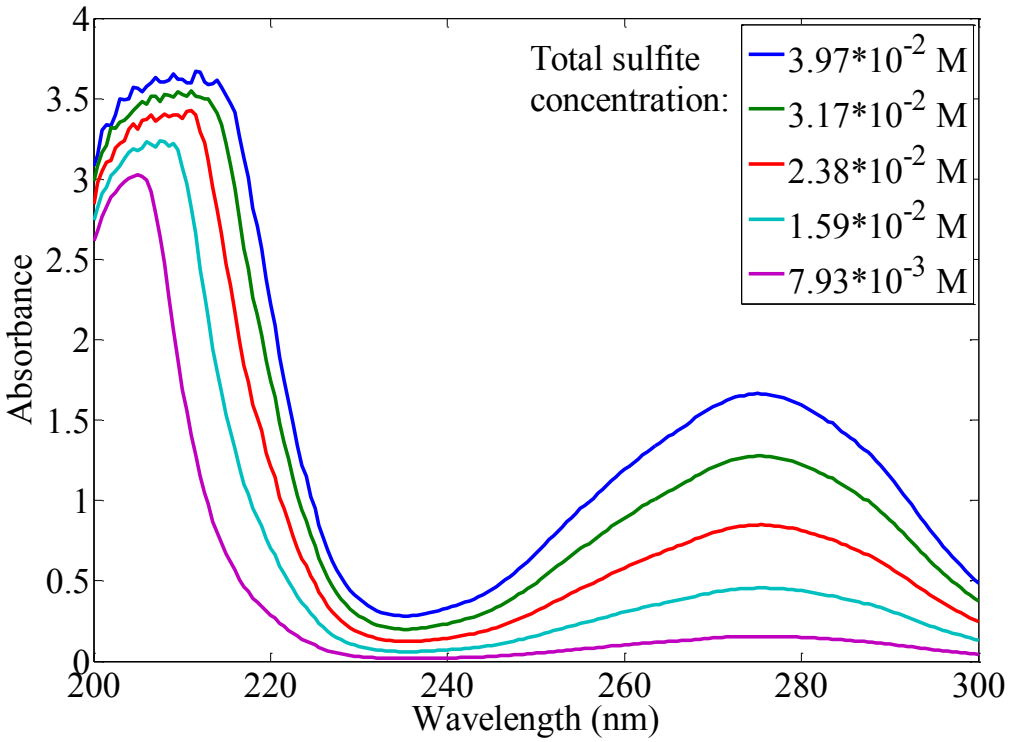

Figure 3-2: Sulfite absorption spectra at pH 2.45.

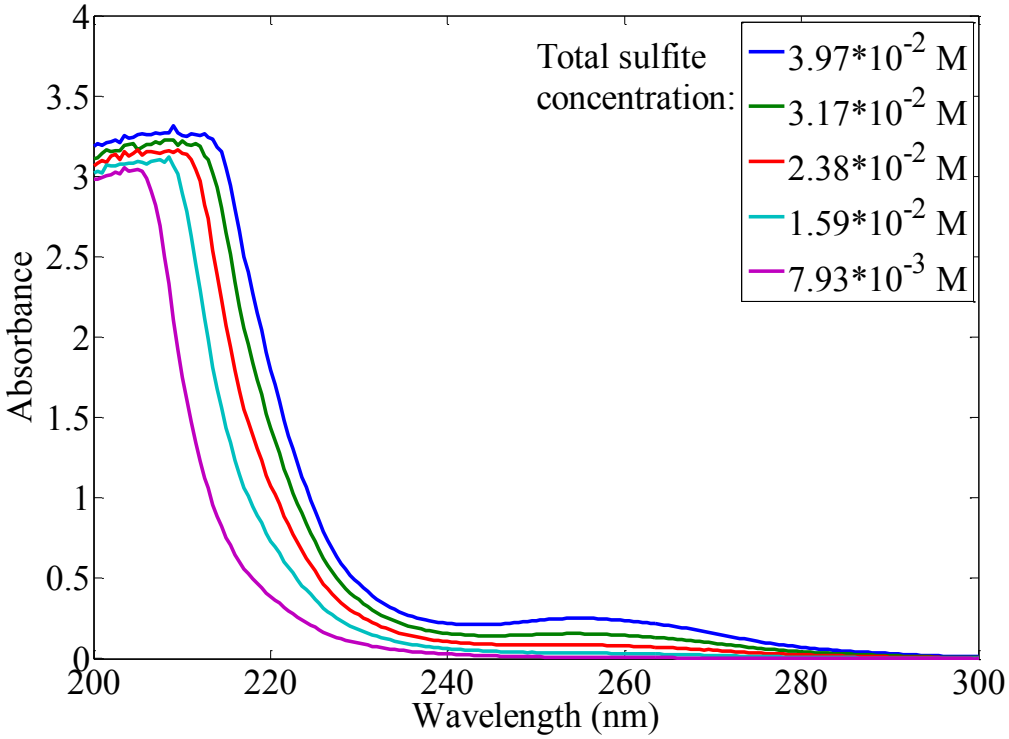

Figure 3-3: Sulfite absorption spectra at pH 5.18.

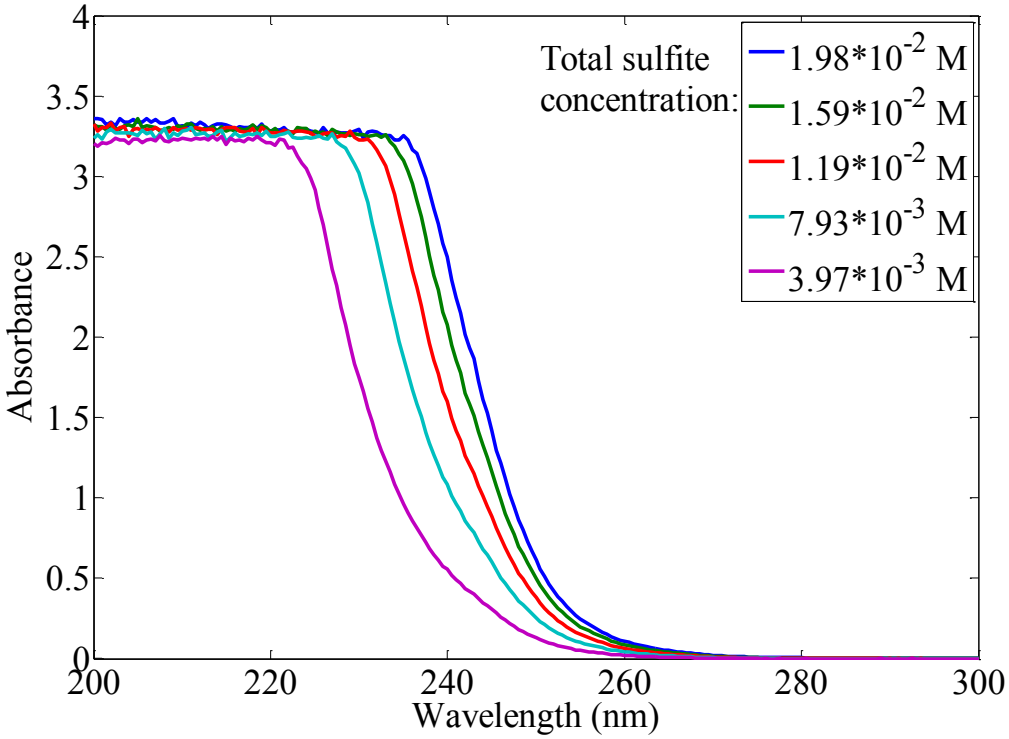

Figure 3-4: Sulfite absorption spectra at pH 7.51.

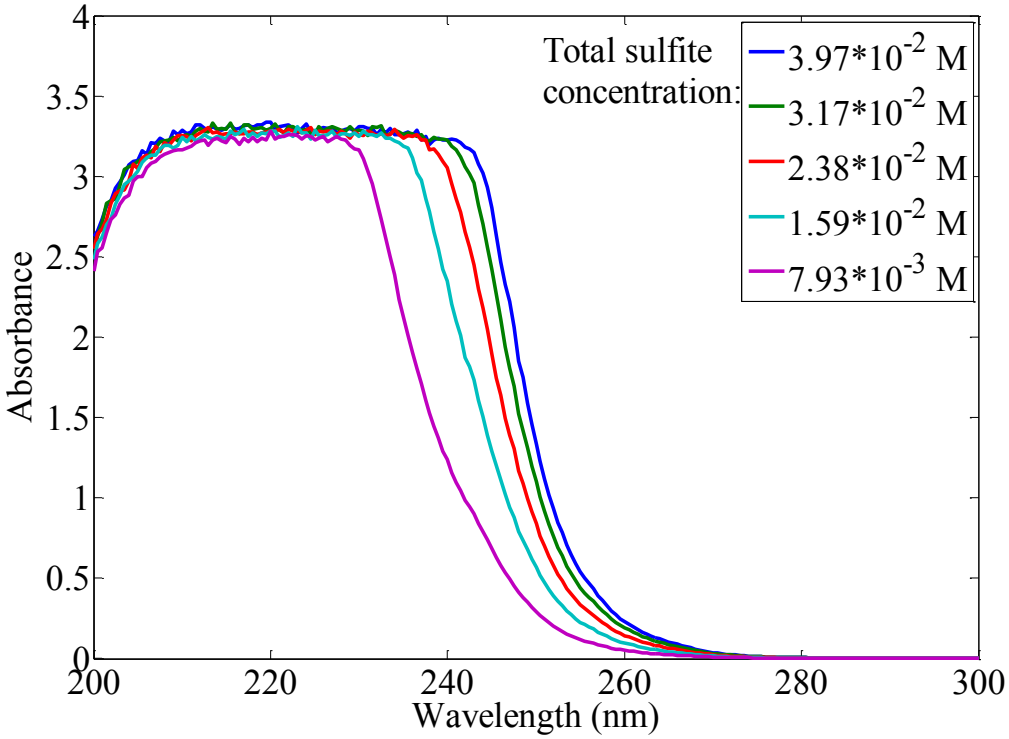

Figure 3-5: Sulfite absorption spectra at pH 9.0.

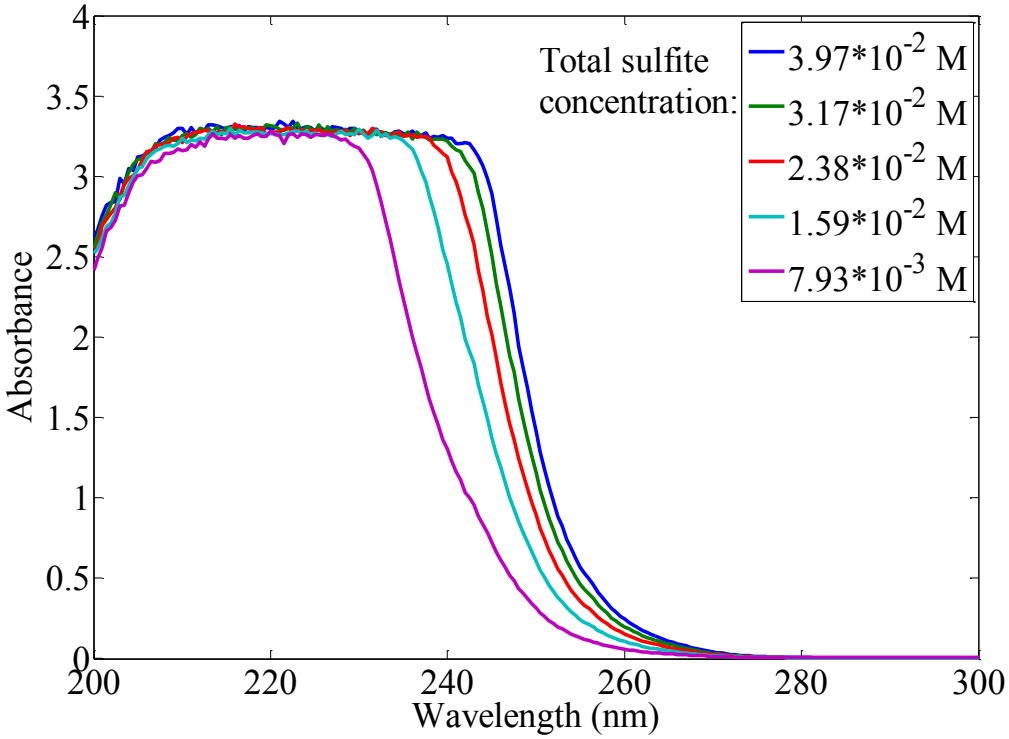

Figure 3-6: Sulfite absorption spectra at pH 10.86.

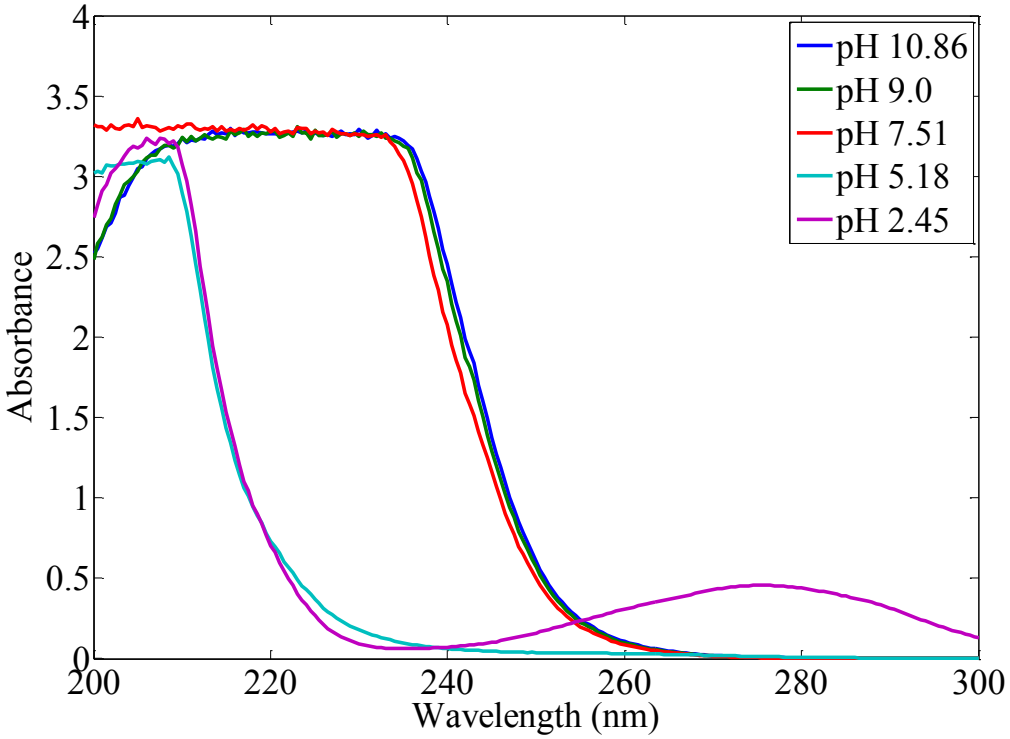

Figure 3-7: Sulfite (0.0159 M) absorption spectra at different pH.

The UV absorption peak of sulfite varies with pH and concentration. The absorbance values between 200 – 240 nm are high (>1). At such high absorbance, the accuracy of the measurement is unreliable, and the estimation of peaks and respective peak wavelengths are based on visual judgment. Sulfite has two peaks, one around 275 nm and the other around 205 nm. The peak around 275 nm decreases as pH increases from 2.45 to 5.18 and is consistent with the presence of sulfurous acid in solution. The peak around 205 nm appears to shift towards higher wavelengths (≅220 nm) and increases with increasing pH and sulfite concentration, and is consistent with the presence of sulfite in solution. Due to the high absorbances, the estimate about the peak

wavelength lacks accuracy. At basic pH, sulfite solutions absorb UV light strongly at around 220 nm, while the absorbance at 254 nm is relatively low. Thus, UV light around 220 nm could be effective at activating sulfite solutions at basic pH. Table 3.1 presents the molar absorptivities of sulfite solutions at 254 nm at various pH that were also shown in Chapter 2. UV-L was more strongly absorbed at low pH where sulfurous acid predominates and at high pH where sulfite predominates.

Table 3-1: Sulfite molar absorptivity at 254 nm.

pH	Molar absorptivity ($M^{-1}cm^{-1}$)
2.5	25.5
5.2	7.6
7.5	15.2
9.0	17.4
10.9	18.2

3.3.2 Model for degradation of target by reductant/UV

To aid in understanding the effects of various variables tested, a simple model is presented below to explain perchlorate degradation. It assumes that the target (perchlorate) is reduced by reacting with a radical ($SO_3^{\bullet-}$) which is formed when a reductant (SO_3^{2-}) absorbs UV light during irradiation. The reducing radical($SO_3^{\bullet-}$) is assumed to be scavenged by reacting with other species in the system. The model

assumes that the reductant (SO_3^{2-}) is the only major UV absorbing species in the solution.

Table 3-2: Nomenclature.

I^*	Light flux (einstein/m^2-s)
ε'	Molar absorptivity or molar extinction coefficient (M^{-1} m^{-1})
L	Total thickness of reactor in direction of light path (m)
A	UV light absorbing compound (SO_3^{-2}) that forms radicals upon irradiation
R	Radical that reacts with target compound ($SO_3^{\cdot-}$)
T	Target compound (ClO_4^-)
S	Radical scavengers
ϕ	Sulfite quantum yield
r	Rate of reaction
k	Rate constant

$$A + hv \xrightarrow{1} R$$

$$R + T \xrightarrow{2} products$$

$$R + S \xrightarrow{3} products$$

Conducting mass balance on radical concentration:

$$\frac{d[R]}{dt} = r_1 - r_2 - r_3$$

Assuming steady state,

$$\frac{d[R]}{dt} = r_1 - r_2 - r_3 = 0$$

$$\therefore r_1 = r_2 + r_3$$

where,

$$r_2 = k_T[R][T]$$

$$r_3 = k_S[R][S]$$

$$\therefore r_1 = k_T[R][T] + k_S[R][S]$$

$$\therefore [R] = \frac{r_1}{k_T[T] + k_S[S]}$$

$$r_1 = \phi r_{abs} = \phi \varepsilon'[A] I^*$$

where,

$$I^* = I_0^* e^{-\varepsilon'[A]x}$$

The average light flux over the depth of the reactor:

$$I_{avg}^* = \frac{I_0^*(1 - e^{-\varepsilon'[A]L})}{\varepsilon'[A]L}$$

$$\therefore r_1 = \frac{\phi I_0^*(1 - e^{-\varepsilon'[A]L})}{L}$$

Rate of degradation of target compound:

$$r_2 = k_T[R][T]$$

$$\therefore r_2 = k_T[T] \frac{r_1}{k_T[T] + k_S[S]}$$

$$\therefore r_2 = \frac{k_T[T]}{k_T[T] + k_S[S]} \times \frac{\phi I_0^*(1 - e^{-\varepsilon'[A]L})}{L}$$

Comparing r_2 with a pseudo first-order target degradation reaction,

$$r_2 = k_2[T] = \frac{k_T[T]}{k_T[T] + k_S[S]} \times \frac{\phi I_0^*(1 - e^{-\varepsilon'[A]L})}{L}$$

$$\therefore k_2 = \frac{k_T}{k_T[T] + k_S[S]} \times \frac{\phi I_0^*(1 - e^{-\varepsilon'[A]L})}{L} \quad (3\text{-}1)$$

The relevant reaction for perchlorate degradation by sulfite anion radical produced by sulfite/UV-L is:

$$\therefore k_2 = \frac{k_{ClO_4^-}}{k_{ClO_4^-}[ClO_4^-] + k_S[S]} \times \frac{\phi_{SO_3^{2-}} I_0^*(1 - e^{-\varepsilon'[SO_3^{2-}]L})}{L} \quad (3\text{-}2)$$

The behavior at low and high reagent concentrations can be seen by using an expansion for the exponential function ($\exp(x) = 1+x + x^2/2! + x^3/3! + \ldots$).

$$\therefore \left(1 - e^{-\varepsilon'[A]L}\right) \approx \varepsilon'[A]L + \frac{(\varepsilon'[A]L)^2}{2!} + \frac{(\varepsilon'[A]L)^3}{3!} + \cdots$$

If the extent of absorption $(\varepsilon'[A]L)\ is \ll 1$,

$$\left(1 - e^{-\varepsilon'[A]L}\right) \approx \varepsilon'[A]L$$

$$\therefore k_2 = \frac{k_T}{k_T[T] + k_S[S]} \times \frac{\phi I_0^* \varepsilon'[A]L}{L} \tag{3-3}$$

If the extent of absorption $(\varepsilon'[A]L)\ is \gg 1$,

$$\left(1 - e^{-\varepsilon'[A]L}\right) \approx 1$$

$$\therefore k_2 = \frac{k_T}{k_T[T] + k_S[S]} \times \frac{\phi I_0^*}{L} \tag{3-4}$$

When sulfite is the only compound absorbing light, then the average rate of light absorption is:

$$r_{light,avg} = \frac{I_0^*(1 - e^{-\varepsilon'[A]L})}{L} \tag{3-5}$$

The quantum yield for the target is:

$$\phi_T = \frac{r_2}{r_{light,avg}}$$

$$\therefore \phi_T = \frac{\frac{k_T[T]}{k_T[T] + k_S[S]} \times \frac{\phi I_0^*(1 - e^{-\varepsilon'[A]L})}{L}}{\frac{I_0^*(1 - e^{-\varepsilon'[A]L})}{L}}$$

$$\therefore \phi_T = \frac{k_T[T]\phi}{k_T[T] + k_S[S]} \tag{3-6}$$

3.3.3 Effect of pH on perchlorate degradation

Batch kinetic experiments were conducted to investigate the effects of pH (7, 9 and 11) on perchlorate degradation. Kinetic experiments were not conducted at acidic pH as the screening experiments did not show perchlorate removal at that condition. Perchlorate kinetic experiments were conducted with initial concentrations of 0.1 mM perchlorate and 11 mM sulfite. Two sets of experiments, one without air circulation ($T \cong 38^{o}C$) and the other with air circulation ($T \cong 28^{o}C$), were conducted. Experiments without air circulation were conducted at a light intensity of 8 mW/cm^2, measured at the top of the reactor, while the experiments with air circulation were conducted at a light intensity of 7 mW/cm^2. All perchlorate degradation kinetic experiments were conducted with a buffer of 5 mM PO_4^{3-}.

Perchlorate degradation is probably a second-order reaction, where the reaction rate is proportional to the concentration of perchlorate and an unknown radical that degrades perchlorate. For the purpose of quantification, a first-order perchlorate degradation model was fitted to the data using the Levenberg-Marquardt algorithm in MATLAB and a first-order rate constant that minimizes the sum of squared residuals was calculated was calculated. Data at the latter experiment times are strongly affected by sulfite loss, which decreases the rate of perchlorate degradation. Data beyond 15 hours of irradiation were excluded from the regressions so that the calculated values of rate constants will represent conditions that are more like a first-order degradation. A first-order degradation model was fitted to sulfite loss during perchlorate degradation and the first-order rate constants were calculated.

The results of the perchlorate kinetic experiments with and without air circulation at different pH are presented in Figures 3-8 and 3-9 respectively. The solid lines represent the first-order degradation model fitted to the kinetic data. The first-order rate constants for perchlorate degradation at different pH are presented in Figure 3-10.

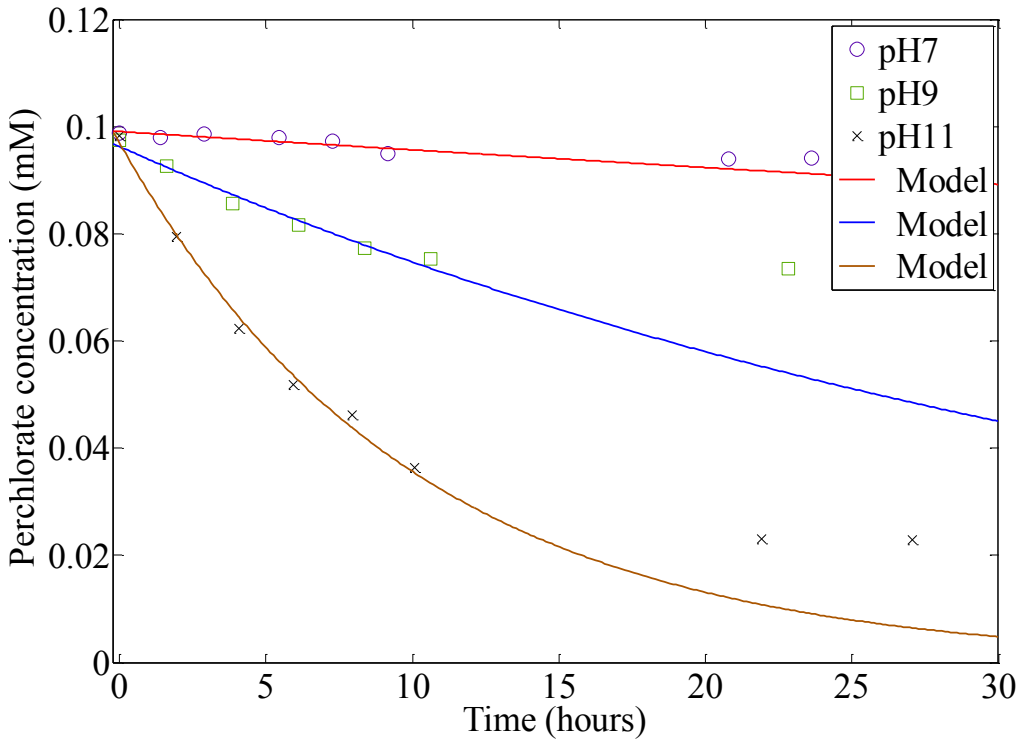

Figure 3-8: Perchlorate degradation by sulfite/UV-L at various pH (8 mW/cm2, 11 mM sulfite concentration, without air circulation, T=38^{o} C).

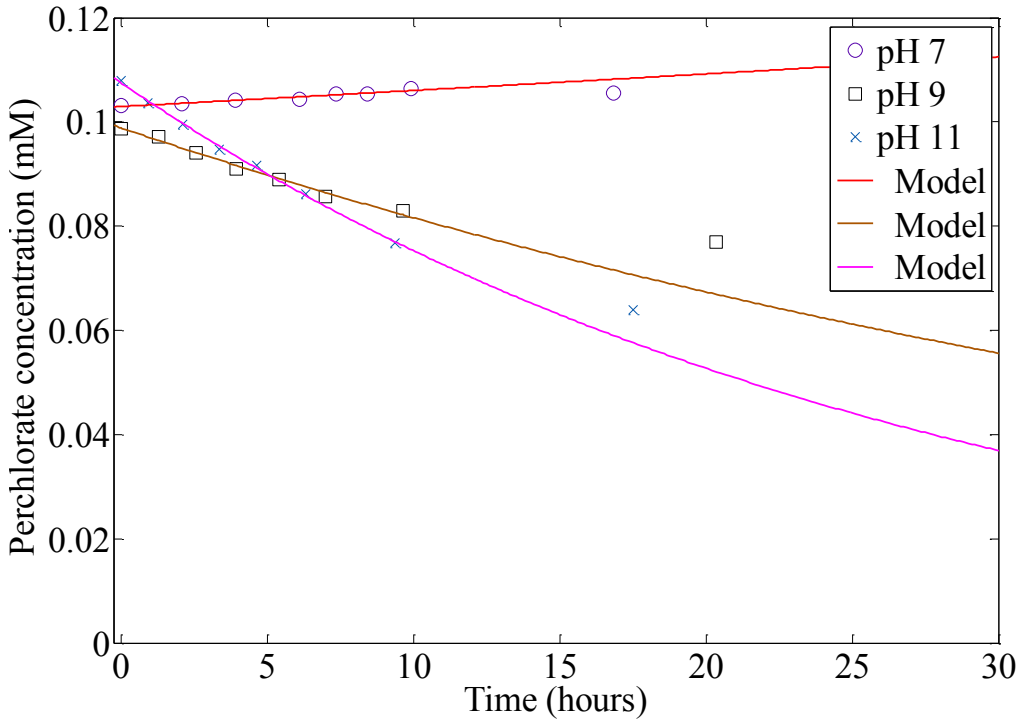

Figure 3-9: Perchlorate degradation by sulfite/UV-L at various pH (7 mW/cm^2, 11 mM sulfite concentration, with air circulation, T≅ 28^o C).

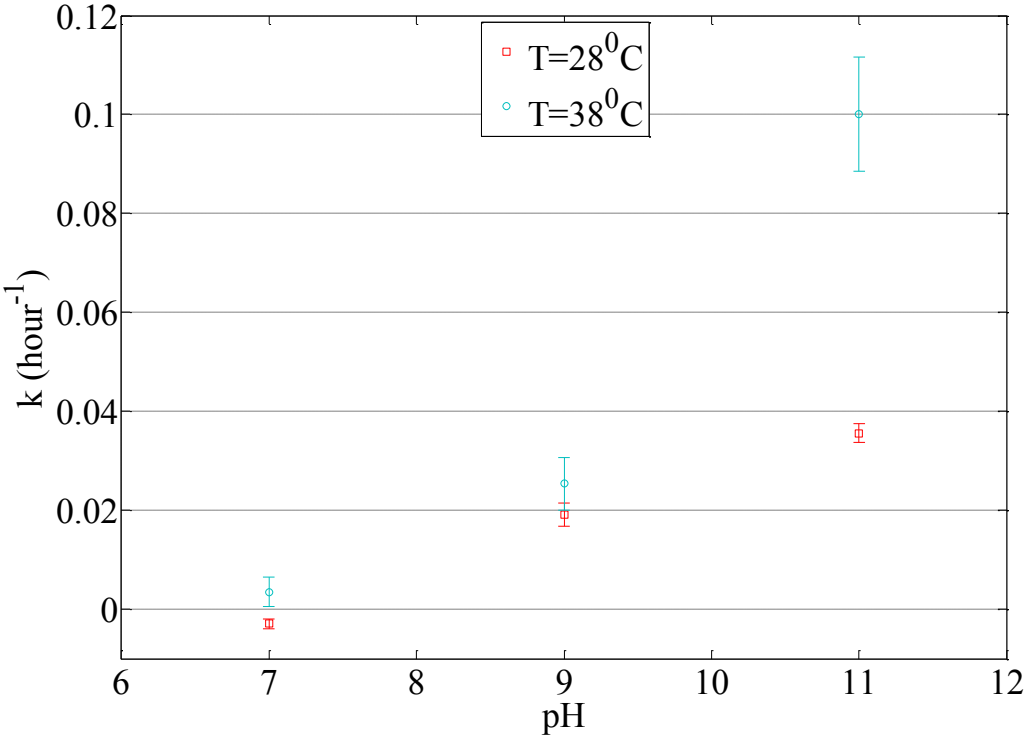

Figure 3-10: First-order rate constants for perchlorate degradation by sulfite/UV-L at various pH (7 mW/cm2, 11 mM sulfite concentration).

As shown in Figures 3-8, 3-9, and 3-10, for experiments with and without air circulation, there is little to no perchlorate removal at neutral pH and the rate of perchlorate degradation by sulfite/UV-L increases with increasing pH and temperature. From equation 3-2, it can be seen that an increase in the concentration of sulfite (SO_3^{-2}), leads to increase in the pseudo first-order rate constant. The concentration of the sulfite ion would increase with increasing pH so an increasing rate constant should result and this is in accordance with observed results. The concentration of the sulfite anion (SO_3^{2-}) increases with pH (Figure 3-1) so more light will be absorbed and more radicals will be produced at higher pH. However, this does not explain the pronounced increase in

efficiency and rate of removal of perchlorate at pH 11, where the increase in sulfite anion concentration is marginal compared to pH 9. Figure 3-10 shows that an increase in temperature is generally favorable for perchlorate degradation, especially at pH 11, where the first-order rate constant for perchlorate degradation more than doubled at the higher temperature.

The effectiveness of UV-L in stimulating contaminant degradation was measured for each experiment by calculating the quantum yields for removal of perchlorate (ϕ_p) and sulfite (ϕ_s) using Equation 3-7. These quantum yields are the ratios of molecules of perchlorate/sulfite degraded per photon of light absorbed by sulfite. The quantum yields are used as a measure of the efficiency of the sulfite/UV-L system in activating sulfite and degrading perchlorate. The molar absorptivity values of sulfite presented in Table 3-1 were used for these calculations.

$$\phi = \frac{r_0 N_A l h c}{I_0 \left(1 - 10^{-\varepsilon C_s l}\right) \lambda_{254}} \tag{3-7}$$

where I_0 = irradiance entering reactor (J/m^2-s), ε = molar absorptivity of sulfite (m^2/mole), C_s=concentration of sulfite (mole/m^3), l = depth of reactor (m), λ_{254} = wavelength of UV light (m), r_0 = initial rate of removal of compound = (k_{model}*initial concentration of perchlorate/sulfite (mole/m^3-s), N_A = Avogadro's number (1/mole), h = Planck's constant (J-s), c = speed of light (m/s).

The quantum yields for the removal of perchlorate are shown in Figure 3-11.

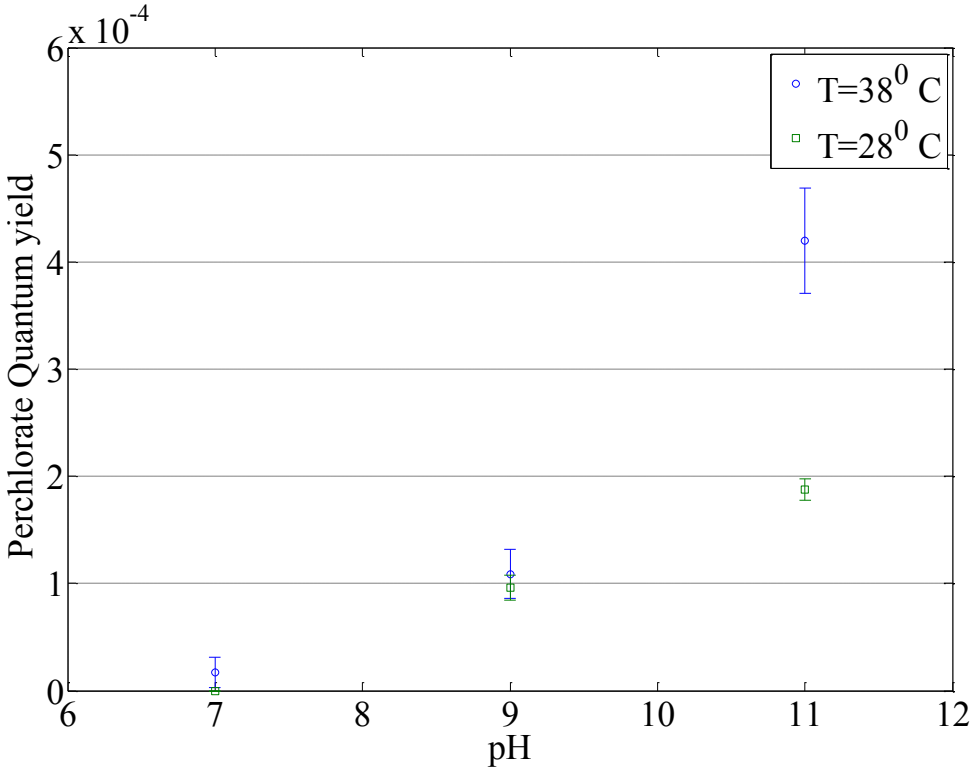

Figure 3-11: Quantum yield for perchlorate degradation by sulfite/UV-L at various pH (7 mW/cm^2, 11 mM sulfite concentration).

As shown in Figure 3-11, for experiments with and without air circulation, the efficiency of perchlorate degradation by sulfite/UV-L increases with increasing pH and temperature. Figure 3-11 shows that an increase in temperature is generally favorable for perchlorate quantum yield, especially at pH 11, where the perchlorate quantum yield more than doubled at the higher temperature. These results indicate that higher OH^- concentrations and higher temperatures are conducive to the mechanism that leads to perchlorate degradation.

For perchlorate kinetic experiments with air circulation, the concentration of sulfite was monitored by UV-spectrophotometry and is presented in Figure 3-12. The first-order rate constants for sulfite loss at different pH are presented in Figure 3-13.

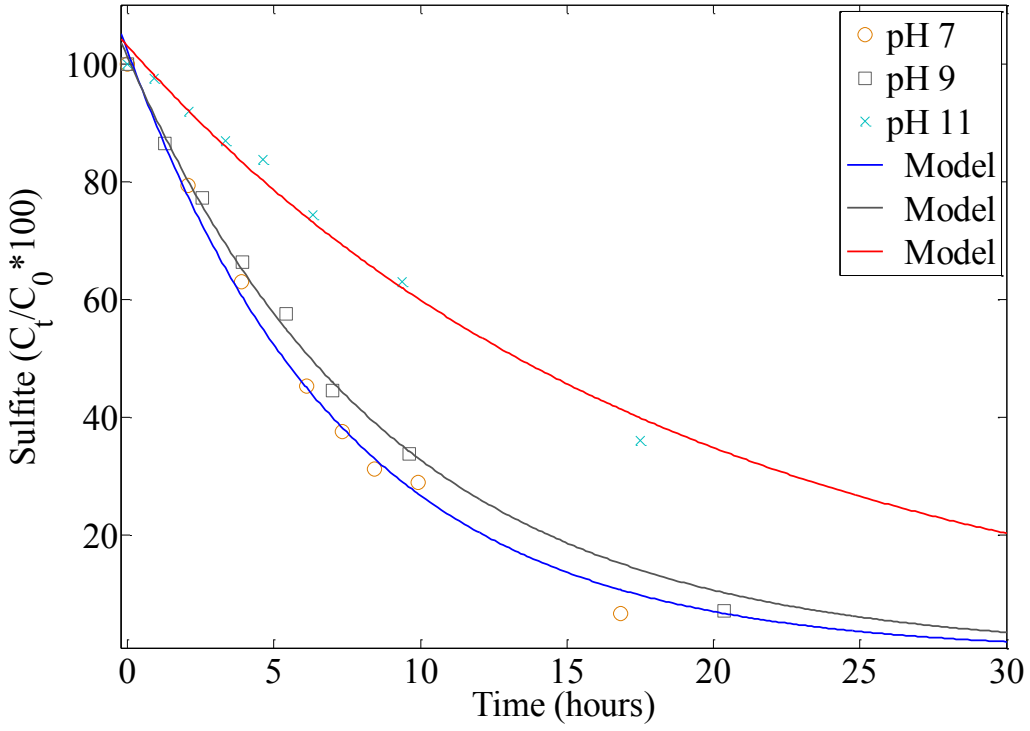

Figure 3-12: Sulfite loss during perchlorate degradation by sulfite/UV-L at various pH (7 mW/cm^2, 11 mM sulfite concentration, with air circulation, T≅ 28^o C).

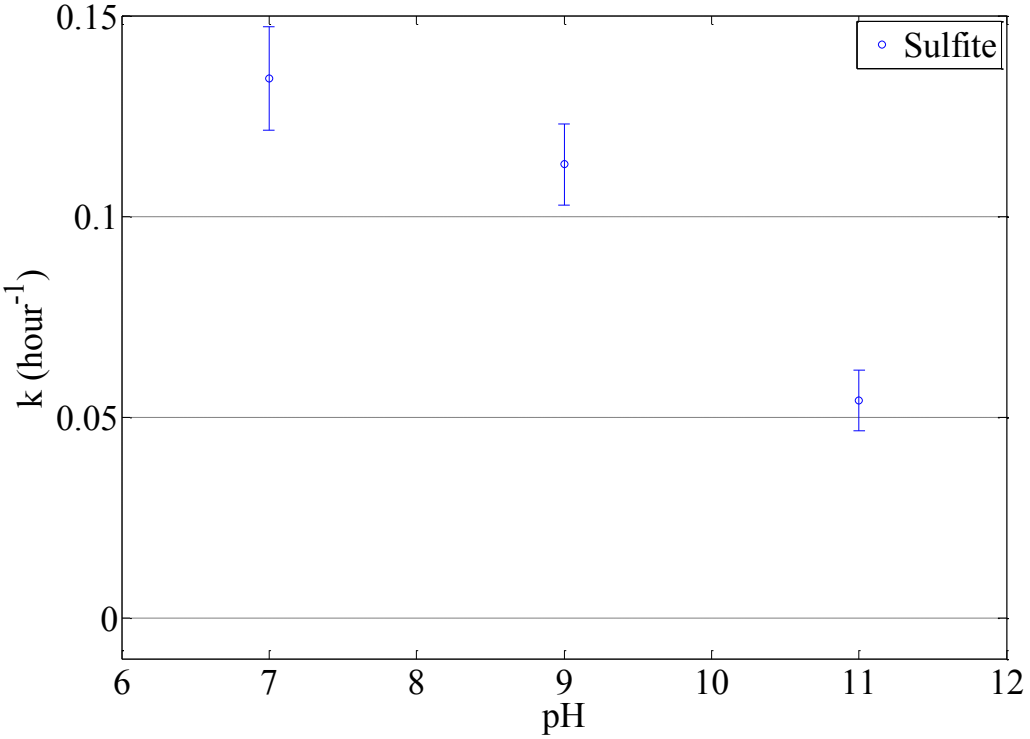

Figure 3-13: First-order rate constants of sulfite loss at various pH (7 mW/cm^2, 11 mM sulfite concentration, with air circulation, T≅ 28^o C).

Figures 3-12 and 3-13 indicate that the increasing pH results in decreasing first-order rate constant for sulfite.

The quantum yields for the sulfite loss are shown in Figure 3-14.

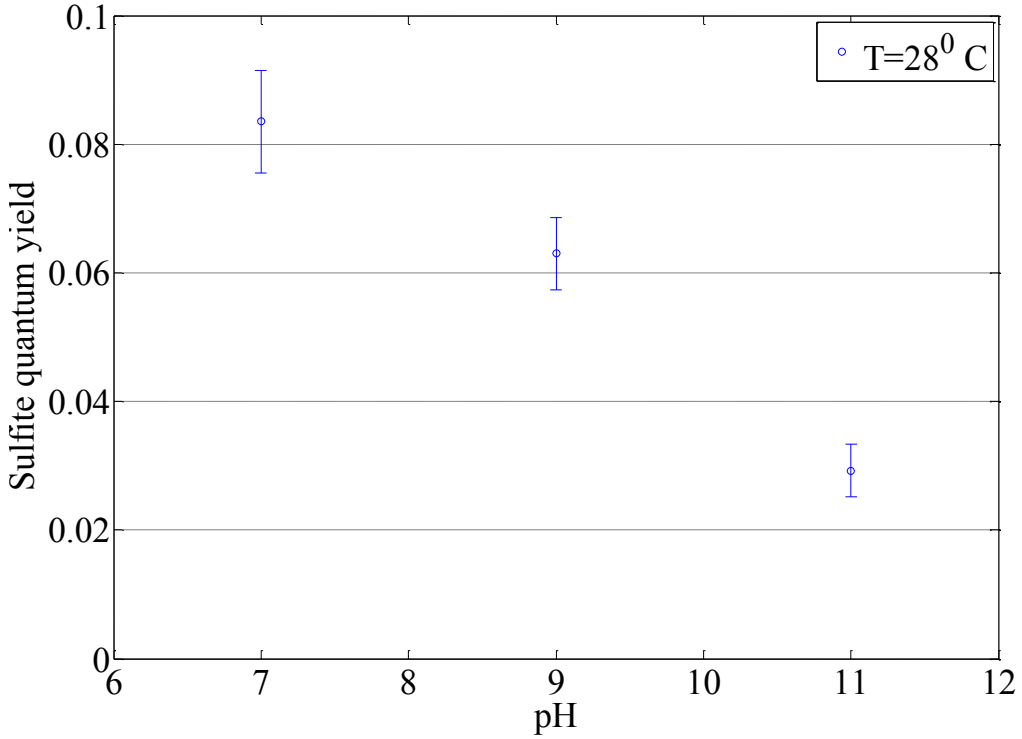

Figure 3-14: Quantum yield for sulfite loss during perchlorate degradation by sulfite/UV-L at various pH (7 mW/cm^2, 11 mM sulfite concentration, with air circulation, T≅28^{o}C).

Figure 3-14 indicates that the increasing pH results in decreasing quantum yields for sulfite.

The calculated quantum yield at pH 9 (0.063±0.0056) is considerably lower than the value at pH 9 (0.39±0.04) reported by Fischer and Warneck [8]. The difference between the reported and observed values of quantum yield of sulfite could be due to the fact that the values reported by Fisher and Warneck were obtained from experiments conducted using argon-saturated solutions, while the values reported here were obtained from experiments conducted with solutions saturated with 95% N_2 and 5 % H_2.

3.3.4 Effect of light intensity on perchlorate degradation

Batch kinetic experiments were conducted to investigate the effects of light intensity on perchlorate degradation. These experiments were conducted with initial concentrations of 0.1 mM perchlorate and 11 mM sulfite. Two sets of experiments were conducted. The set without air circulation used light intensities of 1.45, 4, 7, 12 and 20 mW/cm^2. The set with air circulation used 2.1, 7 and 9.8 mW/cm^2. A first-order perchlorate degradation model was fitted to the data and a first-order-rate constant was calculated. Data for perchlorate that was strongly affected by the loss of sulfite were excluded from fitting, in order to use a data set that more closely followed first-order kinetics. A first-order degradation model was also fitted to sulfite loss during perchlorate degradation and the first-order rate constants were calculated. The results of the perchlorate kinetic experiments with and without air circulation are presented in Figures 3-15 and 3-16, respectively. The first-order rate constants for perchlorate degradation at different light intensities are presented in Figure 3-17.

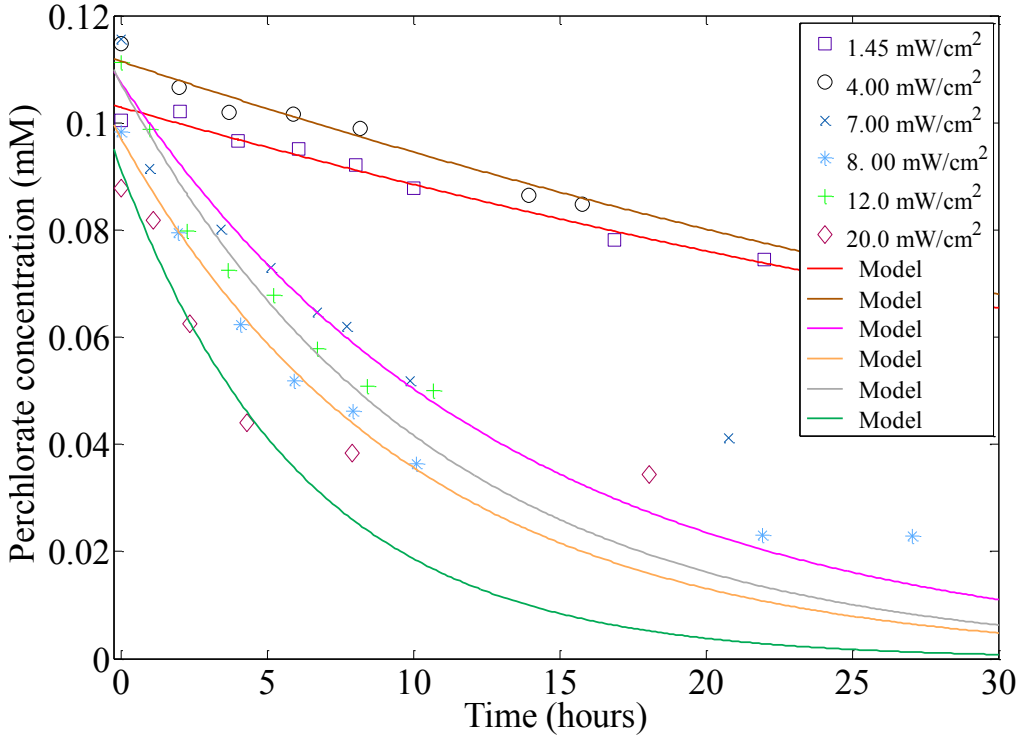

Figure 3-15: Perchlorate degradation by sulfite/UV-L at different light intensities (pH 11, 11 mM sulfite concentration, without air circulation).

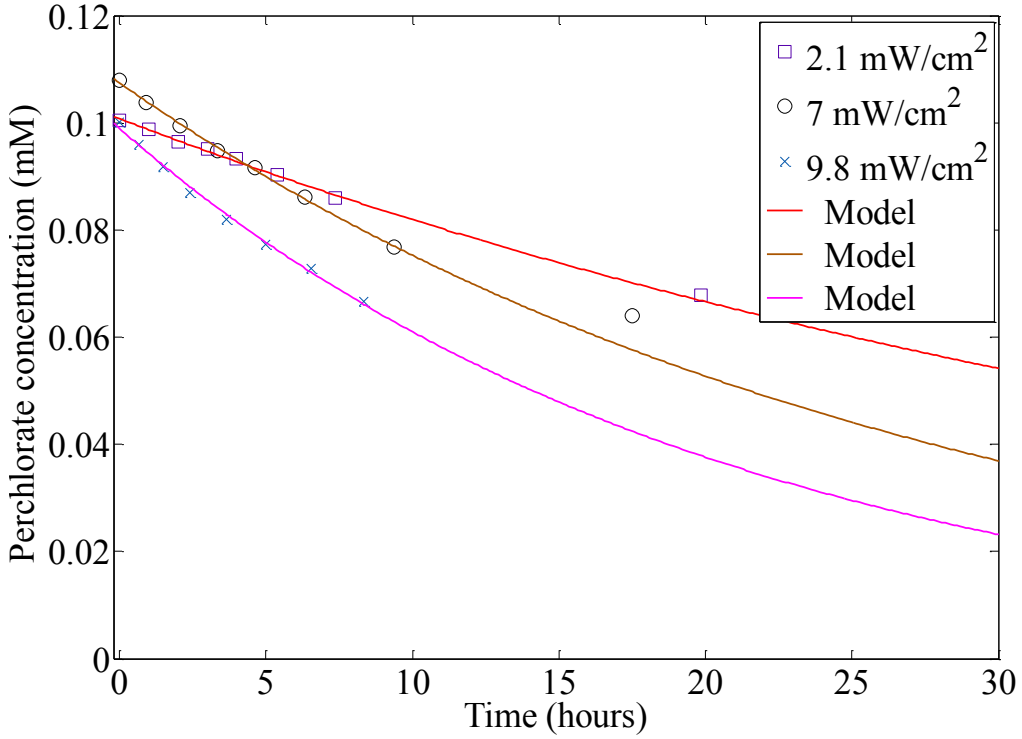

Figure 3-16: Perchlorate degradation by sulfite/UV-L at different light intensities (pH 11, 11 mM sulfite concentration, with air circulation, T≅ 30° C).

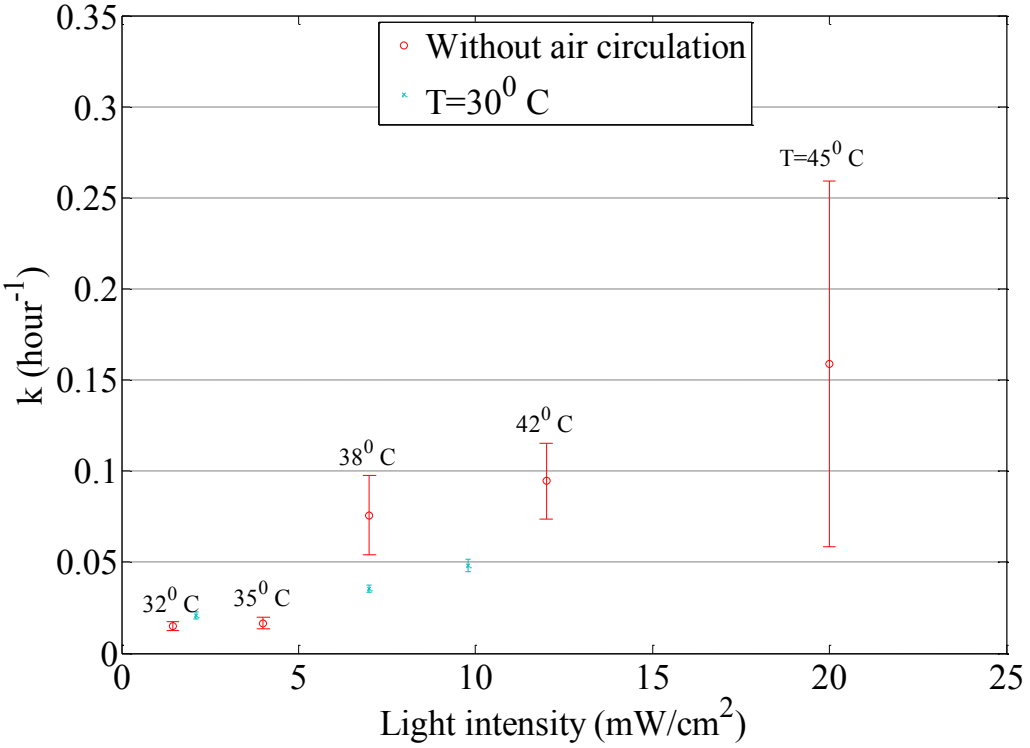

Figure 3-17: First-order rate constants for perchlorate degradation by sulfite/UV-L at different light intensities (pH 11, 11 mM sulfite concentration).

Figure 3-15 shows that even at higher light intensities, perchlorate removal is incomplete. This incomplete degradation of perchlorate and the deviation of the data from the first-order perchlorate degradation model at latter experiment times is caused by consumption of sulfite by photochemical reaction as shown in Figure 3-19 *(24, 25, 45)*. The actual degradation reaction is believed to be the result of reaction between radicals produced by photolysis of sulfite, so as the concentration of sulfite decreases, the rate of degradation of perchlorate decreases and deviates from the assumed first-order perchlorate degradation model.

Figures 3-15, 3-16, and 3-17 indicate faster rates of perchlorate removal at higher light intensities. This is due to the increase in the number of perchlorate-degrading radicals produced when the higher light intensity leads to increased light absorption by sulfite. This is in accordance with equation 3-2, which shows that an increase in influent light intensity (I_0), leads to an increase in the pseudo-first-order rate constant. However, for the experiments without air circulation, the effects of light intensity on perchlorate degradation are partially masked by the effects of varying temperature on perchlorate degradation. In these experiments, higher temperatures were observed at higher light intensities, because the higher light intensities were obtained by placing the reactor closer to the bulb. Therefore, the observed increase in the rate of perchlorate degradation with light intensity is due to a combination of the actual effect of higher light intensity causing an increase in the number of radicals produced and the effect of temperature, which would cause faster rates of perchlorate degradation.

Quantum yields for perchlorate degradation are presented in Figure 3-18.

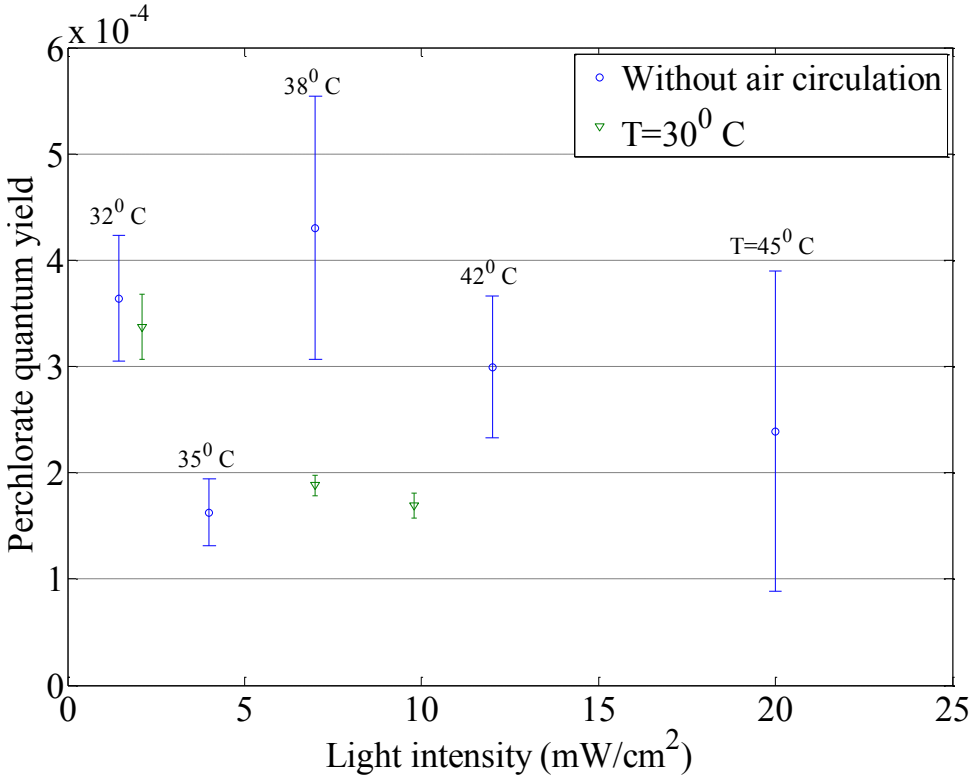

Figure 3-18: Quantum yield for perchlorate degradation by sulfite/UV-L at different light intensities (pH 11, 11 mM sulfite concentration).

Figure 3-18 indicates that perchlorate degradation efficiency decreases with increasing light intensity in experiments with air circulation, but there is substantial variability in experiments without air circulation. At higher light intensities, the concentration of scavengers could increase. As shown in equation 3-6, increase in the scavenger concentration leads to a decrease in the target quantum yield. Thus, with increasing light intensity, perchlorate degradation efficiency decreases. Greater temperatures point to greater perchlorate degradation efficiency as indicated by higher quantum yields. In summary, greater perchlorate degradation efficiency is achieved with a combination of lower light intensity and lower temperature.

Sulfite loss during the perchlorate degradation experiments with and without air circulation are presented in Figures 3-19 and 3-20. The first-order rate constants for sulfite loss at different light intensities are presented in Figure 3-21.

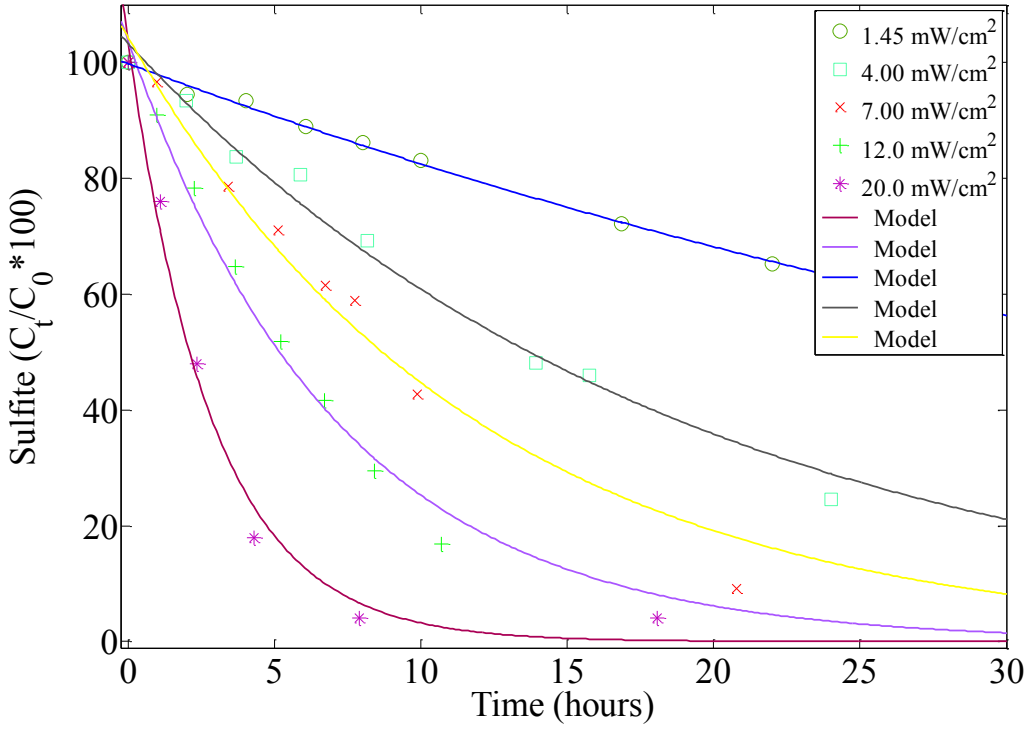

Figure 3-19: Sulfite loss during perchlorate degradation by sulfite/UV-L at different light intensities (pH 11, 11 mM sulfite concentration, without air circulation).

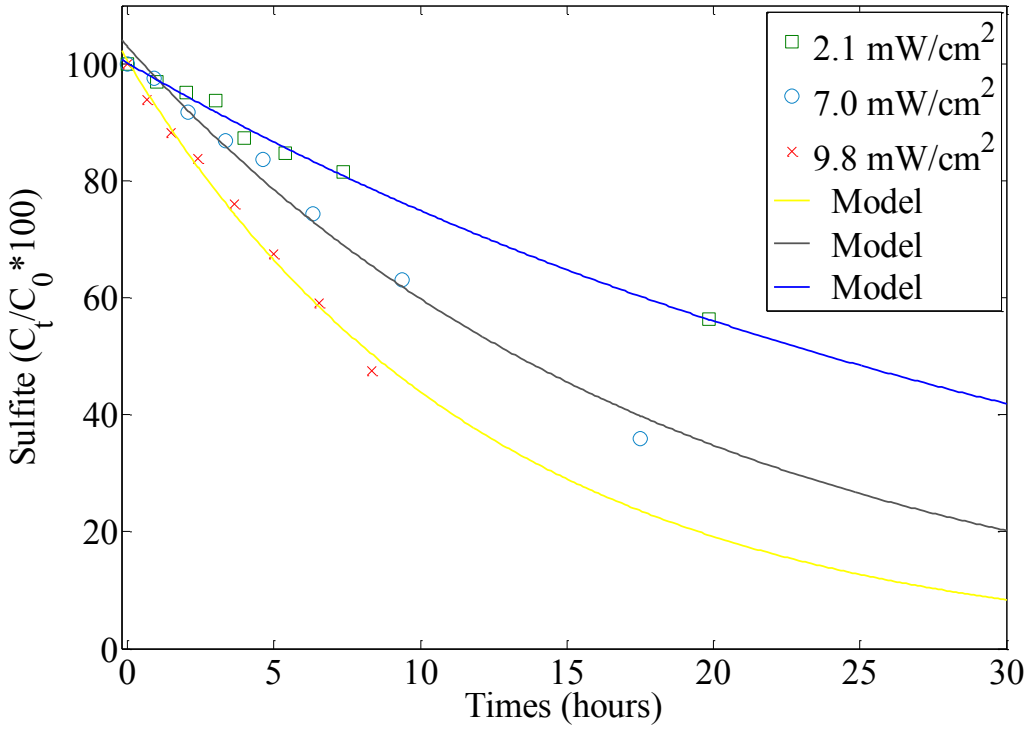

Figure 3-20: Sulfite loss during perchlorate degradation by sulfite/UV-L at different light intensities (pH 11, 11 mM sulfite concentration, with air circulation, T≅ 30° C).

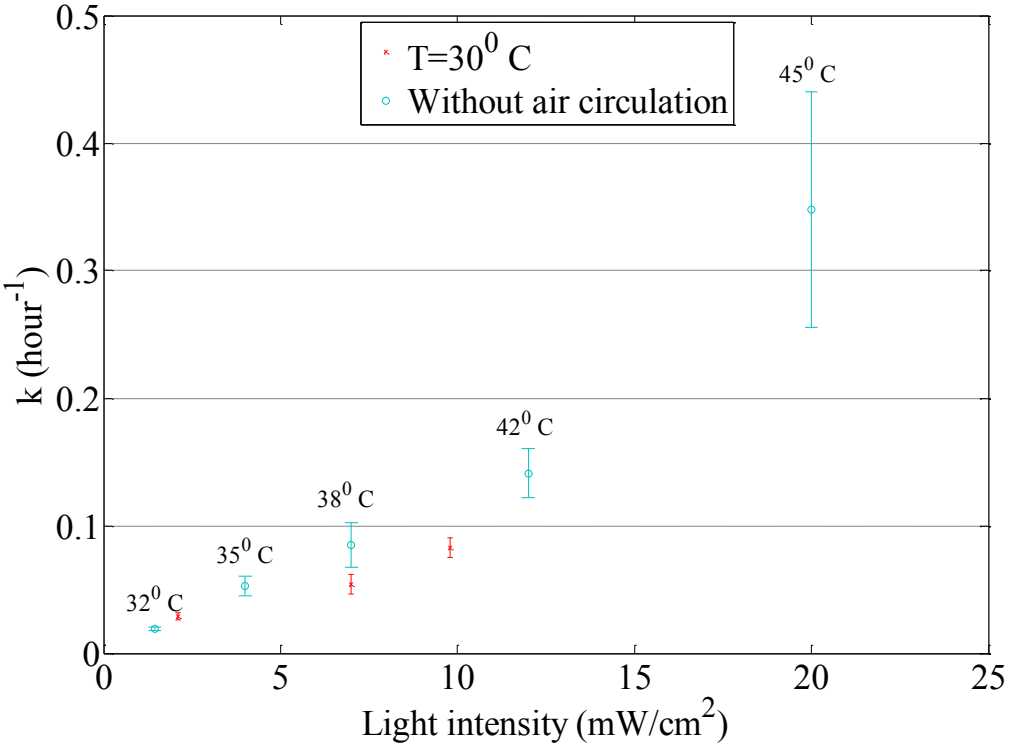

Figure 3-21: First-order rate constants for sulfite loss during sulfite/UV-L at different light intensities (pH 11, 11 mM sulfite concentration).

As expected, Figures 3-19, 3-20 and 3-21 indicate that higher light intensities result in faster loss of sulfite due to increased rates of photolysis of sulfite by UV-L. Figure 3-21 indicates that greater perchlorate degradation efficiency is achieved at a combination of lower light intensity and lower temperature.

Quantum yields for sulfite loss are presented in Figure 3-22.

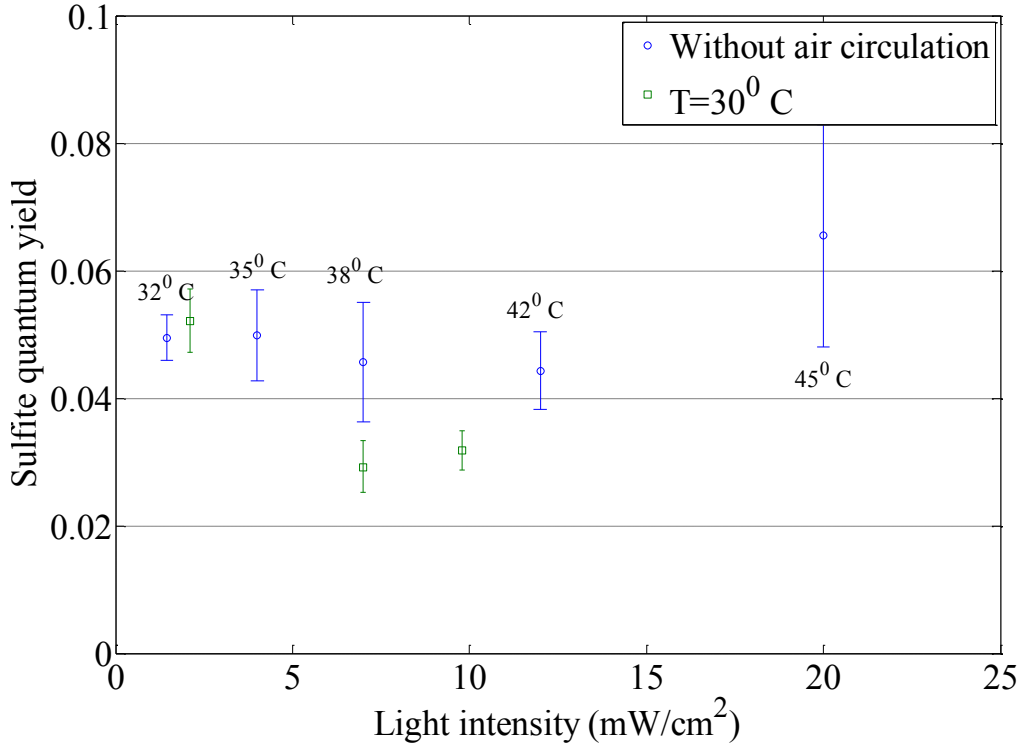

Figure 3-22: Quantum yield for sulfite loss during perchlorate degradation by sulfite/UV-L different light intensities (pH 11, 11 mM sulfite concentration).

Figure 3-22 shows that the quantum yield for sulfite loss does not vary with changing light intensity. Except for the experiment at 2.1 mW/cm^2 with air circulation (30^0 C), the quantum yield decreases with a decrease in temperature, indicating that the photolysis of sulfite by UV-L is more efficient at higher temperatures.

3.3.5 Effect of sulfite concentration on perchlorate degradation

Batch kinetic experiments were conducted to investigate the effects of sulfite concentration on perchlorate degradation. Perchlorate kinetic experiments were conducted with initial concentrations of 0.1 mM perchlorate at 7 mw/cm^2 light intensity.

One set of experiments with air circulation were conducted with sulfite concentrations of 1.26, 3.76, 11, 37.5 and 110.8 mM. A first-order perchlorate degradation model was fitted to the perchlorate data and a first-order rate constant was calculated. A first-order degradation model was fitted to sulfite loss during perchlorate degradation and the first-order rate constants calculated. The results of the perchlorate kinetic experiments are presented in Figure 3-23. Data on sulfite loss during the perchlorate degradation experiments are presented in Figure 3-24. The first-order rate constants for perchlorate degradation and sulfite loss at different sulfite concentration are presented in Figure 3-25.

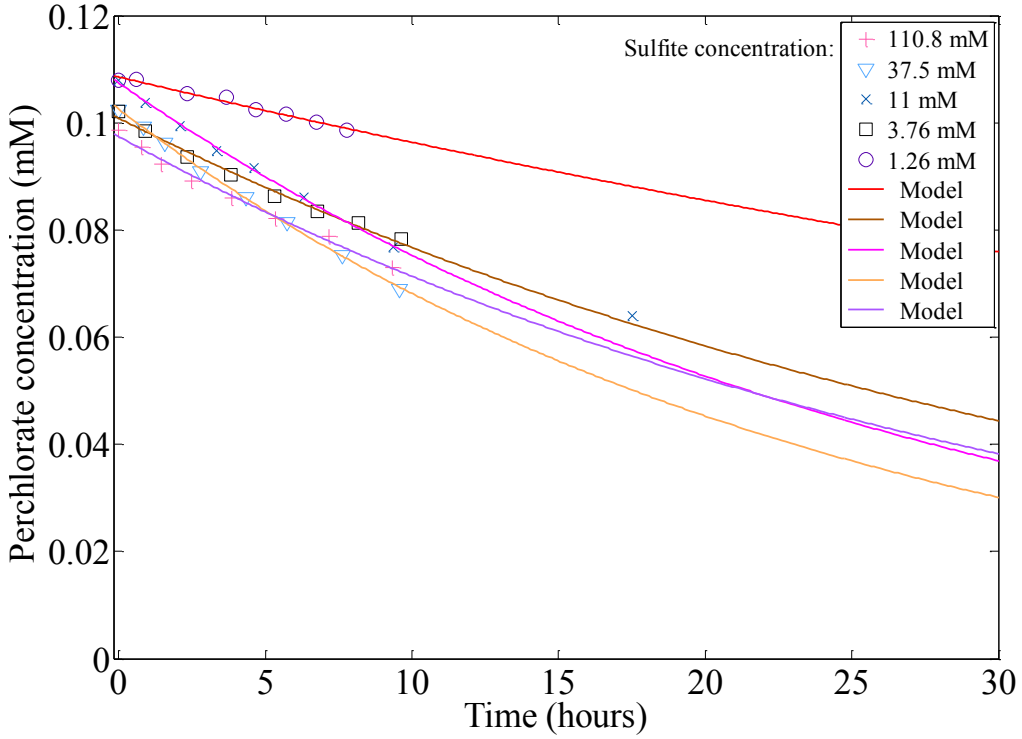

Figure 3-23: Perchlorate degradation by sulfite/UV-L at different sulfite concentrations (pH 11, 7 mW/cm^2, with air circulation, T≅ 30^o C).

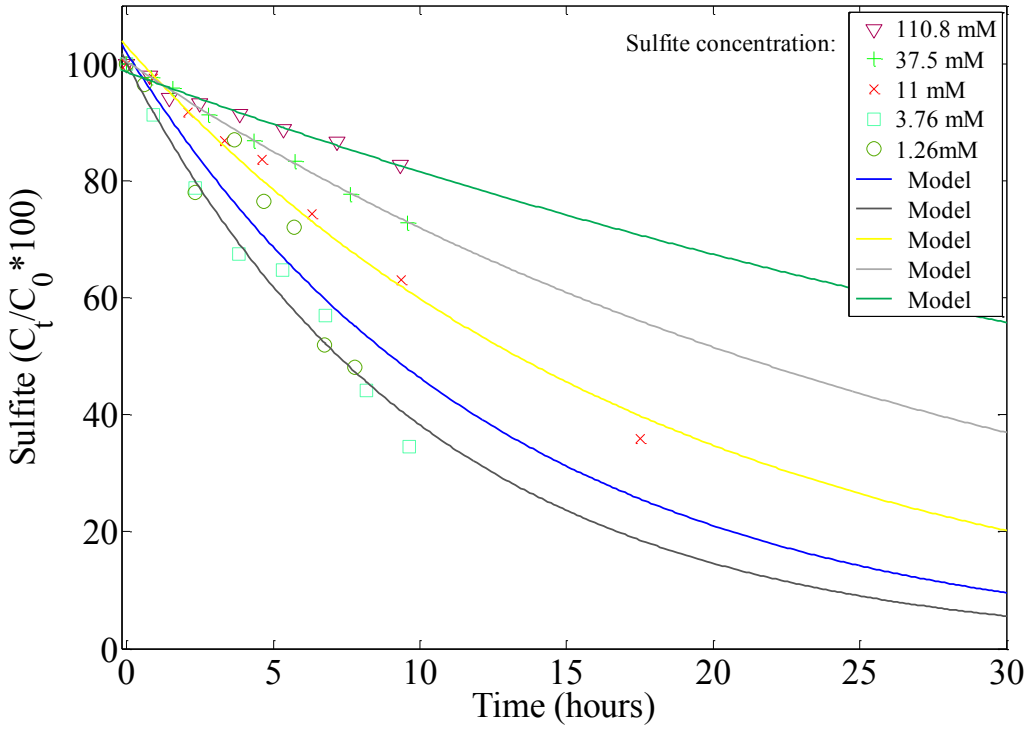

Figure 3-24: Sulfite loss during perchlorate degradation by sulfite/UV-L at different sulfite concentrations (pH 11, 7 mW/cm^2, with air circulation, T≅ 30^o C).

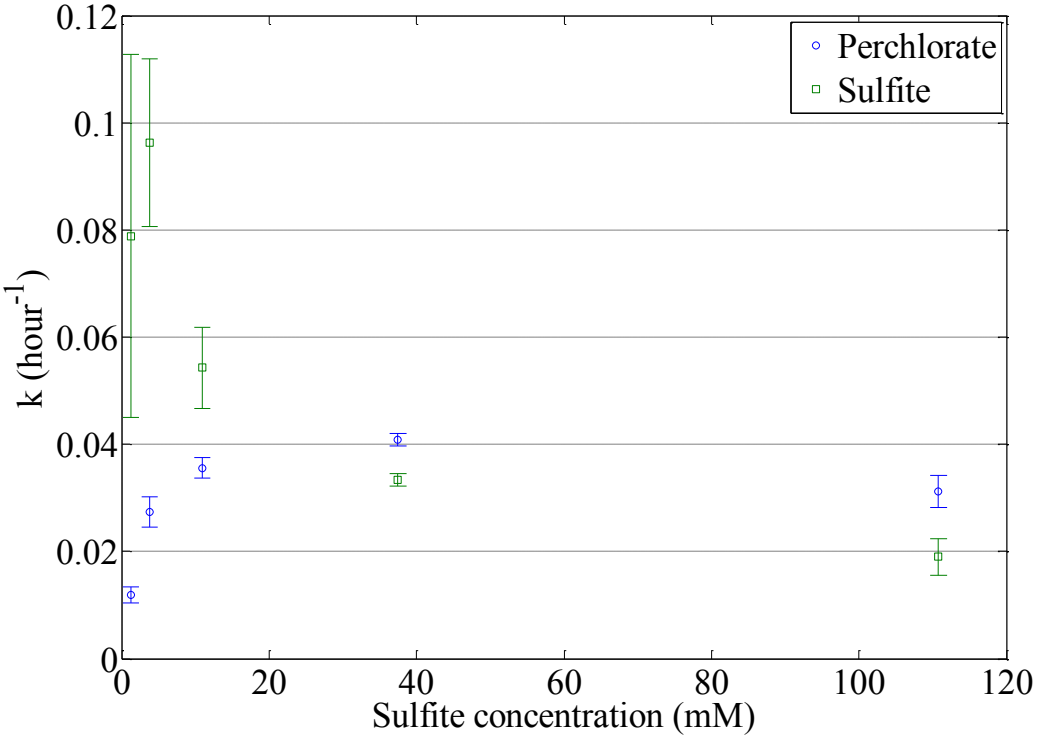

Figure 3-25: First-order rate constants of perchlorate degradation and sulfite loss at different sulfite concentrations (pH=11, 7 mW/cm^2, with air circulation, T≅ 30^o C).

From equation 3-2, the pseudo first-order rate constant is proportional to $(1-e^{-\varepsilon CsL})$. At low sulfite concentrations, little UV light is absorbed, resulting in almost all the light passing through the reactor ($e^{-\varepsilon CsL}\cong 1$), leading to little perchlorate degradation. At higher concentrations of sulfite ($e^{-\varepsilon CsL}\cong 0$), higher absorbance of UV light by the sulfite solution, leading to greater production of radicals, resulting in faster rates of degradation of perchlorate. As indicated by equations 3-3 and 3-4, at low sulfite concentrations, the perchlorate degradation rate is proportional to the sulfite concentration; at high sulfite concentrations, the degradation rate is independent of sulfite concentration.

At the highest sulfite concentration (110.8 mM), little to no light is available at the lower levels of the reactor. All the light is absorbed by the upper levels of the reactor, where radical concentration will be high, but perchlorate availability would be low because there is little mixing in the reactor. At the lower levels, negligible radical concentrations lead to little to no perchlorate removal. Therefore, the system would act like two reactors placed one over the other, with the bottom reactor receiving no light, leading to relative decrease in the overall perchlorate degradation. Table 3-3 presents absorbance and the percentage transmittance of light at 254 nm in the reactors at the different sulfite concentrations tested.

Table 3-3: Percent transmittance and absorbance of 254 nm wavelength at different sulfite concentrations at pH 11.

Sulfite concentration (mM)	Absorbance at pH 11 at 254 nm	Percent transmittance at pH 11 at 254 nm	$(1-e^{-\varepsilon Cs2L})/(1-e^{-\varepsilon Cs1L})$	k_2/k_1
1.26	0.022932	95	-	-
3.76	0.068432	85	3.0	2.2
11	0.2002	63	2.5	1.4
37.5	0.6825	21	2.1	1.1
110.8	2.01656	1	1.3	0.7

Table 3-3 shows that at concentrations of sulfite greater than 11 mM, light intensity through the reactor decreases substantially. This results in underutilization of

sulfite at the lower regions of the reactor, leading to decreased production and availability of radicals that can degrade perchlorate. As predicted by equation 3-2, the ratio of the pseudo first-order rate constants at different sulfite concentrations (k_2/k_1) is similar to the ratio of the respective light absorption $(1-e^{-\varepsilon Cs2L})/(1-e^{-\varepsilon Cs1L})$. Though the observed ratios (k_2/k_1) are lower than the expected ratios $[(1-e^{-\varepsilon Cs2L})/(1-e^{-\varepsilon Cs1L})]$, the trend of k_2/k_1 decreasing with increasing sulfite concentration is similar to that predicted by the model. The values may be lower than predicted by the model, because a greater share of the radicals at higher sulfite concentrations may be scavenged by competing reactions and unavailable for reacting with perchlorate.

Quantum yields for perchlorate degradation and sulfite loss at different sulfite concentrations are presented in Figures 3-26 and 3-27 respectively.

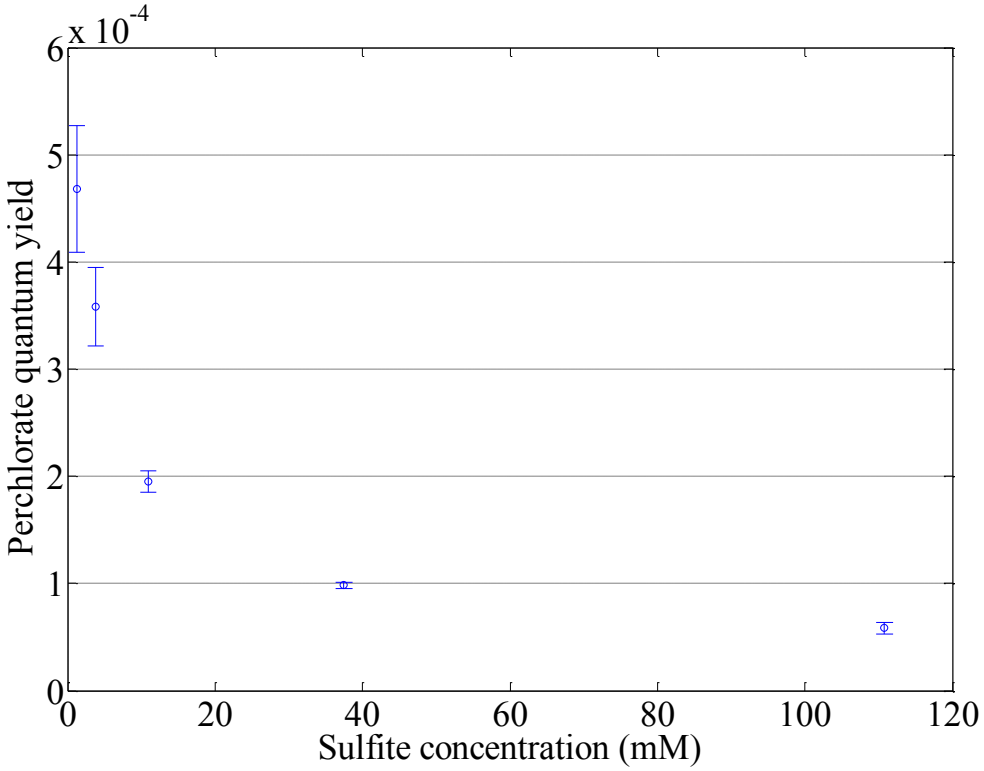

Figure 3-26: Quantum yield for perchlorate degradation by sulfite/UV-L at different sulfite concentrations (pH 11, 7 mW/cm^2, with air circulation, T≅ 30^o C).

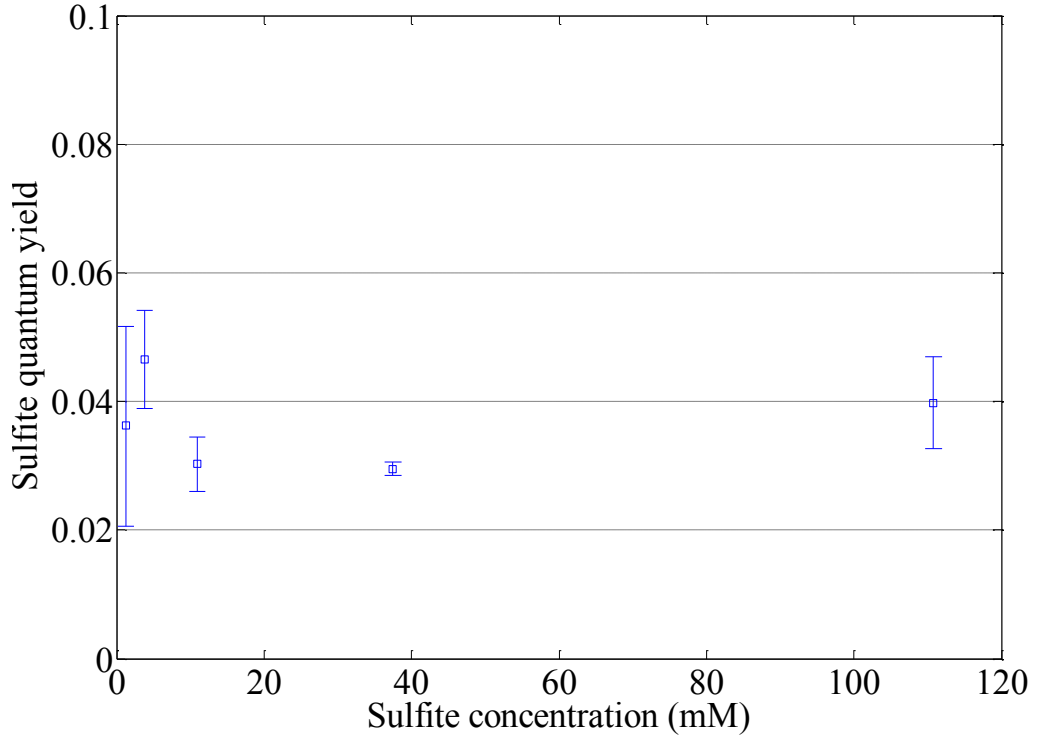

Figure 3-27: Quantum yield for sulfite loss during perchlorate degradation by sulfite/UV-L at different sulfite concentrations (pH 11, 7 mW/cm^2, with air circulation, T≅ 30^o C).

Figure 3-26 indicates rapidly decreasing efficiency of perchlorate degradation with increasing sulfite concentration. Table 3-3 and equation 3-1 show that with an increase in sulfite concentration ([A]), the light intensity across the reactor (I_0(1-exp(-ε'[A]L)) increases, leading to greater changes in the concentrations of radicals through the reactor. With poor mixing in the reactor, the radical production could occur in regions where perchlorate has been depleted, resulting in poor utilization of the radicals. Such underutilization of sulfite at different regions within the reactor at higher sulfite concentrations leads to decreasing perchlorate degradation efficiency with increasing sulfite concentration. Figure 3-27 indicates that there is no variation of sulfite quantum

yield with variation in sulfite concentration, which is consistent with what has been reported in the literature *(45)*.

3.3.6 Perchlorate degradation product analysis

Identification and analysis of products of the perchlorate degradation was conducted for the batch kinetic experiment conducted at pH 11, 0.1 mM perchlorate, 3.76 mM sulfite and 7 mW/cm^2 light intensity. The compounds chlorate (ClO_3^-) and chloride (Cl^-) were identified and quantified. Chlorite (ClO_2^-) was not detected in solution. The perchlorate, chlorate and chloride concentrations are presented in Figure 3-28. The experimental results are presented in Appendix B.

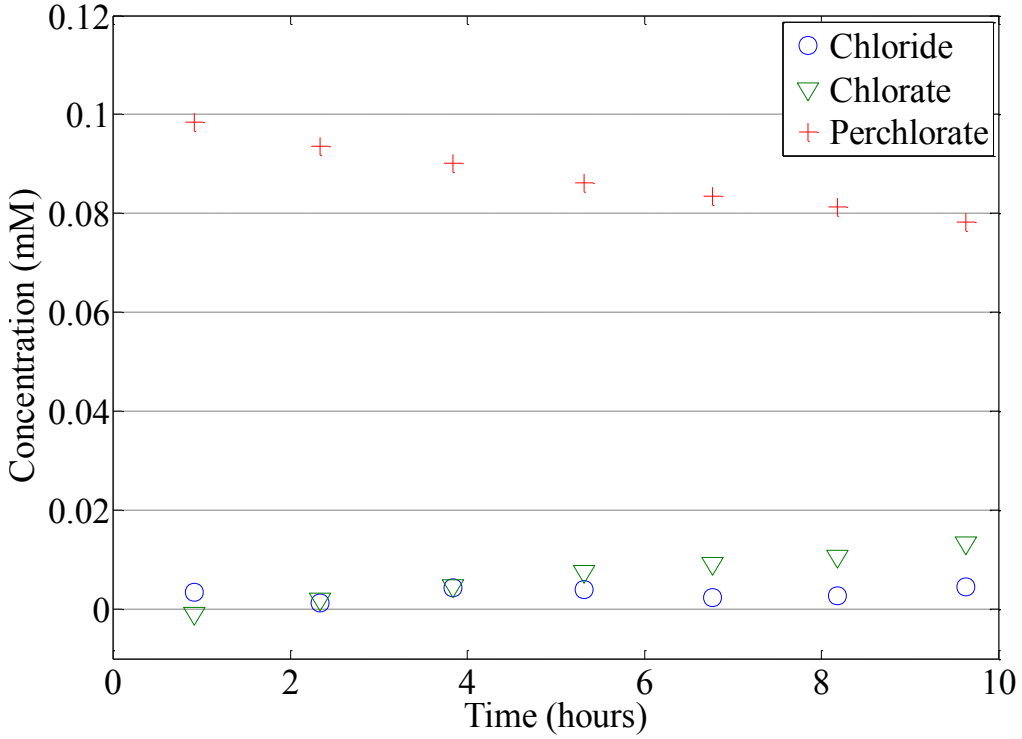

Figure 3-28: Identification of products of perchlorate degradation by UV-L sulfite (pH 11, 0.1 mM perchlorate, 3.76 mM sulfite and 7 mW/cm^2).

Figure 3-28 indicates increasing chlorate and chloride concentrations with decreasing perchlorate concentration. Chloride recovery, calculated by totaling the concentrations of perchlorate, chlorate and chloride in solution at each sampling time is presented in Table 3-4.

Table 3-4: Chloride mass balance.

Irradiation time in hours	Perchlorate concentration in mM	Chlorate concentration in mM	Chloride concentration in mM	Chloride recovery (mM)
0.0	0.102	0.000	0.000	0.102
0.9	0.098	0.000	0.003	0.101
2.3	0.094	0.002	0.001	0.097
3.8	0.090	0.005	0.004	0.099
5.3	0.086	0.007	0.004	0.098
6.8	0.083	0.009	0.002	0.095
8.2	0.081	0.011	0.003	0.095
9.6	0.078	0.013	0.005	0.096

From Table 3-4, satisfactory chloride recovery is observed among perchlorate, chlorate and chloride. This lends credence to the hypothesis that perchlorate is reduced to chlorate by sulfite radical anions through an oxygen abstraction mechanism, and chlorate is further reduced to chloride by the reducing radicals in solution or by sulfite itself *(58)*.

3.3.7 Effect of catalysts on perchlorate degradation

Batch screening experiments were conducted to test the effects of catalysts (Fe^{3+}, Fe^{2+}, Cu, Rb, Mo, Ni, V, Os and W) on perchlorate degradation by sulfite/UV-L. The experiments indicated little or no removal of perchlorate. The presence of catalysts thus does not aid the degradation of perchlorate by sulfite/UV-L. The experimental results are presented in Appendix B.

3.4 Summary

The results of the sulfite/UV-L experiments on perchlorate degradation suggest that perchlorate degradation rate and efficiency improve with an increase in pH. Increased light intensity increases the rate of perchlorate degradation, but decreases the efficiency of perchlorate degradation. The effects of the increase in sulfite concentration on perchlorate degradation rate depend on the UV- light distribution and availability within the reactor. Increase in temperature is beneficial to perchlorate degradation rate and efficiency. Perchlorate is reduced to chlorate and finally to chloride.

4 NITRATE REDUCTION BY THE SULFITE/UV-L ARP

4.1 Introduction

Nitrate is one of the most widespread contaminants of ground water in the US. Sources of nitrate contamination include its use widely as a fertilizer, as well as animal wastes, human wastes, and explosives *(65)*. Nitrate adversely affects human health by causing methemoglobinemia (Blue Baby Syndrome) in infants *(65)* as well as inhibiting iodine uptake by the thyroid gland, leading to thyroid dysfunction. Long term effects to human health due to nitrates include diuresis, which causes increased starchy deposits and hemorrhaging of the spleen *(65)*. For these reasons, a maximum contaminant level has been set at 10 mg/l nitrate-nitrogen in accordance with the Safe Drinking Water Act *(65)*. Significant damage to the environment can result from nitrate through stimulation of algal blooms, which can lead to oxygen deficiency *(65)*.

Ion exchange, reverse osmosis, electrodialysis, permeable reactive barriers, and biodenitrification are some of the methods presently used for removing nitrate from water *(65)*.

Active metals, ammonia, borohydride, formate, hydrazine, hydroxylamine, hydrogen and ferrous iron are some of the chemical reducing agents that have been used to chemically reduce nitrate in the presence of catalysts, or high temperatures and pressures. Electrochemical and photochemical techniques are some of the nitrate reduction mechanisms that employ other energy sources *(41)*.

The results of the preliminary experiments presented in Chapter 2 provide data that show the sulfite/UV-L ARP to be a successful treatment method for nitrate. The sulfite/UV-L ARP involves irradiating target contaminant solutions that contain sulfite with ultraviolet light of 253.7 nm wavelength. The data from the preliminary experiments indicate that the rate of nitrate degradation by sulfite/UV-L ARP increases with an increase in pH.

In this study, the effects of sulfite concentration, light intensity, and pH on the ability of the sulfite/UV-L ARP to degrade nitrate were studied and the products of nitrate degradation by the sulfite/UV-L ARP were investigated.

The degradation of nitrate to simple compounds by the sulfite/UV-L ARP indicates that it holds promise of being developed into a commercially viable alternative to the present nitrate treatment technologies.

4.2 Materials and Methods

4.2.1 Materials

Chemical reagents and samples were prepared in an anaerobic chamber (Coy Laboratory Products Inc.) containing an atmosphere of 95% N_2 and 5% H_2. Deaerated deionized water (ddw) was used to make all solutions and was prepared by deoxygenating ultra-pure water (18 MΩ cm) with 99.99% nitrogen for 2 h and then with the atmosphere in anaerobic chamber for 12 h. Aqueous solutions and chemicals sensitive to redox reaction were deoxygenated in an airlock (Coy Laboratory Products Inc.) and kept in the anaerobic chamber. Target compounds and reductant for this

research were ACS (American Chemical Society) grade or higher and were used as received.

4.2.2 Analytical procedures

Nitrate and nitrite anions were measured to monitor and identify the products of nitrate degradation. All of the analytes (NO_3^-, NO_2^-) were analyzed by ion chromatography on a Dionex 500 ion chromatograph equipped with a 4-mm Dionex AS–16 analytical and guard column. Analysis of nitrate and nitrite was conducted with 10 mM sodium hydroxide eluent at 1.25 mL/min flow rate with a 250 μL sample. The absorption spectra of sulfite solutions were measured by a Thermo Spectronic Helios Gamma UV-Vis Spectrophotometer using Starna Cells, which are rectangular UV quartz cells with a stopper and a 10-mm light path length.

4.2.3 Reactor systems

Ultraviolet light from low pressure bulbs (UV-L) was provided by a Phillips TUV PL-L36W/4P lamp positioned above the reactors, with both lamp and reactors contained within an enclosure. The UV-L source produced UV light with a wavelength of 253.7 nm. Kinetic experiments on degradation of nitrate were conducted using cylindrical quartz reactors obtained from Starna cells (Atascadero, CA, USA). The reactors have an interior diameter of 47 mm and depth of 10 mm. A UV512C Digital UV C Meter obtained from General Tools (New York City, NY, USA) was used to measure the light intensity at the point where light entered the reactor. Air circulation by a fan

inside the UV enclosure was employed to reduce temperature increase for some of the UV irradiation experiments.

4.3 Results and Discussion

4.3.1 Effect of pH on nitrate degradation

Batch kinetic experiments were conducted to investigate the effects of pH (3, 5, 7, and 9) on nitrate degradation. Two sets of experiments, one without air circulation and the other with air circulation, were conducted. Nitrate kinetic experiments were conducted with initial concentration of 0.16 mM nitrate. Experiments with air circulation were conducted with an initial concentration of 2.8 mM sulfite and at a light intensity measured at the top of the reactor of 2.8 mW/cm^2, while the experiments without air circulation were conducted with initial concentration of 8.5 mM sulfite and at a light intensity of 4 mW/cm^2. Among the experiments without air circulation, the experiments at pH 7 and pH 9 involve total irradiation times around 20 minutes and thus little to no temperature increase occurred. For the experiments without air circulation and at pH 3 and pH 5, the total irradiation time was around 10 and 4 hours, respectively, and thus temperature increased to around 35^0C. All nitrate degradation kinetic experiments were conducted with a buffer of 5 mM PO_4^{3-}.

Nitrate degradation is probably a second-order reaction, where the reaction rate is proportional to the concentrations of nitrate and an unknown radical that degrades nitrate. For simplicity, a first-order nitrate degradation model was fitted to the data and a first-order rate constant that minimizes the sum of squared residuals was calculated.

A simple two-step, first-order nitrate degradation model is assumed.

$$NO_3^- \xrightarrow{k_1} NO_2^-$$

$$NO_3^- \xrightarrow{k_2} products$$

The relationship between a pseudo-first-order rate constant for degradation of a target compound that reacts with a free radical (equation 3-1) was developed in Chapter 3 and can be applied to nitrate degradation.

$$k_2 = \frac{k_{NO_3^-}}{k_{NO_3^-} C_{NO_3^-} + k_S[S]} \times \frac{\phi_{SO_3^{2-}} I_0^* \left(1 - e^{-\varepsilon' C_{SO_3^{2-}} L}\right)}{L} \quad (4\text{-}1)$$

where I_0^* = Light flux entering reactor (einstein/m^2-s), ε'= Molar absorptivity or molar extinction coefficient (M^{-1} m^{-1}), L = Total thickness of water in reactor in direction of light path (m), C_{SO32-}= concentration of UV light absorbing compound (sulfite) that forms radicals upon irradiation, C_{NO3-}= concentration of target compound (nitrate), [S]= concentration of radical scavenger, k=rate constant of relevant reaction, ϕ_{SO32-}= sulfite quantum yield.

Solving the mass balance for nitrite in a batch system with two-step, first-order degradation kinetics gives:

$$C_{NO_2^-} = \frac{k_1 C_{NO_3^- initial}}{(k_2 - k_1)} \times (e^{-k_1 t} - e^{-k_2 t}) \quad (4\text{-}2)$$

The effectiveness of UV-L in stimulating contaminant degradation was measured for each experiment by calculating the quantum yields for removal of nitrate (ϕ_n) using

Equation 4-3. These quantum yields are the ratios of molecules of nitrate degraded per photon of light absorbed by sulfite. The quantum yields are used as a measure of the efficiency of the sulfite/UV-L system under consideration, in degrading nitrate in the reactor system. The molar absorptivity values of sulfite presented in Chapter 2 were used for these calculations. When the experiment's pH is not the same as the pH where the absorptivities were measured, the nearest measurement was used (e.g. pH 7.5 molar absorptivity was used for pH 7 kinetic experiment).

$$\phi = \frac{r_0 N_A lhc}{I_0 \left(1 - 10^{-\varepsilon C_s l}\right) \lambda_{254}} \tag{4-3}$$

where I_0 = irradiance entering reactor (J/m^2-s), ε = molar absorptivity of sulfite (m^2/mole), C_s=concentration of sulfite (mole/m^3), l = depth of reactor (m), λ_{254} = wavelength of UV light (m), r_0 = initial rate of removal of compound = (k_{model}*initial concentration of nitrate (mole/m^3-s), N_A = Avogadro's number (1/mole), h = Planck's constant (J-s), c = speed of light (m/s). The relevant rate constants are presented in Appendix C.

The results of the nitrate kinetic experiments with and without air circulation at different pH are presented in Figures 4-1 and 4-2, respectively. For the purpose of quantification, a first-order perchlorate degradation model was fitted to the data using the Levenberg-Marquardt algorithm in MATLAB and a first-order rate constant that minimizes the sum of squared residuals was calculated was calculated. The values for the first-order rate constant for nitrate degradation at different pH are presented in Figure

4-3. The solid lines in all of these figures represent the first-order degradation model that was fitted to the kinetic data.

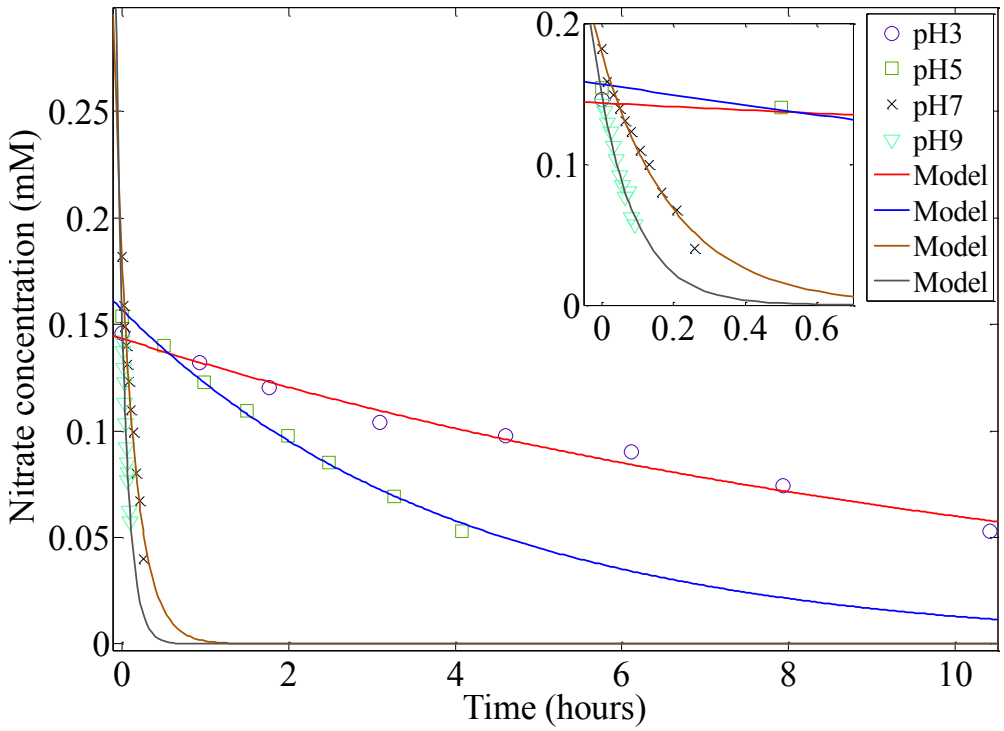

Figure 4-1: Nitrate degradation by sulfite/UV-L at various pH (4 mW/cm^2, 8.5 mM sulfite concentration, without air circulation).

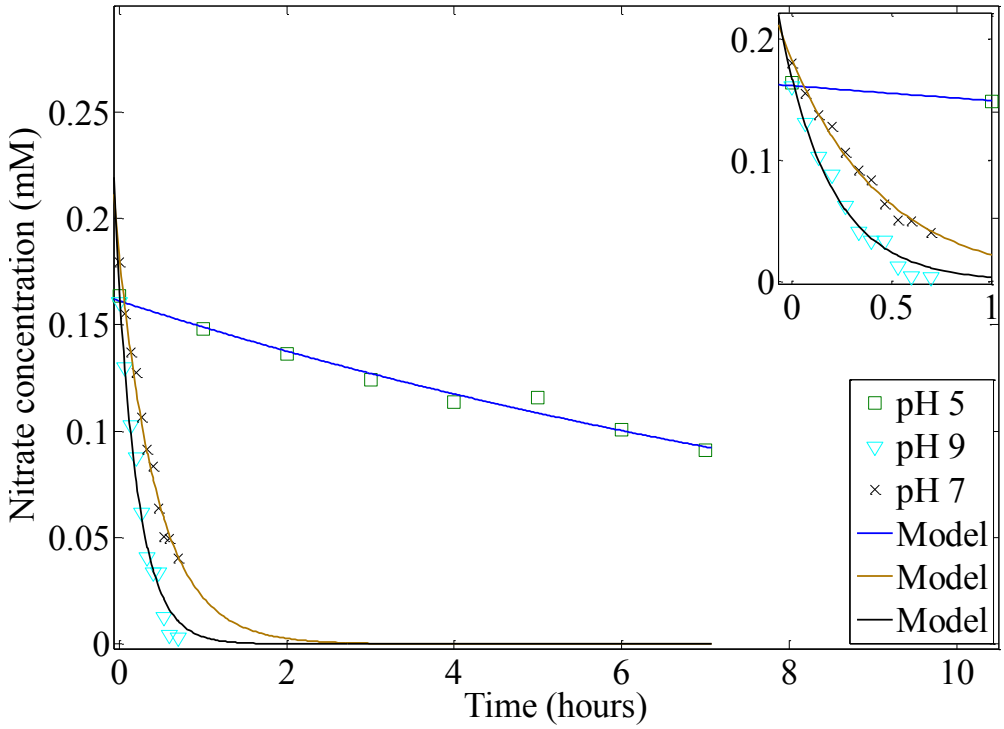

Figure 4-2: Nitrate degradation by sulfite/UV-L at various pH (2.8 mW/cm^2, 2.8 mM sulfite concentration, with air circulation, T≅ 27^o C).

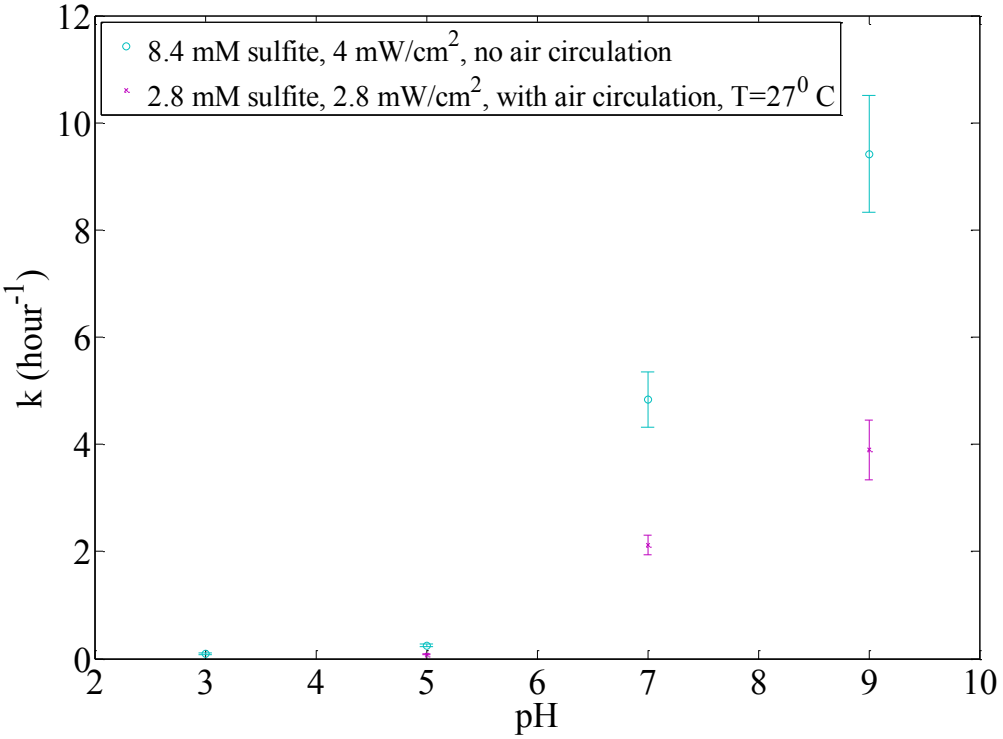

Figure 4-3: First-order rate constants for nitrate degradation by sulfite/UV-L at various pH.

Figures 4-1, 4-2, and 4-3 show that for experiments with and without air circulation, there is little nitrate removal at acidic pH and the rate of nitrate degradation by sulfite/UV-L increases with increasing pH. Figure 4-3 indicates that higher initial rates of nitrate formation occur with increasing pH, in accordance with the nitrate degradation profiles at different pH (Figures 4-1, 4-2). Equation 4-1 shows that an increase in molar absorptivity or concentration of sulfite (SO_3^{-2}) leads to an increase in the pseudo-first-order rate constant due to increased absorbance of light. As shown in Figures 3-1, 3-2, 3-3 and 3-7, the other sulfite species (H_2SO_3 and HSO_3^-) which are predominant at acidic pH, absorb light and can produce radicals/reductants. Irradiation of

HSO_3^- is known to produce $SO_2^{\bullet-}$ and $OH^\bullet$ *(66)*. These radicals could lead to nitrate degradation. Figures 4-1 and 4-2 show that the degradation of nitrate by the products of irradiation of H_2SO_3 and HSO_3^- is slower than the degradation of nitrate by the products of irradiation of SO_3^{2-}. H_2SO_3 and HSO_3^- can compete with SO_3^{2-} for UV light, possibly slowing down the reduction of nitrate. The concentration of the sulfite anion (SO_3^{2-}) increases with pH (Figure 3-1), so more light will be absorbed and more radicals will be produced at higher pH. This would lead to an increased rate constant at higher pH, which is in accordance with observed results. These results indicate that higher SO_3^{2-} and OH^- concentrations are conducive to the mechanism that leads to nitrate degradation.

The quantum yields for removal of nitrate (ϕ_n) are shown in Figure 4-4.

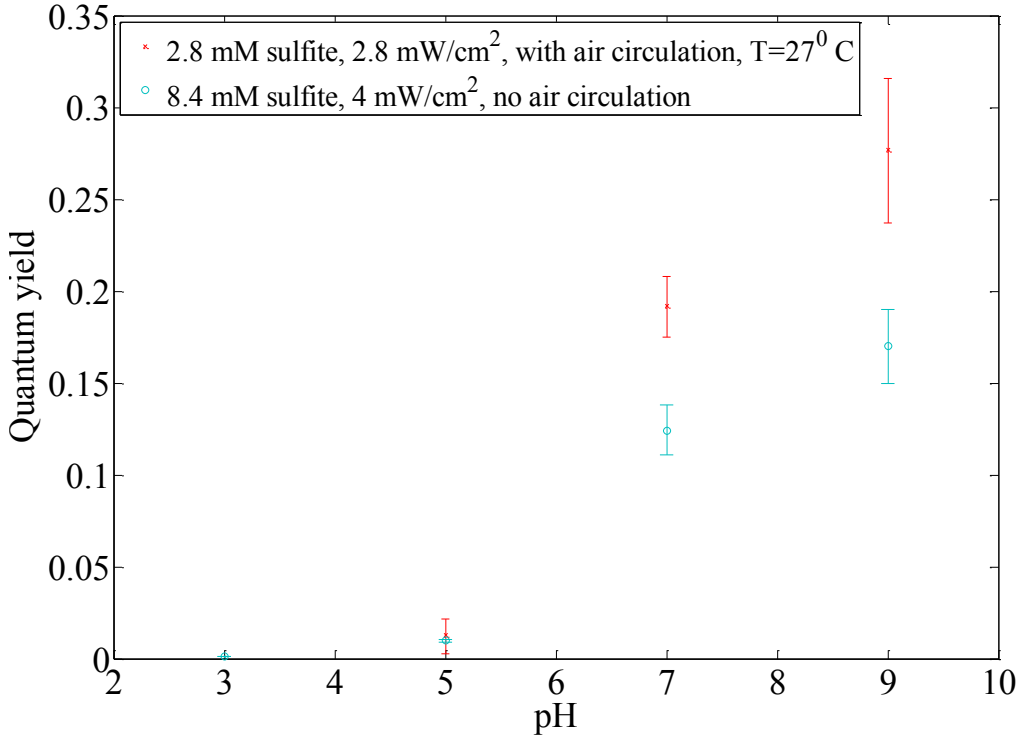

Figure 4-4: Quantum yields for nitrate degradation by Sulfite/UV-L at various pH.

Figure 4-4 shows that for experiments with and without air circulation, the efficiency of nitrate degradation by sulfite/UV-L increases with increasing pH.

The nitrite concentrations during the nitrate kinetic experiments with air circulation at different pH are presented in Figure 4-5. The solid lines represent a first-order degradation model (equation 4-2) that was fitted to the kinetic data.

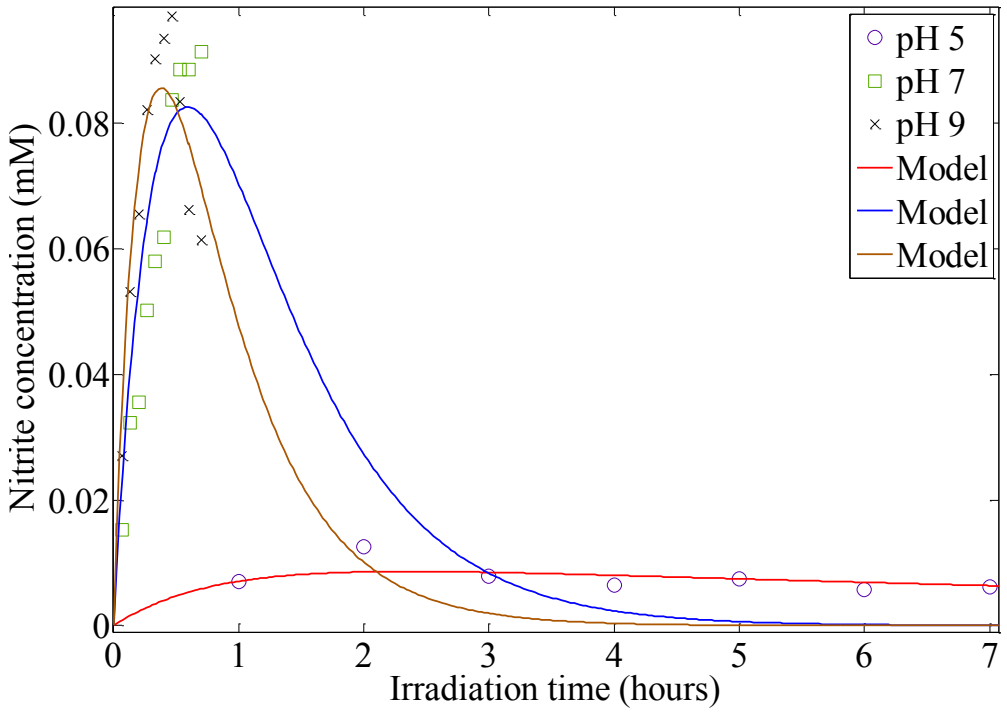

Figure 4-5: Nitrite concentration during nitrate degradation by sulfite/UV-L at various pH (2.8 mM sulfite, 2.8 mW/cm^2, with air circulation, T=27^0 C).

Nitrite concentration profiles shown in Figure 4-5 follow a trend of increasing nitrite concentration, followed by decreasing nitrite concentration. Since nitrate degradation rate increases with increasing pH, the point of change from net increase in nitrite concentration to net decrease in nitrite concentration occurs earlier with increasing pH.

Fitting equation 4-2 to the nitrite data, values for the first-order rate constant for nitrite degradation were obtained at different pH and they are presented in Figure 4-7.

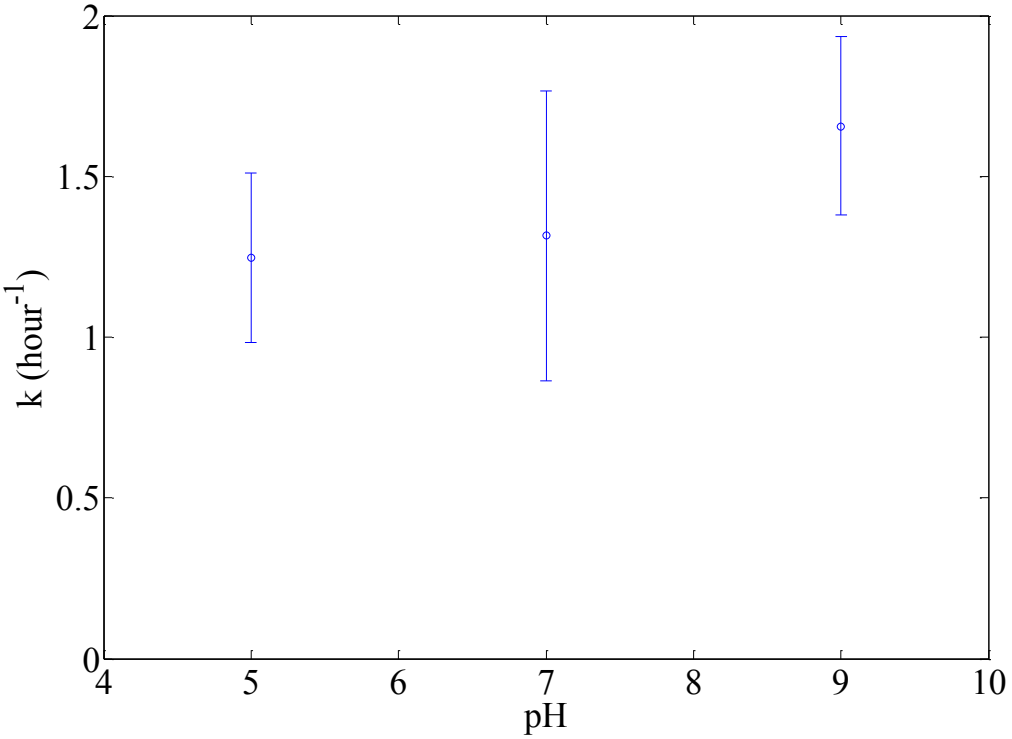

Figure 4-6: First-order rate constant for nitrite degradation during nitrate degradation by sulfite/UV-L at various pH (2.8 mM sulfite, 2.8 mW/cm^2, with air circulation, T=27^0 C).

Figure 4-6 indicates that the first-order nitrite degradation rate constant is similar at different pH.

For nitrate kinetic experiments with air circulation, the concentration of sulfite was monitored by UV-spectrophotometry and is presented in Figure 4-5.

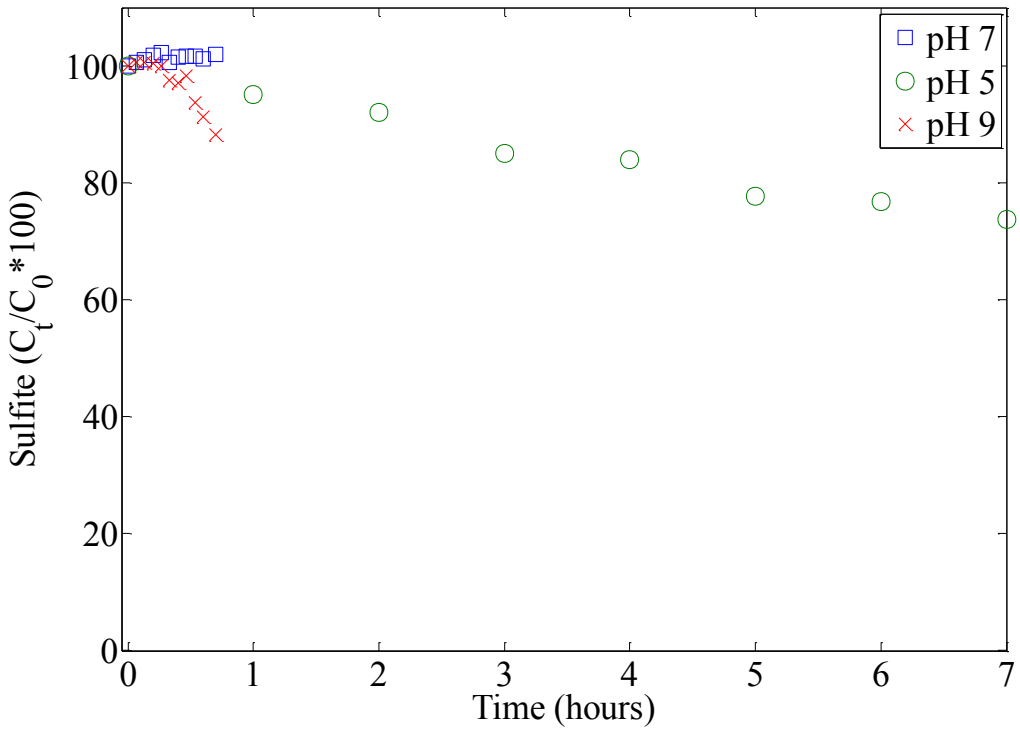

Figure 4-7: Sulfite loss during nitrate degradation by sulfite/UV-L at various pH (2.8 mW/cm^2, 2.8 mM sulfite concentration, with air circulation, T≅ 27^o C).

Figure 4-7 indicates that for the range of light intensities, irradiation time periods and sulfite concentrations used in these experiments; there is little change in the sulfite concentration during the course of the reaction. A greater rate removal of sulfite occurs at pH 9, with neutral pH having the lowest rate of nitrate loss. Sulfite loss at pH 5 is higher than that at neutral pH. This could because H_2SO_3 and HSO_3^- are consumed at a faster rate by irradiation, leading to greater loss of total sulfite.

4.3.2 Effect of light intensity on nitrate degradation

Batch kinetic experiments were conducted to investigate the effects of light intensity on nitrate degradation. These experiments were conducted with initial concentrations of 0.16 mM nitrate and 2.8 mM sulfite, with air circulation and at light intensity of 2.8 mW/cm^2.

The results of the nitrate kinetic experiments with air circulation are presented in Figure 4-8. The solid lines represent a first-order nitrate degradation model that was fitted to the data. The first-order-rate constants that minimize the sum of squared residuals were calculated and are presented in Figure 4-9.

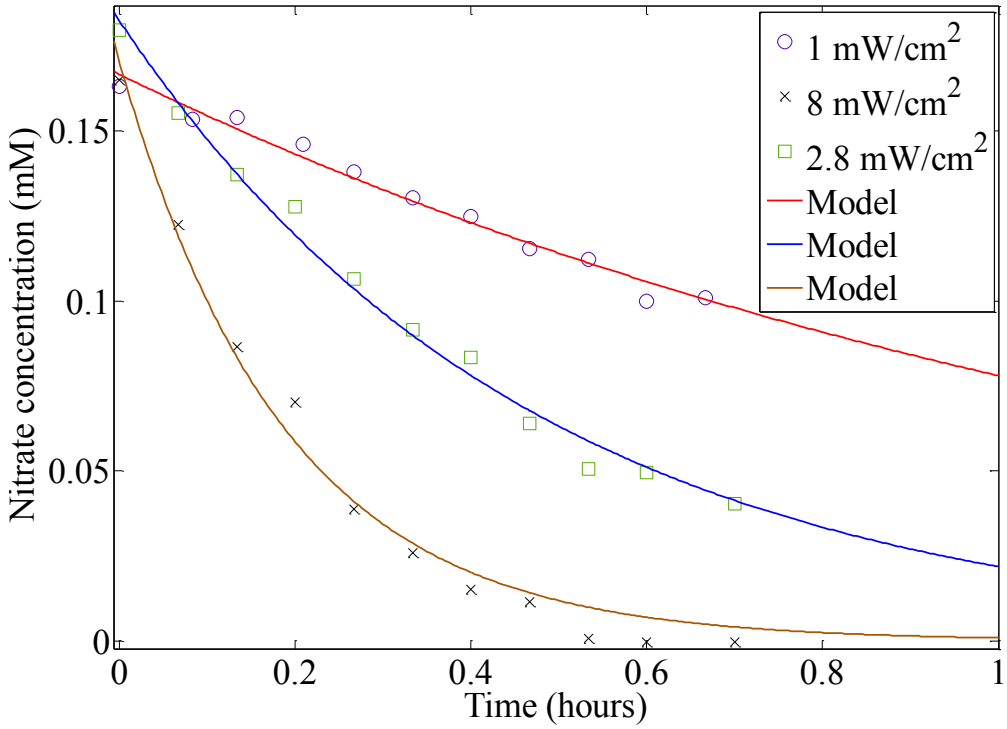

Figure 4-8: Nitrate degradation by sulfite/UV-L at different light intensities (pH 7, 2.8 mM sulfite concentration, with air circulation, T≅27^0 C).

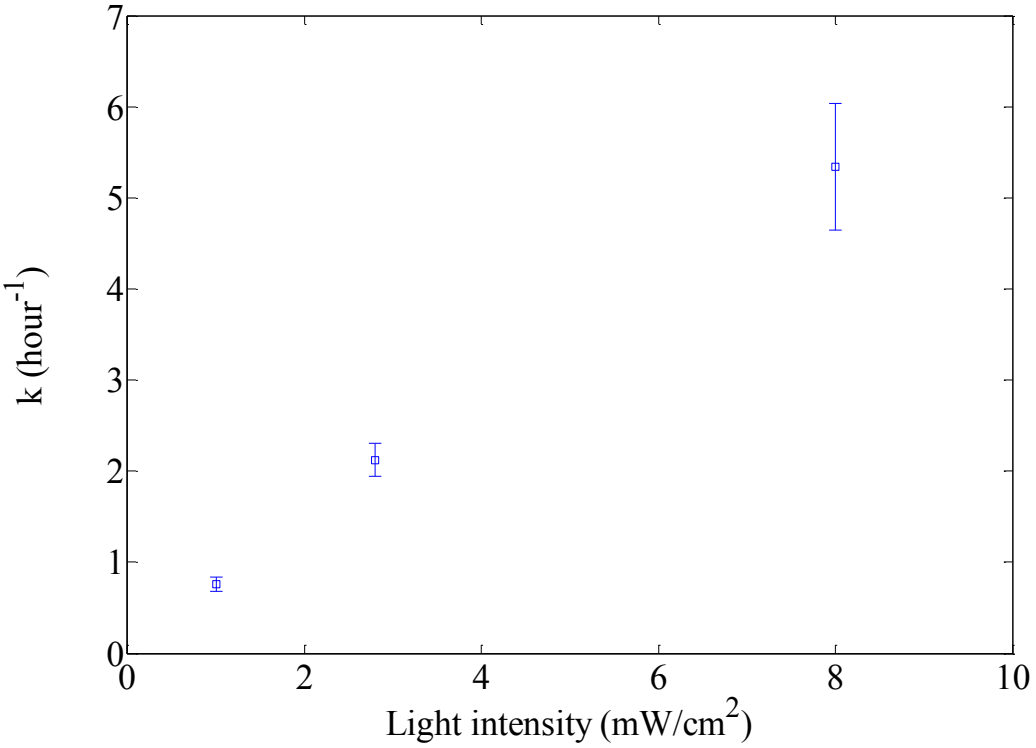

Figure 4-9: First-order rate constants for nitrate degradation by sulfite/UV-L at different light intensities (pH 7, 2.8 mM sulfite concentration, with air circulation, T≅27^0 C).

Figures 4-8, and 4-9 indicate faster rates of nitrate removal at higher light intensities. This is due to the increase in the number of nitrate-degrading radicals produced when the higher light intensity leads to increased light absorption by sulfite. This is in accordance with equation 4-1, which shows that an increase in influent light intensity I_0, leads to a linear increase in the pseudo-first-order rate constant.

The ratios of influent light intensities are compared with the ratios of nitrate pseudo-first-order rate constants in Table 4-1.These data indicate that the change in light intensity corresponds well with the observed change in the pseudo-first-order rate constant.

Table 4-1: Comparison of change in light intensity with nitrate pseudo-first-order rate constants.

Influent light intensity (mW/cm^2)	$I_{0\,2}/I_{0\,1}$	k_2/k_1
1	-	-
2.8	2.8	2.8
8	2.9	2.5

Quantum yields for nitrate degradation are presented in Figure 4-10.

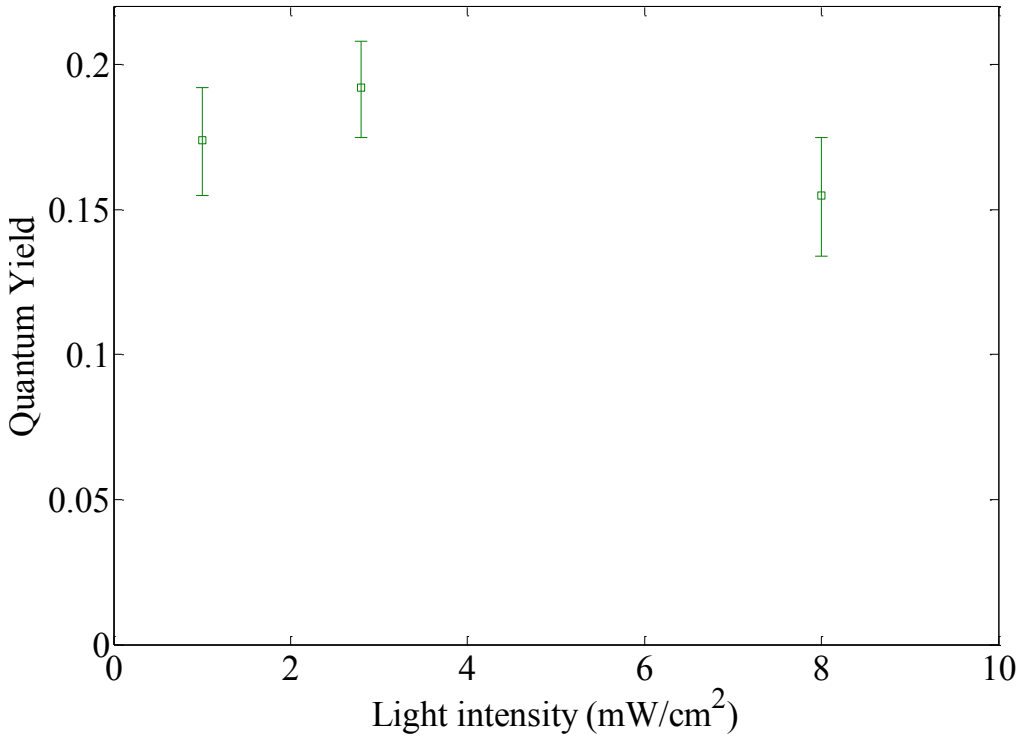

Figure 4-10: Quantum yields for nitrate degradation by sulfite/UV-L at different light intensities (pH 7, 2.8 mM sulfite concentration, with air circulation, T≅27^0 C).

From Figure 4-10, for the range of light intensities tested, the effect of light intensity on nitrate quantum yield is not clear and appears to have no effect. Similar to the perchlorate quantum yield, it is believed that the nitrate quantum yield will decrease (relatively slowly since rate of degradation of nitrate is relatively fast), with increasing light intensity, especially at higher light intensities. Decrease in quantum yield is believed to be due to increase in the scavenging reactions with increase in light intensity/number of radicals.

The nitrite concentrations during the nitrate kinetic experiments with air circulation at different light intensities are presented in Figure 4-11. The solid lines represent the first-order degradation model (equation 4-2) fitted to the kinetic data.

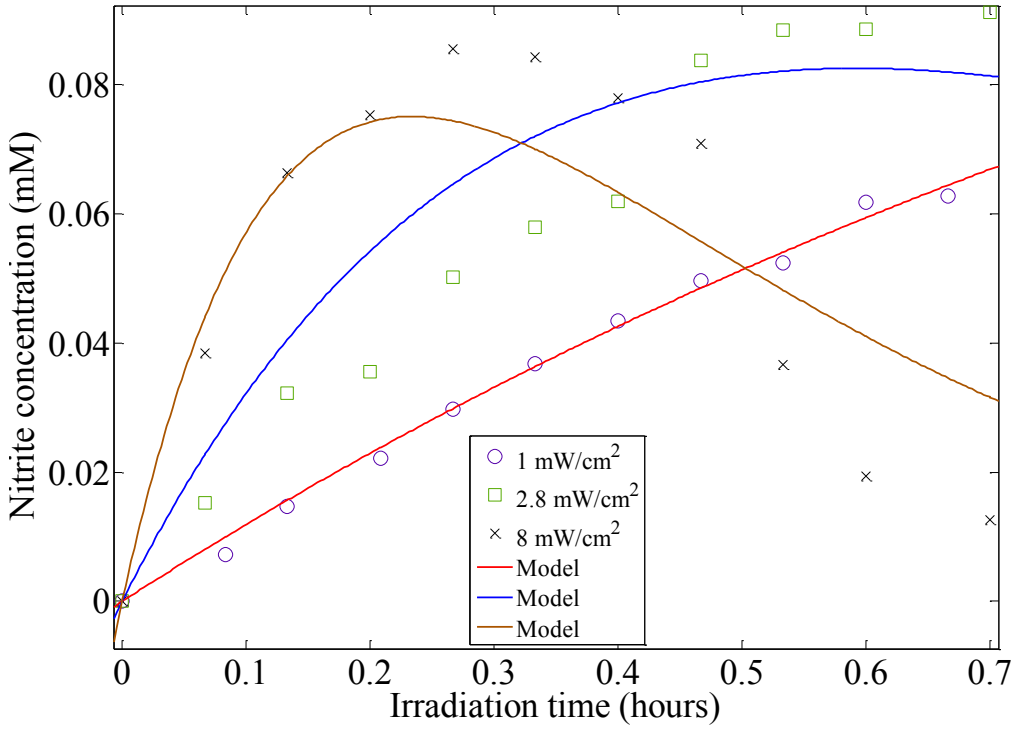

Figure 4-11: Nitrite concentration during nitrate degradation by sulfite/UV-L at different light intensities (pH 7, 2.8 mM sulfite concentration, with air circulation, T≅27^0 C).

Figure 4-11 indicates that higher initial rates of nitrite formation occur with increasing light intensity, which is in accordance with the nitrate degradation profiles at different light intensities (Figure 4-8). Nitrite concentration profiles follow a trend of increasing nitrite concentration, followed by decreasing nitrite concentration. Since nitrate degradation rate increases with increasing light intensity, the point of change from net increase in nitrite concentration to net decrease in nitrite concentration occurs earlier with increasing light intensity.

The first-order rate constants for nitrite degradation at different light intensities were obtained by fitting Equation 4-2 to nitrite concentrations and the results are presented in Figure 4-12.

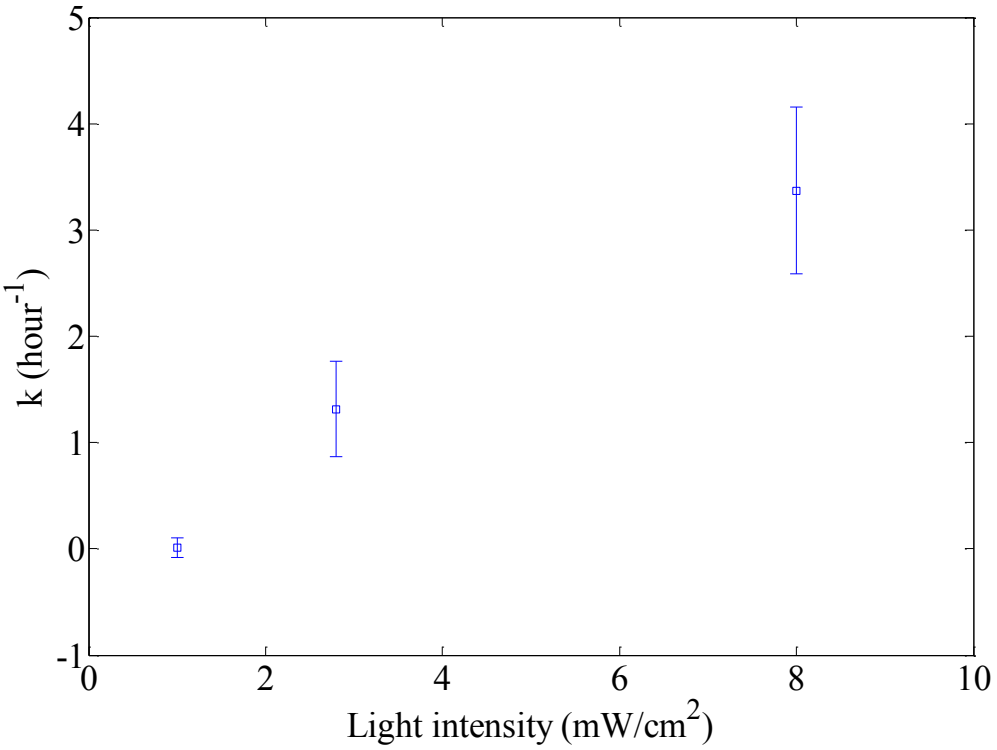

Figure 4-12: First-order rate constant for nitrite degradation during nitrate degradation by sulfite/UV-L at different light intensities (pH 7, 2.8 mM sulfite concentration, with air circulation, T≅27^0 C).

Figure 4-12 indicates that the first-order nitrite degradation rate constant increases with increasing light intensity, similar to the nitrate degradation rate constant.

Applying equation 3-1 to nitrite degradation, the ratios of influent light intensities are compared with the ratios of nitrite pseudo-first-order rate constants in Table 4-1.These data indicate that at the higher light intensities, the change in light

intensity corresponds well with the observed change in the pseudo-first-order rate constant. The low nitrite pseudo-first-order rate constant at 1 mW/cm^2, which is believed to be due to low rate of nitrate removal, exaggerates the ratio of increase of the pseudo-first-order rate constant at lower light intensities.

Table 4-2: Comparison of change in light intensity with nitrite pseudo-first-order rate constants.

Influent light intensity (mW/cm^2)	$I_{0\,2}/I_{0\,1}$	k_2/k_1
1	-	-
2.8	2.8	118
8	2.9	2.6

Sulfite loss during the nitrate degradation experiments with air circulation are presented in Figure 4-13.

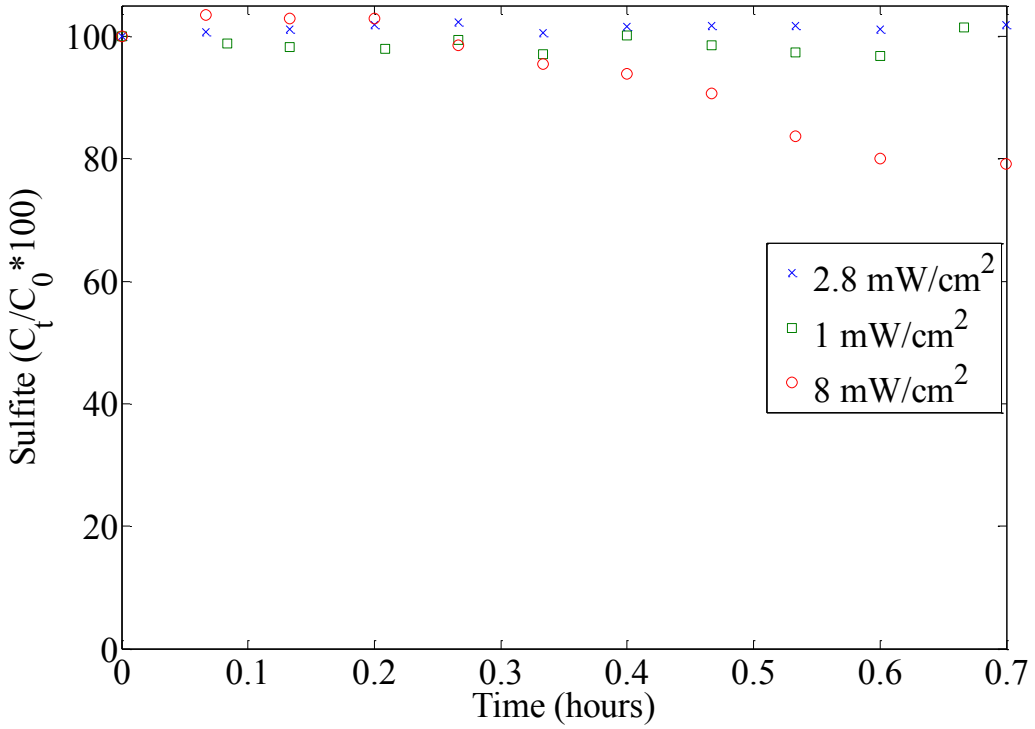

Figure 4-13: Sulfite loss during nitrate degradation by sulfite/UV-L at different light intensities (pH 7, 2.8 mM sulfite concentration, with air circulation, T≅27^0 C).

Figure 4-13 indicates that for the irradiation times and light intensities under consideration, there is little loss of sulfite during nitrate degradation, although there is some loss of sulfite at the highest light intensity.

4.3.3 Effect of sulfite concentration on nitrate degradation

Batch kinetic experiments were conducted to investigate the effects of sulfite concentration on nitrate degradation. These kinetic experiments were conducted with initial nitrate concentrations of 0.16 mM and with 2.8 mw/cm^2 light intensity. One set of experiments were conducted with air circulation and with sulfite concentrations of 0.94

mM, 2.8 mM and 8.4 mM. A first-order nitrate degradation model was fitted to the nitrate data and first-order rate constants that minimize the sum of squared residuals were calculated. The results of the nitrate kinetic experiments are presented in Figure 4-14. The solid lines represent the first-order nitrate degradation model that was fitted to the data. The first-order rate constants for nitrate degradation at different sulfite concentration are presented in Figure 4-15.

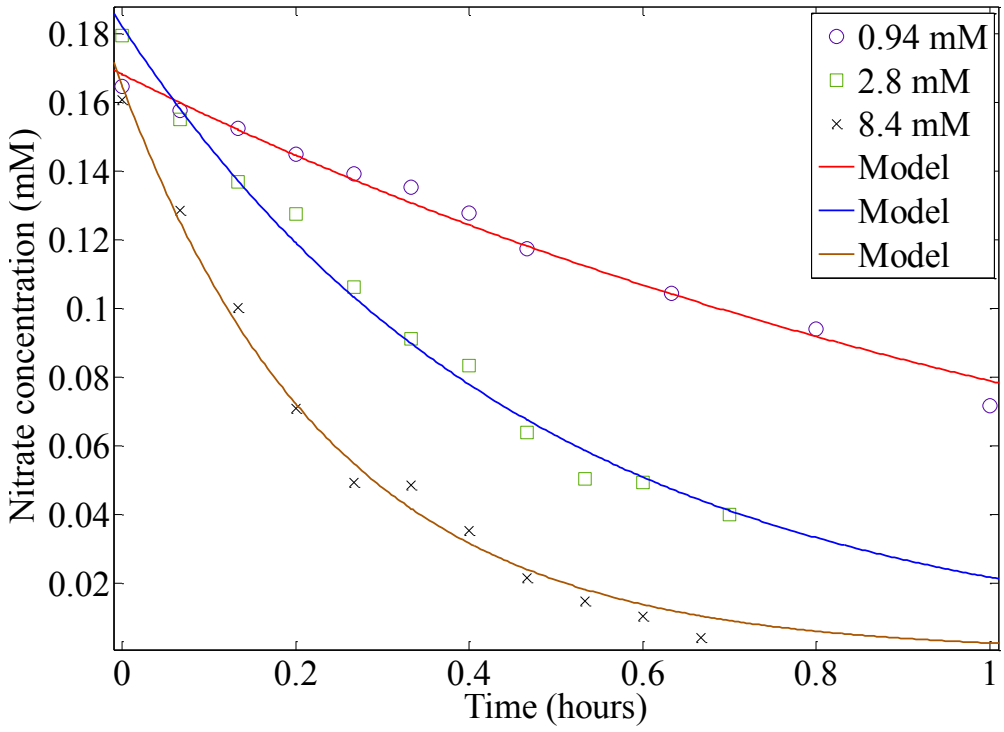

Figure 4-14: Nitrate degradation by sulfite/UV-L at different sulfite concentrations (pH 7, 2.8 mW/cm^2, with air circulation, T≅ 27^o C).

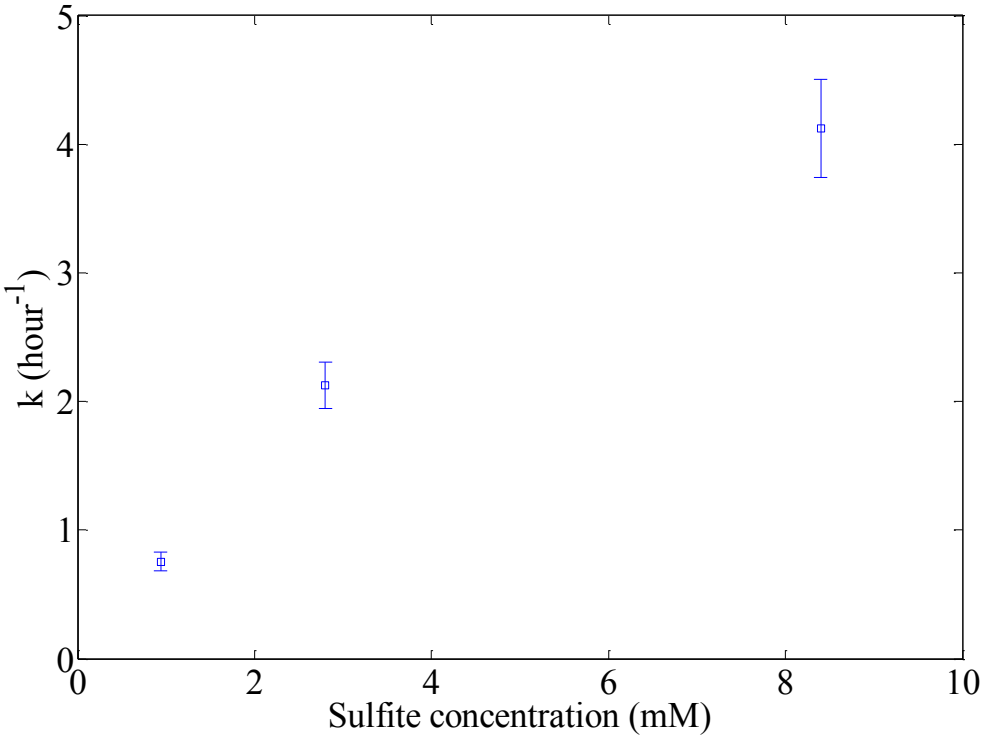

Figure 4-15: First-order rate constants for nitrate degradation by sulfite/UV-L at different sulfite concentrations (pH 7, 2.8 mW/cm^2, with air circulation, T≅ 27^o C).

Figures 4-14 and 4-15 indicate higher rates of nitrate degradation at higher sulfite concentrations. Equation 4-1 shows how the concentration of sulfite affects the pseudo-first-order rate constant for degradation of nitrate.

At low sulfite concentrations, the absorbance is low and little UV light is absorbed ($e^{-\varepsilon CsL}\cong 1$). This leads to slower nitrate degradation due to lower rates of radical formation. At higher concentrations of sulfite, the absorbance of light is high and almost all of the UV light is absorbed ($e^{-\varepsilon CsL}\cong 0$). A further increase in sulfite concentration will have no effect, because it will not increase the amount of light absorbed. Table 4-3

presents absorbance and the percentage transmittance of light at 254 nm in the reactors at the different sulfite concentrations tested.

Table 4-3: Percent transmittance and absorbance of 254 nm wavelength at different sulfite concentrations at pH 7.

Sulfite concentration (mM)	Absorbance at pH 7 at 254 nm	Percent transmittance at pH 7 at 254 nm	$(1-e^{-\varepsilon Cs2L})$ $/(1-e^{-\varepsilon Cs1L})$	k_2/k_1
1	0.015	97	-	-
2.8	0.043	91	2.7	2.8
8.4	0.128	75	2.7	1.9

As indicated by equation 3-3, at low sulfite concentrations, the target degradation rate is linearly proportional to the sulfite concentration. Table 4-3 shows that, as predicted by equation 4-1 and 3-4, the ratio of the pseudo-first-order rate constants at different sulfite concentrations (k_2/k_1) is similar to the ratio of the respective light absorption [$(1-e^{-\varepsilon Cs2L})$ $/(1-e^{-\varepsilon Cs1L})$]. The observed ratio ($k_2/k_1$) is lower than the expected ratio [$(1-e^{-\varepsilon Cs2L})$ $/(1-e^{-\varepsilon Cs1L})$] at higher sulfite concentration, as a greater share of the radicals at higher sulfite concentrations will be scavenged by the relatively faster competing reactions rather than reacting with nitrate.

Quantum yields for nitrate degradation are presented in Figure 4-16.

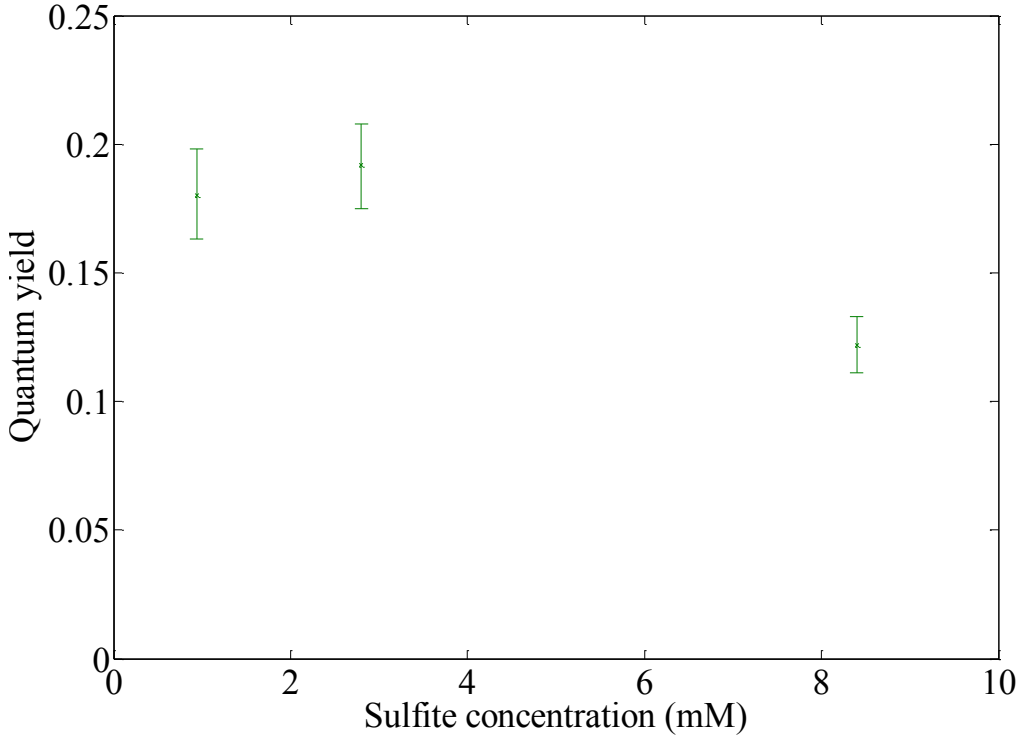

Figure 4-16: Quantum yields for nitrate degradation by sulfite/UV-L at different sulfite concentrations (pH 7, 2.8 mW/cm^2, with air circulation, T≅ 27^o C).

Since the observed ratio (k_2/k_1) is lower than the expected ratio [$(1-e^{-\varepsilon Cs2L})$ /$(1-e^{-\varepsilon Cs1L})$] at higher sulfite concentration, the quantum yield for nitrate degradation decreases with increasing sulfite concentration, as indicated by Figure 4-16. Another reason for the decreasing nitrate quantum yield is underutilization of sulfite at different regions within the reactor at higher sulfite concentrations. This is caused by slow mixing that leads to non-uniformity in concentrations, which is not described by the model shown in Equation 4-1.

The nitrite concentrations during the nitrate kinetic experiments with air circulation at different sulfite concentrations are presented in Figure 4-17. The solid lines represent the first-order degradation model (equation 4-2) fitted to the kinetic data.

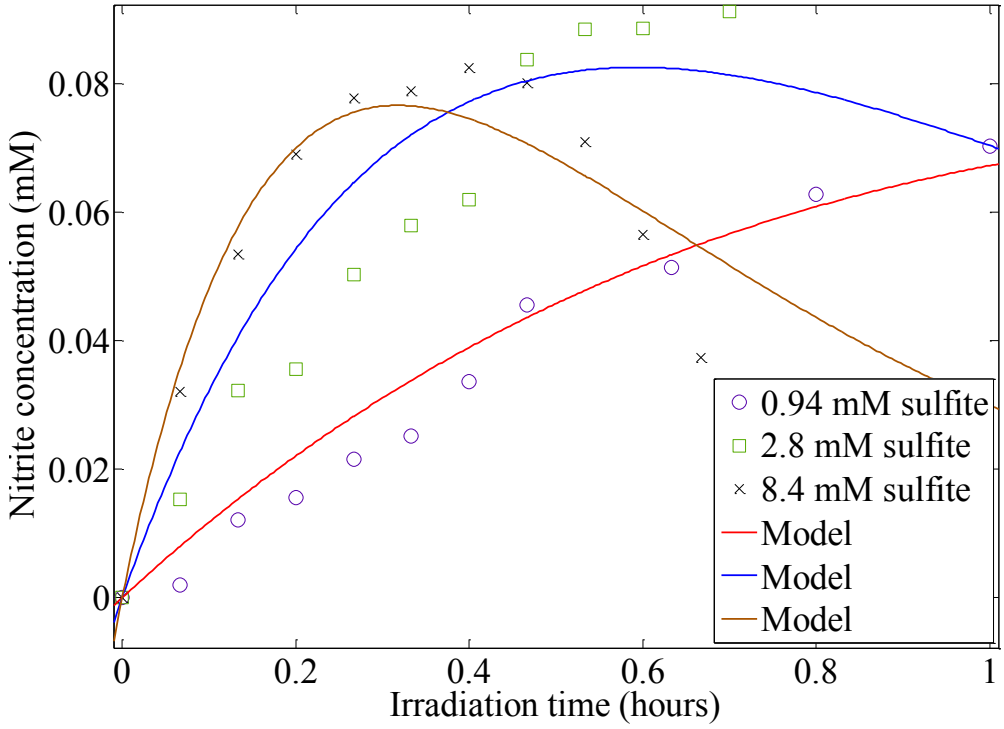

Figure 4-17: Nitrite concentration during nitrate degradation by sulfite/UV-L at different sulfite concentrations (pH 7, 2.8 mW/cm^2, with air circulation, T≅ 27^o C).

Figure 4-17 indicates higher initial rates of nitrite formation with increasing sulfite concentration, which is in accordance with the nitrate degradation profiles at different sulfite concentration (Figure 4-14). Nitrite concentration profiles follow a trend of increasing nitrite concentration e, followed by a decreasing nitrite concentration.

Since nitrate degradation rate increases with increasing sulfite concentration, the point of change from net increase in nitrite concentration to net decrease in nitrite concentration occurs earlier with increasing sulfite concentration.

The first-order rate constants for nitrite degradation at different sulfite concentrations were obtained by fitting Equation 4-2 to nitrite concentrations and the results are presented in Figure 4-12.

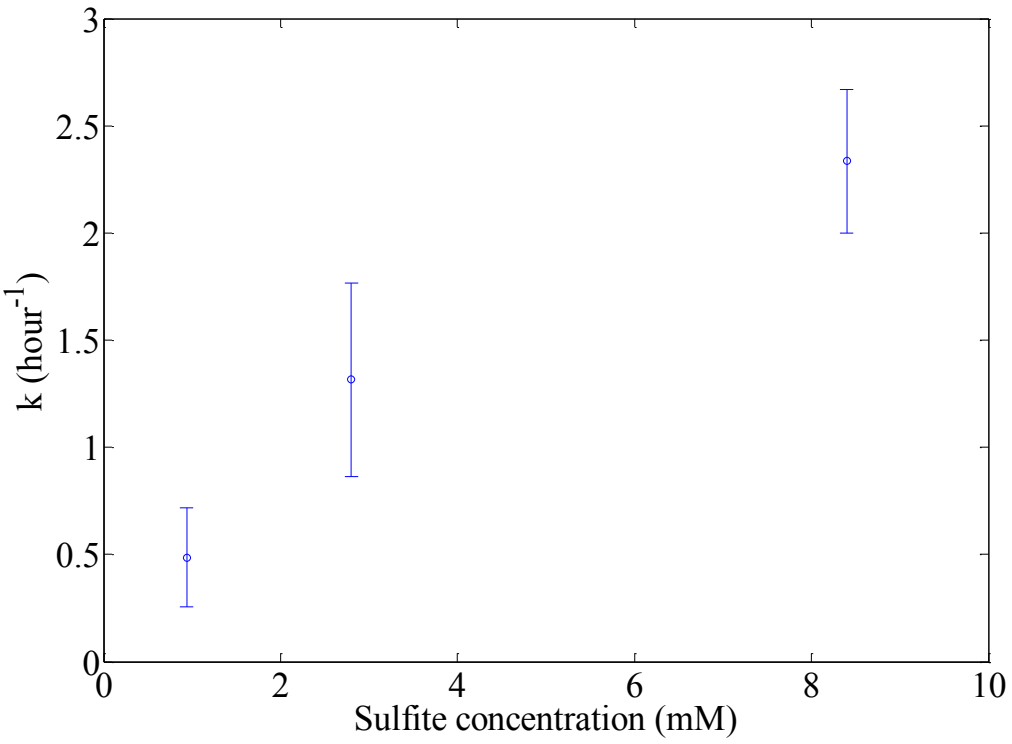

Figure 4-18: First-order rate constant for nitrite degradation during nitrate degradation by sulfite/UV-L at different sulfite concentrations (pH 7, 2.8 mW/cm^2, with air circulation, T≅ 27^o C).

Figure 4-19 indicates that the first-order nitrite degradation rate constant increases with increasing sulfite concentration, similar to the nitrate degradation rate constant.

Data on sulfite loss during the nitrate degradation experiments are presented in Figure 4-19.

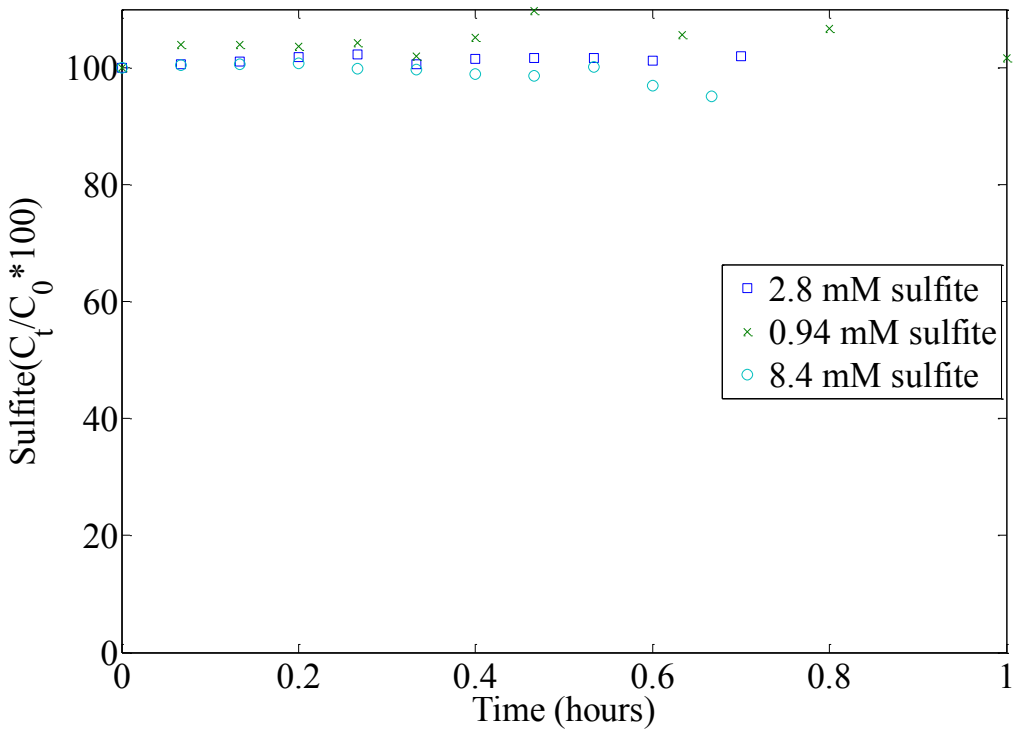

Figure 4-19: Sulfite loss during nitrate degradation by sulfite/UV-L at different sulfite concentrations (pH 7, 2.8 mW/cm^2, with air circulation, T≅ 27^o C).

Figure 4-19 indicates that there is little sulfite loss over the experimental time periods.

A summary of the perchlorate degradation kinetic experiments and experimental results is presented in Appendix B.

4.4 Summary

The results of the sulfite/UV-L experiments on nitrate degradation suggest that nitrate degradation rate and efficiency improve with an increase in pH. Increased light intensity and increased sulfite concentrations increase the rate of nitrate degradation. However, the efficiency of nitrate degradation as measured by the quantum yield decreases at the highest sulfite concentration tested. Nitrite is one of the intermediate products of nitrate degradation and its degradation behavior is similar to that of nitrate.

5 MECHANISTIC MODEL

5.1 Introduction

A preliminary kinetic model that simulates radical reactions occurring in Advanced Reduction Processes is presented in this chapter. Part of this model was developed by others. Reactions relevant to sulfite/UV-L degradation of perchlorate/nitrate were collected from available literature. The model includes a description of the production of reactive species ($SO_3^{\bullet-}$, e_{aq}^-) from sulfite as functions of intensity of UV-L and concentrations of sulfite. Reactions for these species with other compounds that are often found in water were included. A total of 89 reactions and 33 species were considered. Reactions for the target compound and possible reactive species were included and coefficients for these reactions were obtained by conducting non-linear regressions on data produced by the kinetic experiments conducted with air circulation. Solutions to the model were determined using the MATLAB function "ode15s", which solves equations numerically by backward differentiation formulas. The relevant MATLAB files are presented in Appendix D.

5.2 Results and Discussion

5.2.1 Perchlorate kinetic model

The model was applied to the data obtained from perchlorate kinetic experiments conducted with air circulation. The combination of sulfite quantum yield and rate constant of perchlorate degradation by $SO_3^{\bullet-}$ that gives the least weighted sum of squared errors between the modeled sulfite and perchlorate concentrations and the observed

concentrations are presented in Table 5-1. The combination that minimized the following value was chosen.

$$WSSE = \sum_{i=1}^{n} \left[\left(\frac{C_{\text{expt,perch,i}} - C_{\text{model,perch,i}}}{C_{\text{initial,perch}}} \right)^2 + \left(\frac{C_{\text{expt,sulfite,i}} - C_{\text{model,sulfite,i}}}{C_{\text{initial,sulfite}}} \right)^2 \right] \quad (5\text{-}1)$$

$$SSE_{sulfite} = \sum_{i=1}^{n} \left(C_{\text{expt,sulfite,i}} - C_{\text{model,sulfite,i}} \right)^2 \quad (5\text{-}2)$$

$$SSE_{perch} = \sum_{i=1}^{n} \left(C_{\text{expt,perch,i}} - C_{\text{model,perch,i}} \right)^2 \quad (5\text{-}3)$$

Table 5-1: Values of sulfite quantum yield and perchlorate degradation rate constant.

UV reading (mW/cm^2)	pH	Sulfite concentration (mM)	Sulfite quantum yield	Rate constant of reaction between $SO_3^{\bullet-}$ and ClO_4^- (L/mol-s)	$\frac{\sqrt{\frac{SSE_{sulfite}}{n-2}}}{C_{avg,sulfite}}$	$\frac{\sqrt{\frac{SSE_{perch}}{n-2}}}{C_{avg,perch}}$	WSSE
7	7	11.08	0.11	0	0.0709	0.0209	0.0099
7	9	11.08	0.04	380	0.0787	0.0097	0.0135
7	11	11.08	0.02	940	0.0817	0.0092	0.0254
7	11	110.8	0.03	420	0.0244	0.0174	0.0044
7	11	37.5	0.02	710	0.0400	0.0056	0.0076
7	11	3.76	0.03	1120	0.0744	0.0059	0.0152
7	11	1.26	0.02	810	0.1032	0.0068	0.0374
9.8	11	11.08	0.02	1160	0.0320	0.0061	0.0038
2.1	11	11.08	0.03	780	0.0151	0.0071	0.0013

The values of perchlorate degradation rate constant were held constant and the values of sulfite quantum yield that give the least sum of squared errors (not weighted) between the modeled sulfite and observed concentrations were calculated. The average of the sulfite quantum yields at similar pH was calculated, because it is expected that the quantum yields will be the same under similar conditions. The standard deviation of the modeled sulfite quantum yields over similar pH values is 0.0059. This average value was then used to calculate the perchlorate degradation rate constants that gave the least sum of squared errors between the modeled perchlorate and observed concentrations. These values are presented in Table 5-2.

Table 5-2: Modified values of sulfite quantum yield and perchlorate degradation rate constant.

UV reading (mW/cm^2)	pH	Sulfite concentration (mM)	Sulfite quantum yield with rate constant held constant	Averaged sulfite quantum yield that was held constant to calculate the rate constant	Rate constant (L/mol-s) of reaction between $SO_3^{\bullet-}$ and ClO_4^- when sulfite quantum yield was constant	$\frac{\sqrt{\frac{SSE_{sulfite}}{n-2}}}{C_{avg,sulfite}}$	$\frac{\sqrt{\frac{SSE_{perch}}{n-2}}}{C_{avg,perch}}$	WSSE
7	7	11.08	0.11	0.11	0	0.0709	0.0209	0.0099
7	9	11.08	0.035	0.035	390	0.0247	0.0116	0.0019
7	11	11.08	0.016	0.022	920	0.1129	0.0082	0.0482
7	11	110.8	0.026	0.022	500	0.0260	0.0176	0.0048
7	11	37.5	0.016	0.022	680	0.0615	0.0058	0.0178
7	11	3.76	0.027	0.022	1250	0.1040	0.0079	0.0297
7	11	1.26	0.020	0.022	780	0.1070	0.0069	0.0402
9.8	11	11.08	0.019	0.022	1130	0.0636	0.0059	0.0145
2.1	11	11.08	0.031	0.022	900	0.0614	0.0060	0.0173

The rate constants in Table 5-2 at pH 11, but at different light intensities and sulfite concentrations are not constant and have a standard deviation of 250. The rate constants at different light intensities have a standard deviation of 130. The rate constants at different sulfite concentrations vary considerably, and have a standard deviation of 280. The rate constant at higher sulfite concentrations are relatively low.

The model considers that only SO_3^{2-} absorbs light and forms radicals. Thus, the sulfite quantum yields at pH 7 and pH 9, where SO_3^{2-} is present in relatively low concentration compared to pH 11, are higher than the sulfite quantum yield at pH 11. The model tries to assign the loss of total sulfite only to loss of SO_3^{2-} , and does not

consider possible absorption of light by the other sulfite species. The model assumes that only $SO_3^{\bullet-}$ degrades perchlorate. It is possible that other reductants formed in the system leads to degradation of perchlorate.

The predictions of kinetic model fitted to the concentrations of perchlorate and sulfite during perchlorate kinetic experiments at various pH are presented in figures 5-1 and 5-2 respectively. The values for averaged quantum yield and rate constant in Table 5-2 were used to generate the estimate.

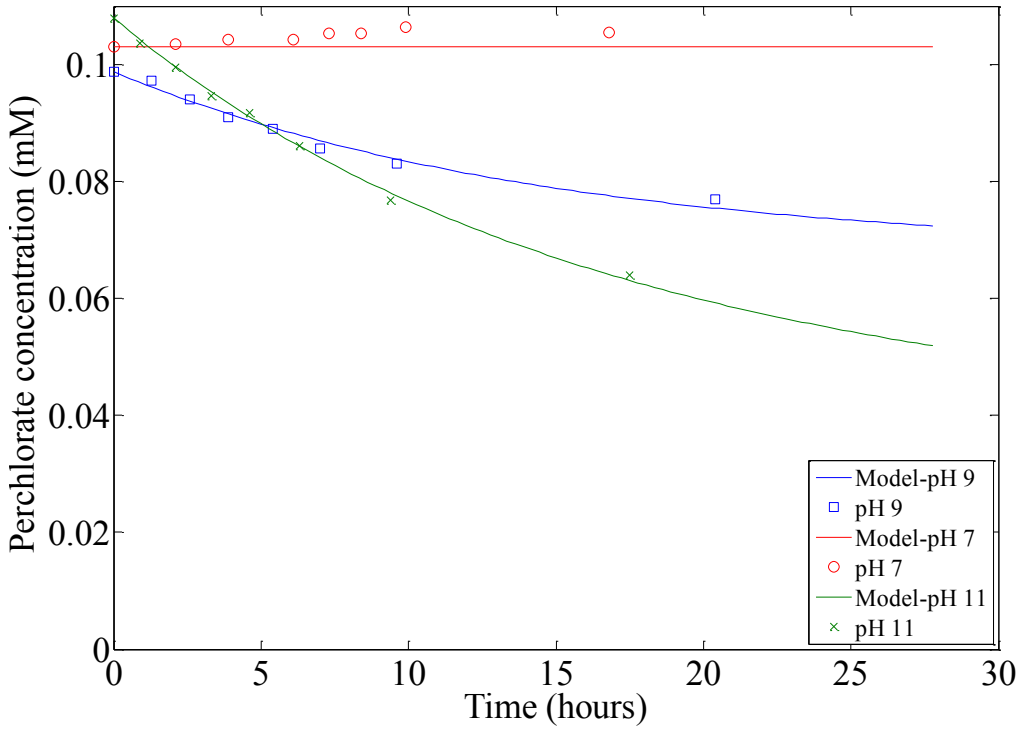

Figure 5-1: Kinetic model of perchlorate degradation by sulfite/UV-L at various pH (7 mW/cm^2, 11 mM sulfite concentration, with air circulation, T≅ 28^o C).

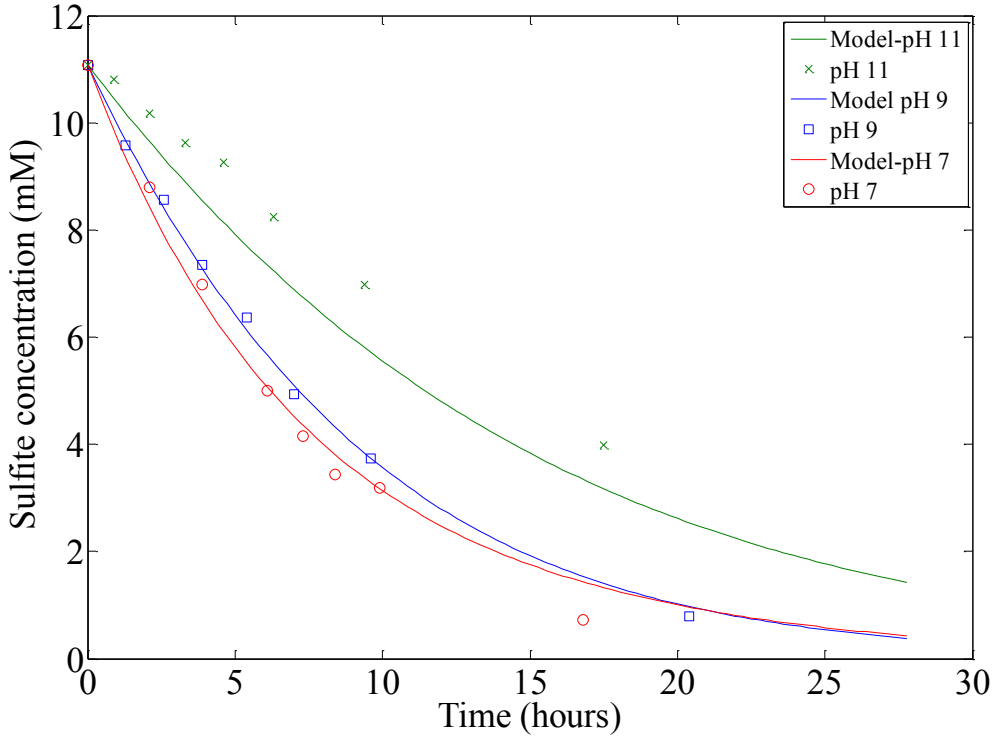

Figure 5-2: Kinetic model of sulfite loss during perchlorate degradation by sulfite/UV-L at various pH (7 mW/cm^2, 11 mM sulfite concentration, with air circulation, T≅ 28^o C).

The model fits the perchlorate and sulfite data well, except at pH 11, where it under estimates the sulfite concentrations. This is because the average sulfite quantum yield was used to simulate the data, rather than one specific to pH11.

The predictions of kinetic model fitted to the concentrations of perchlorate and sulfite during perchlorate kinetic experiments at various sulfite concentrations are presented in figures 5-3 and 5-4 respectively. The values for averaged quantum yield and rate constant presented in Table 5-2 were used to generate the estimate.

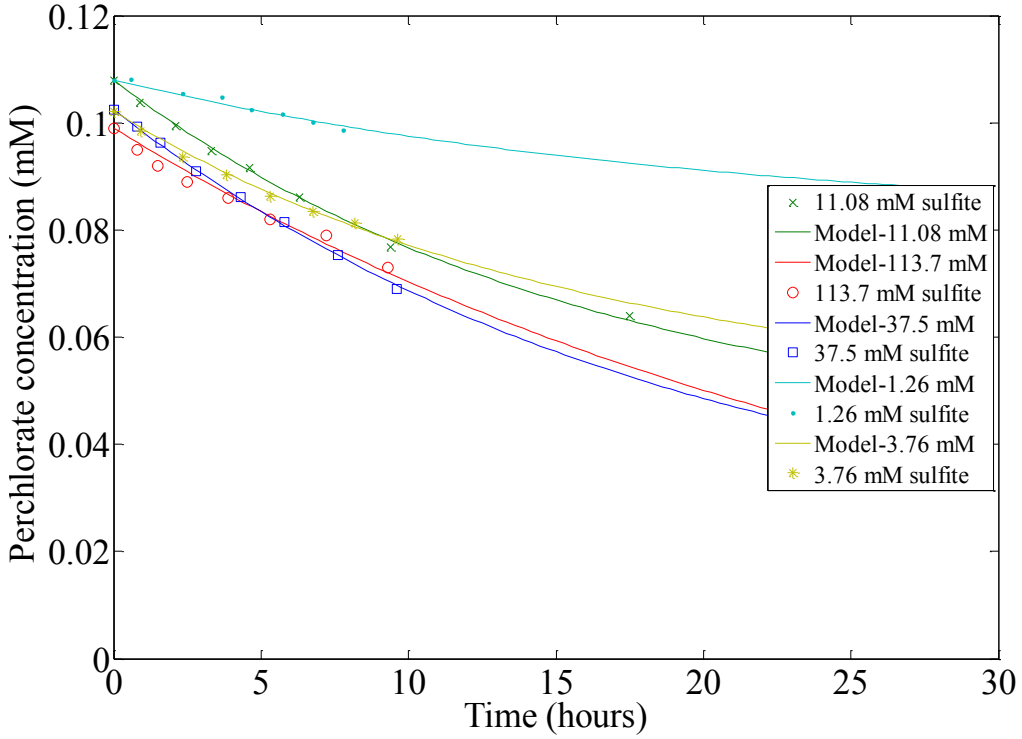

Figure 5-3: Kinetic model of perchlorate degradation by sulfite/UV-L at different sulfite concentrations (pH 11, 7 mW/cm^2, with air circulation, T≅ 30^o C).

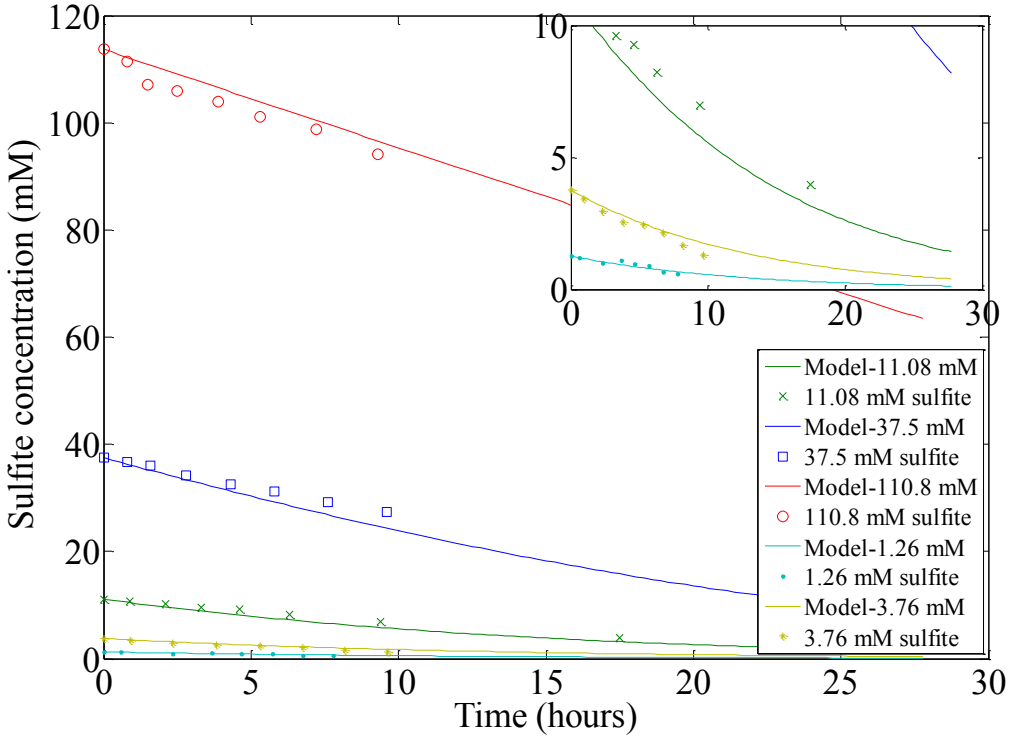

Figure 5-4: Kinetic model of sulfite loss during perchlorate degradation by sulfite/UV-L at different sulfite concentrations (pH 11, 7 mW/cm^2, with air circulation, T≅ 30^o C)

The model fits the perchlorate data well. For the sulfite data, the model deviates from the experimental data due to the usage of the average sulfite quantum yield. There is no apparent trend in the model over or under estimating the data.

The predictions of the kinetic model fitted to the concentrations of perchlorate and sulfite during perchlorate kinetic experiments at various light intensities are presented in figures 5-5 and 5-6 respectively. The values for averaged quantum yield and rate constant in Table 5-2 were used to generate the estimate.

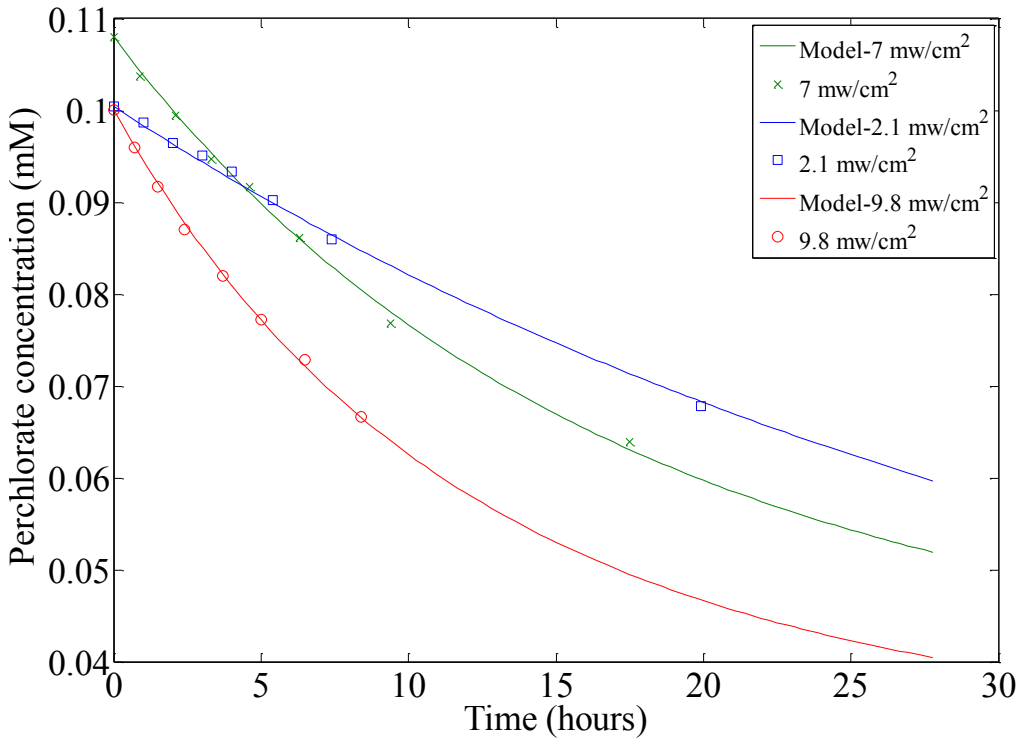

Figure 5-5: Kinetic model of perchlorate degradation by sulfite/UV-L at different light intensities (pH 11, 11 mM sulfite concentration, with air circulation, T≅ 30^{o} C).

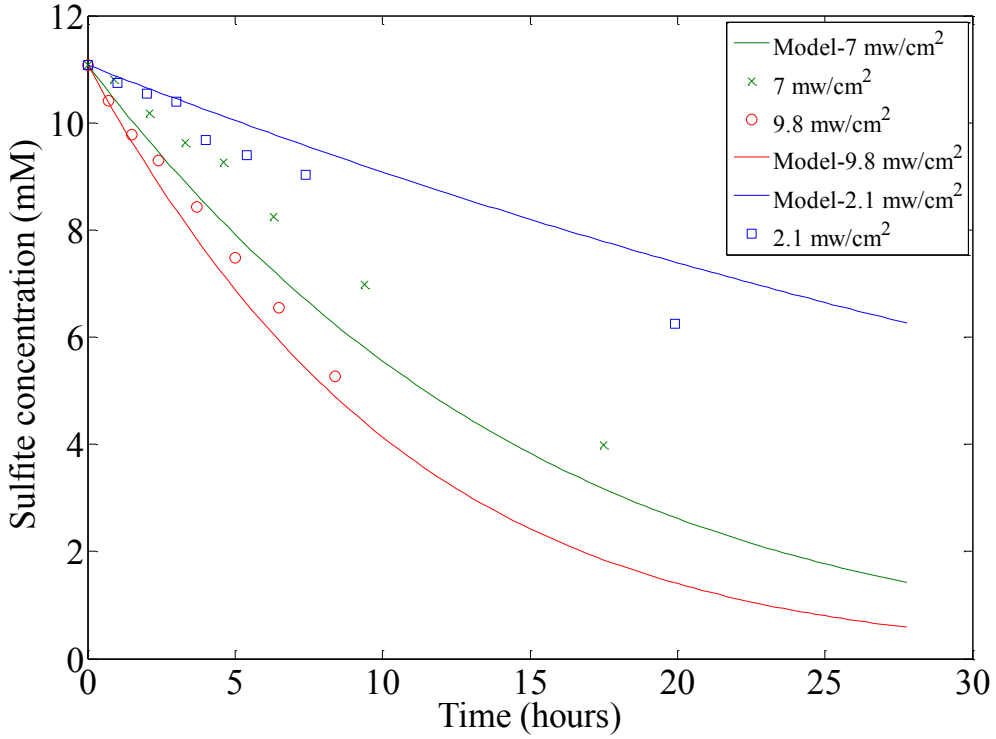

Figure 5-6: Kinetic model of sulfite loss during perchlorate degradation by sulfite/UV-L at different light intensities (pH 11, 11 mM sulfite concentration, with air circulation, T≅ 30° C).

The model fits the perchlorate data well. For the sulfite data, the model deviates from the experimental data due to the usage of the average sulfite quantum yield. The model underestimates the sulfite concentration at higher light intensities and overestimates the sulfite concentration at lower light intensities.

5.2.2 Nitrate kinetic model

The model was applied to the data obtained from nitrate kinetic experiments conducted with air circulation. The model considers degradation of nitrate by reaction with $H^{\bullet}$, e_{aq} and $SO_3^{\bullet-}$. The values of the reaction rate constants of nitrate degradation by

$H^{\bullet}$ and e_{aq} that are available in the literature were used. The combination of sulfite quantum yield and rate constant of nitrate degradation by $SO_3^{\bullet-}$ that gives the least sum of squared errors between the modeled sulfite and nitrate concentrations and the observed concentrations are presented in Table 5-3.

Table 5-3: Values of sulfite quantum yield and nitrate degradation rate constant.

UV reading (mW/cm^2)	pH	Sulfite concentration (mM)	Sulfite quantum yield	Rate constant of reaction between $SO_3^{\bullet-}$ and NO_3^- (L/mol-s)	$\frac{\sqrt{\frac{SSE_{sulfite}}{n-2}}}{C_{avg,sulfite}}$	$\frac{\sqrt{\frac{SSE_{nitrate}}{n-2}}}{C_{avg,nitrate}}$	WSSE
2.8	7	0.94	0.14	1.93e17	0.0953	0.0268	0.0927
2.8	7	2.8	0.14	5.89e4	0.0467	0.0856	0.0537
2.8	7	8.5	0.08	6.32e4	0.0149	0.1989	0.0493
2.8	5	2.8	0.70	80	0.1935	0.0457	0.1718
2.8	9	2.8	0.09	7.54e4	0.0294	0.1404	0.0349
1	7	2.8	0.15	8.53e4	0.0052	0.0208	0.0052
8	7	2.8	0.14	2.57e4	0.0625	0.1799	0.0566

The sulfite quantum yield and nitrate degradation rate constant vary with experimental conditions. The experimental data shows that nitrate is removed at acidic, neutral and basic pH with little to no loss of sulfite. The model considers that only SO_3^{2-} absorbs light and forms radicals and that the other sulfite species are non-reactive, which might not be the case. Irradiation of bisulfite (HSO_3^-) can lead to formation of aqueous electrons, which can degrade nitrate. Thus, the sulfite quantum yields calculated at pH 5 will be forced to be higher than they actually are, because the model tries to assign the loss of total sulfite only to loss of the sulfite ion (SO_3^{2-}). The sulfite quantum yields are

relatively high, even though there is not much loss of sulfite during the course of the experiments.

The predictions of the kinetic model fitted to concentrations of nitrate and sulfite during nitrate kinetic experiments at various pH are presented in figures 5-7 and 5-8 respectively.

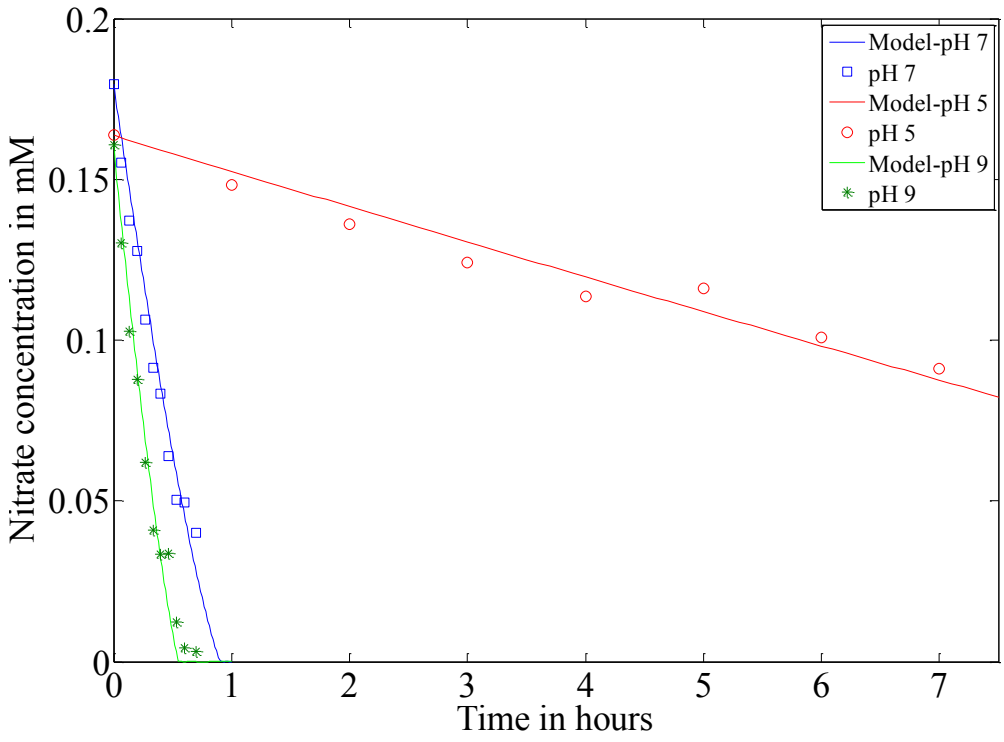

Figure 5-7: Kinetic model for nitrate degradation by sulfite/UV-L at various pH (2.8 mW/cm^2, 2.8 mM sulfite concentration, with air circulation, T≅ 27^o C).

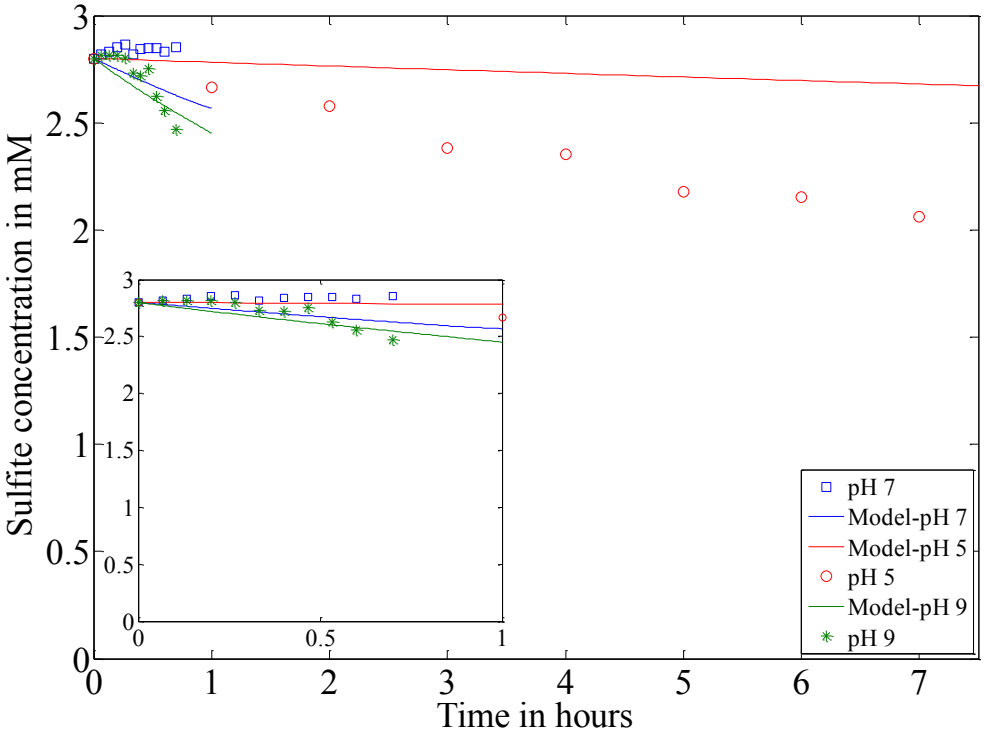

Figure 5-8: Kinetic model for sulfite loss during nitrate degradation by sulfite/UV-L at various pH (2.8 mW/cm^2, 2.8 mM sulfite concentration, with air circulation, T≅ 27^o C).

The model fits the nitrate data well. For the sulfite data, the model deviates from the experimental data at pH 5 because it does not consider photolysis of HSO_3^- and H_2SO_3, which are the sulfite species that are predominant at pH 5. At pH 7, little loss of sulfite is noticed, but the model predicts higher loss. Higher model predictions could be due to the parameter estimation method over-estimating the sulfite yield. This could occur because the procedure chose a value of the sulfite quantum yield to fit both sulfite concentrations and target concentrations. This could lead to quantum yields that are too high to accurately describe sulfite removal. The kinetic model predicts well the sulfite loss at pH 9, where SO_3^{2-} is predominant.

The predictions of the kinetic model fitted to concentrations of nitrate and sulfite during nitrate kinetic experiments at various sulfite concentrations are presented in figures 5-9 and 5-10 respectively.

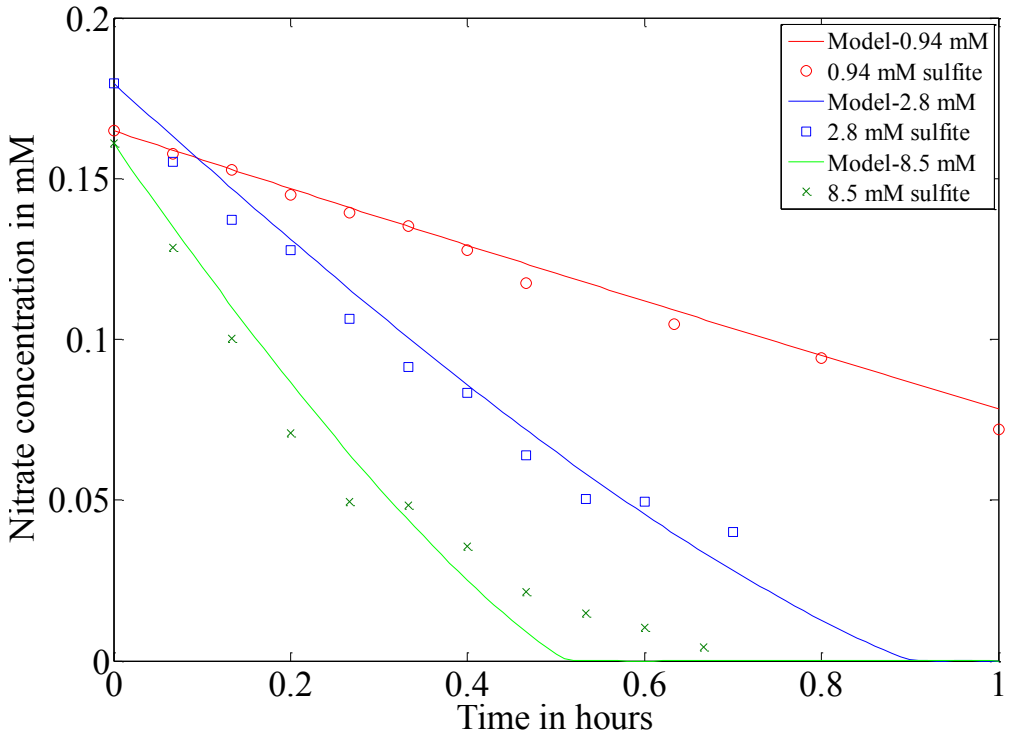

Figure 5-9: Kinetic model for nitrate degradation by sulfite/UV-L at different sulfite concentrations (pH 7, 2.8 mW/cm^2, with air circulation, T≅ 27^o C).

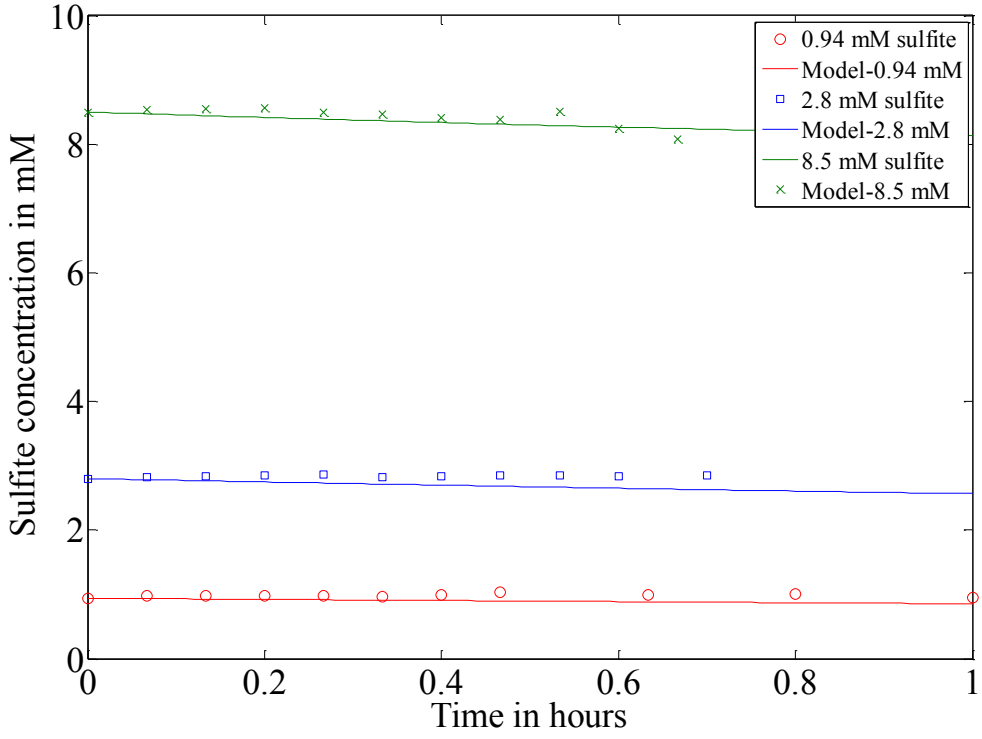

Figure 5-10: Kinetic model for sulfite loss during nitrate degradation by sulfite/UV-L at different sulfite concentrations (pH 7, 2.8 mW/cm^2, with air circulation, T≅ 27^o C).

The model fits the nitrate data well. For the sulfite data, the model underestimates the concentrations of sulfite. All the experiments that look at effects of sulfite concentration were conducted at pH 7. For some reason, there is little to no loss of sulfite in most of the kinetic experiments conducted at pH 7. Thus, for the kinetics experiments that look at effect of sulfite concentration, the model needs to predict a higher decrease in sulfite concentration in order for the model to be able to produce radicals that degrade nitrate.

The kinetic model fitted to concentrations of nitrate and sulfite during nitrate kinetic experiments at various light intensities are presented in figures 5-11 and 5-12 respectively.

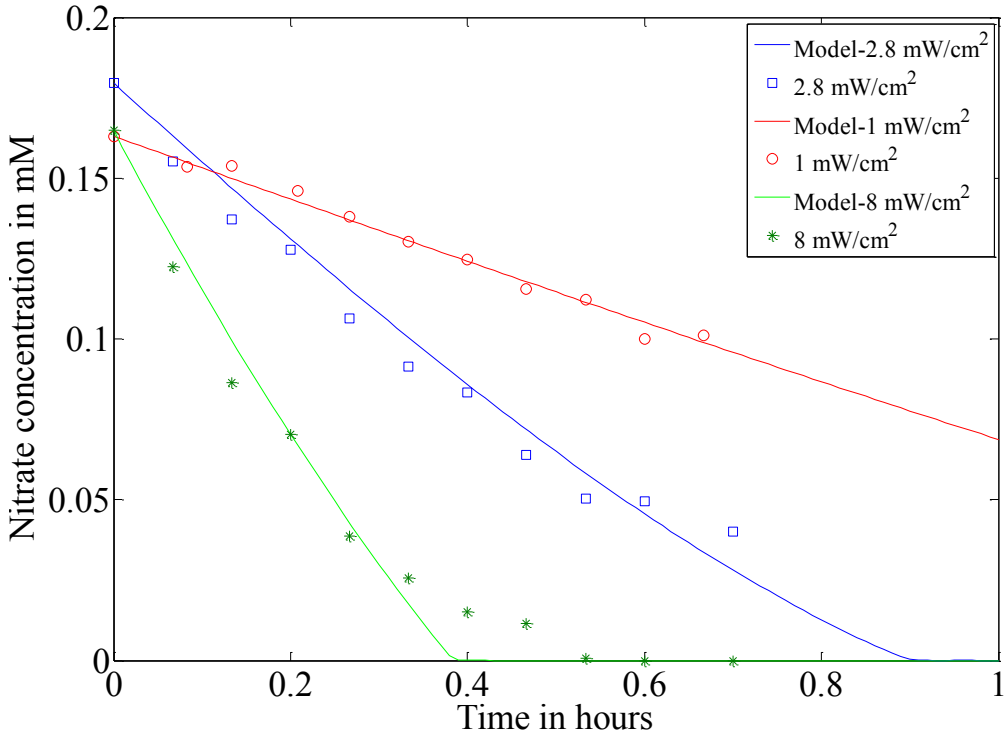

Figure 5-11: Kinetic model for nitrate degradation by sulfite/UV-L at different light intensities (pH 7, 2.8 mM sulfite concentration, with air circulation, T≅27^0 C).

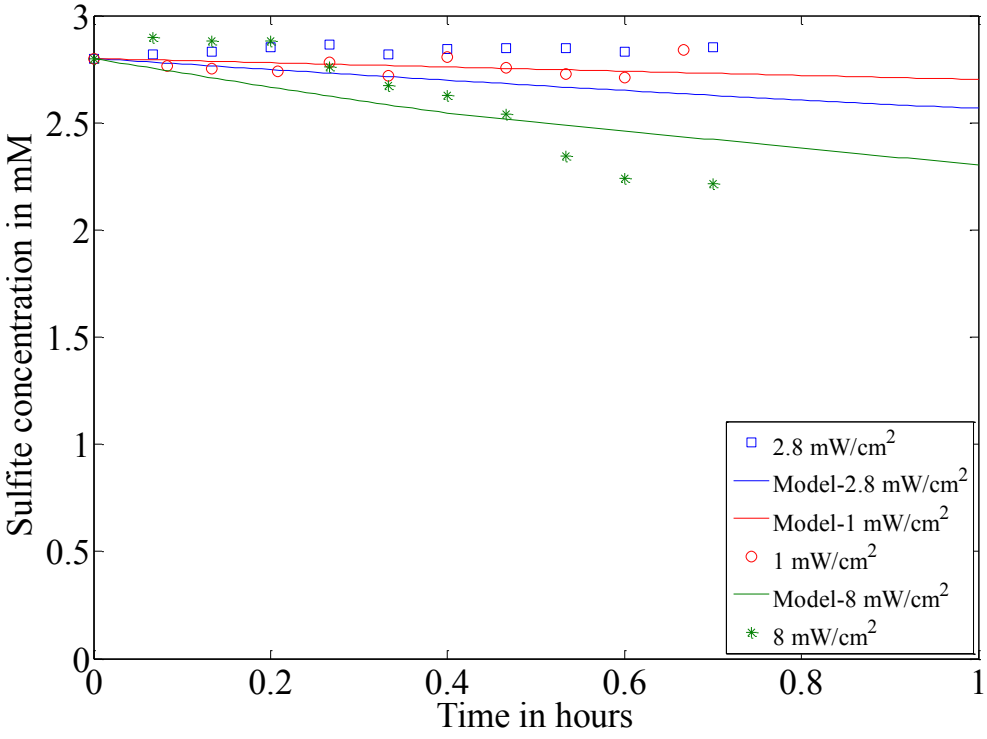

Figure 5-12: Kinetic model for sulfite loss during nitrate degradation by sulfite/UV-L at different light intensities (pH 7, 2.8 mM sulfite concentration, with air circulation, T≅27^0 C).

The model fits the nitrate data well. For the sulfite data, the model the model underestimates the concentrations of sulfite at those light intensities where little loss of sulfite is observed, but nitrate degradation still occurs. It predicts the sulfite loss well at the other light intensities where sulfite loss is observed.

While the model fits the individual experiments well, the sulfite quantum yields and perchlorate degradation rate constants are not independent of the relevant variables, with a different set of quantum yield and rate constant for each experiment. This is the major drawback of the model. In the nitrate degradation experiments where there is

relatively little loss of sulfite but considerable nitrate degradation, the model does not fit the sulfite loss well. The model, when developed further, should estimate the sulfite quantum yields such that they do not vary with light intensity or sulfite concentration. Light intensity and sulfite concentration should not affect sulfite quantum yield as the species stay the same. The parameters can vary with pH, as a change in pH leads to changes in the species of sulfite. The rate constant for perchlorate degradation by the sulfite anion radial should be independent of pH, light intensity or sulfite concentration. The model is far from achieving its goal of successfully simulating the sulfite/UV-L degradation of target compounds.

The model can be improved by finding more reactions relevant to the system, correcting the present reactions for changes in pH and other original experimental conditions, and adding other species that can absorb light and produce radicals.

5.3 Summary

The kinetic model is unable to accurately and consistently predict the behavior of the sulfite/UV-L system. The sulfite quantum yields and degradation rate constants vary with experimental conditions, when they are expected to be constant. The kinetic model presented is a basic model that needs to be improved before it can adequately simulate the sulfite/UV-L system. The model considers irradiation of SO_3^{2-} to be the only mechanism that leads to formation of reductants and radicals. The various reactions considered in the kinetic model do not apply to all of the operating conditions (pH etc) used in the kinetic experiments presented in this research. Such issues limit the ability of

the kinetic model to simulate the sulfite/UV-L system accurately. Nevertheless, the present kinetic model serves as a stepping stone for better models.

6 CONCLUSIONS AND RECOMMENDATIONS

6.1 Conclusions

This research puts forth and validates the Advanced Reduction Processes, a new class of treatment processes which combine a reagent with an activating method to produce highly reactive reductant radicals to reductively degrade oxidized contaminants. The results of this research: 1) demonstrate the ability of various ARPs to effectively degrade a variety of oxidized contaminants, and 2) characterize degradation of perchlorate and nitrate by the most effective ARP tested, the sulfite/UV-L/sulfite ARP. This knowledge could be used to develop an effective method of destroying perchlorate and nitrate in ion exchange regenerant solutions and other contaminated media. This research provides an exciting opportunity to develop effective treatment technologies for oxidized contaminants.

The specific conclusions from this research are:

1. The results of the screening experiments demonstrate that a wide range of ARP can degrade a wide variety of contaminants.
2. The screening experiments indicate that the E-beam and UV-L generally were successful in activating different reagents to degrade the target contaminants. 1,2 DCA, 2,4 DCP and nitrate were more readily degraded compared to perchlorate and PFOA.

3. The ARP that combines sulfite with UV-L provides the most consistently high levels of removal across all contaminants. It is the only combination tested that was able to achieve destruction of perchlorate, indicating its effectiveness.
4. UV-L is more strongly absorbed at low pH where sulfurous acid predominates and at high pH where sulfite predominates. At basic pH, sulfite solutions absorb UV light strongly at around 220 nm, while the absorbance at 254 nm is relatively low.
5. The rate of perchlorate degradation and removal efficiency by UV-L/sulfite increase with increasing pH and temperature, indicating that higher OH^- concentrations and higher temperatures are conducive to the mechanism that leads to perchlorate degradation. No perchlorate removal was observed at acidic pH.
6. Increasing pH results in decreasing quantum yield and first-order rate constant for sulfite loss during perchlorate degradation by UV-L.
7. Faster rates of perchlorate removal and lower levels of degradation efficiency (quantum yield) are observed at higher light intensities.
8. Higher light intensities result in faster loss of sulfite. Quantum yield for sulfite loss does not vary with changing light intensity.
9. Perchlorate degradation rate increases with increasing sulfite concentration until a certain point and then starts decreasing due to lack of mixing within the reactor system used. Efficiency of perchlorate degradation decreases with increasing sulfite concentration.

10. There is no variation of sulfite quantum yield with variation in sulfite concentration.
11. Chlorate and chloride concentrations increase with decreasing perchlorate concentration. Satisfactory chloride recovery is observed among perchlorate, chlorate and chloride.
12. The presence of catalysts (Fe^{3+}, Fe^{2+}, Cu, Rb, Mo, Ni, V, Os and W) did not aid the degradation of perchlorate by sulfite/UV-L.
13. Nitrate degradation rate and efficiency increase with increasing pH. Nitrate removal occurs at acidic pH too.
14. Nitrite is one of the products of nitrate degradation and is itself degraded to other products.
15. For the range of light intensities tested, nitrate degradation increases linearly with increase in light intensity. Nitrite degradation increases with increasing light intensity.
16. For the range of sulfite concentrations tested, nitrate and nitrite degradation rates increase with increasing sulfite concentrations.
17. The kinetic model developed fits the perchlorate, nitrate and sulfite data well but lacks consistency.

6.2 Recommendations

The results described in this research propose some relevant research topics for future work in similar experimental systems. The specific research topics for future research are as follows.

1. Other potential reductants and activating agents can be tested for effectiveness against difficult to reduce oxidized contaminants.
2. Preliminary cost analysis can be conducted to check the commercial viability of the sulfite/UV-L ARP in degrading perchlorate and nitrate.
3. Lamps that emit light at wavelengths where sulfite solutions absorb more strongly than at 254 nm can be tested.
4. Effects of conditions and variables that mimic actual operating conditions (e.g conditions in ion exchange regenerant solutions) can be tested.
5. The effects of temperature on the efficiency of the sulfite/UV-L system can be studied in greater detail.
6. The efficiency of sulfite/UV-L system in degrading perchlorate increases dramatically at higher pH. The reasons for this increase can be studied to understand the process better and aid in increasing its efficiency.
7. Pilot scale studies which are along the lines of UV irradiation systems used in industry can be conducted to check the effects of flow, mixing, temperature and variation in light intensity. Optimum light intensity and sulfite concentrations that strike a balance between target quantum yield and rate of target degradation so as to achieve greater cost effectiveness can be investigated.

8. Effects of serial injection of small amounts of sulfite can be studied to aid in understanding and increasing the efficiency of the sulfite/UV-L system.
9. Conducting in-depth product analysis of perchlorate, nitrate and sulfite during degradation will aid in gathering more information about the system and identifying the reducing species.
10. Various radical and reductant scavengers can be used to identify the reducing/beneficial species that lead to degradation of perchlorate and nitrate.
11. The kinetic model can be improved by modifying the equations for operating conditions, identifying the relevant reducing species, adding relevant product reactions, and considering the possibility of irradiation of other sulfite species producing radicals.

LITERATURE CITED

1. Poyatos, J. M.; Munio, M. M.; Almecija, M. C.; Torres, J. C.; Hontoria, E.; Osorio, F., Advanced oxidation processes for wastewater treatment: state of the art. *Water Air Soil Poll* **2010,** *205*, (1-4), 187-204.

2. Copinet, A.; Bertrand, C.; Govindin, S.; Coma, V.; Couturier, Y., Effects of ultraviolet light (315 nm), temperature and relative humidity on the degradation of polylactic acid plastic films. *Chemosphere* **2004,** *55*, (5), 763-773.

3. Casacci, M.; Thomas, P.; Pacifico, A.; Bonnevalle, A.; Paro Vidolin, A.; Leone, G., Comparison between 308-nm monochromatic excimer light and narrowband UVB phototherapy (311-313 nm) in the treatment of vitiligo--a multicentre controlled study. *Journal of the European Academy of Dermatology and Venereology : JEADV* **2007,** *21*, (7), 956-963.

4. Skov, E. R.; Pisani, J. A.; Beale, S. E., Industrial wastewater treatment using hydroxyl radical oxidation by hydraulically induced cavitation. In *AIChE Spring National Meeting* Proceedings*, Session 86a*, Houston, Texas, **1997**.

5. Kang, J.-W.; Hoffmann, M. R., Kinetics and mechanism of the sonolytic destruction of methyl tert- butyl ether by ultrasonic irradiation in the presence of ozone. *Environmental Science and* Technology **1998,** *32*, (Compendex), 3194-3199.

6. Siddiqui, M. S.; Amy, G. L.; Cooper, W. J.; Kurucz, C. N.; Waite, T. D.; Nickelsen, M. G., Bromate ion removal by HEEB irradiation. *J Am Water Works Ass* **1996,** *88*, (10), 90-101.

7. Nickelsen, M. G.; Cooper, W. J.; Kurucz, C. N.; Waite, T. D., Removal of benzene and selected alkyl-substituted benzenes from aqueous solution utilizing continuous high-energy electron irradiation. *Environmental Science and Technology* **1992,** *26*, (Compendex), 144-144.

8. Haque, K. E., Microwave energy for mineral treatment processes-A brief review. *International Journal of Mineral Processing* **1999,** *57*, (Compendex), 1-24.

9. Mudhoo, A.; Sharma, S. K., Microwave irradiation technology in waste sludge and wastewater treatment research. *Crit Rev Env Sci Tec* **2011,** *41*, (11), 999-1066.

10. Lo, K. V.; Chan, W. I.; Lo, I. W.; Liao, P. H., The effects of irradiation intensity on the microwave-enhanced advanced oxidation process. *Journal of Environmental Science and Health, Part A: Toxic/Hazardous Substances & Environmental Engineering* **2010,** *45*, (2), 257-262.

11. Makarov, S. V., Novel trends in chemistry of sulfur-containing reductants. *Uspekhi Khimii* **2001,** *70*, (Compendex), 1005-1007.

12. Mayhew, S. G., The redox potential of dithionite and sulfur dioxide(1-) from equilibrium reactions with flavodoxins, methyl viologen and hydrogen plus hydrogenase. *European Journal of Biochemistry* **1978,** *85*, (2), 535-547.

13. Neta, P.; Huie, R. E.; Harriman, A., One-electron-transfer reactions of the couple sulfur dioxide/sulfur dioxide radical anion in aqueous solutions. Pulse radiolytic and cyclic voltammetric studies. *Journal of Physical and Chemical Reference Data* **1987,** *91*, (6), 1606-1611.

14. McKenna, C. E.; Gutheil, W. G.; Song, W., A method for preparing analytically pure sodium dithionite. Dithionite quality and observed nitrogenase-specific activities. *Biochimica et Biophysica Acta, General Subjects* **1991,** *1075*, (1), 109-117.

15. Ohlsson, P. I.; Blanck, J.; Ruckpaul, K., Reduction of lactoperoxidase by the dithionite anion monomer. *European Journal of Biochemistry* **1986,** *158*, (3), 451-454.

16. Pukhovskaya, S. G.; Guseva, L. Z.; Makarov, S. V.; Naidenko, E. V., A new procedure for the spectrophotometric determination of nitrogen(II) oxide in solutions. *J Anal Chem+* **2005,** *60*, (1), 21-23.

17. Hara, K.; Sayama, K.; Arakawa, H., UV photoinduced reduction of water to hydrogen in Na2S, Na2SO3, and Na2S2O4 aqueous solutions. *Journal of Photochemistry and Photobiology, A: Chemistry* **1999,** *128*, (1-3), 27-31.

18. Miyawaki, S.; Iimori, T. Reduction bleaching of chemical thermomechanical pulp under microwave irradiation. 2003-82144 2004285534, 2003/03/25., **2004**.

19. Goswami, S.; Maity, A. C.; Das, N. K., Advanced reagent for thionation. Rapid synthesis of primary thioamides from nitriles at room temperature. *Journal of Sulfur Chemistry* **2007,** *28*, (3), 233-237.

20. Surpur, M. P.; Singh, P. R.; Patil, S. B.; Samant, S. D., One-pot synthesis of benzimidazoles from o-nitroanilines under microwaves via a reductive cyclization. *Synthetic Communications* **2007,** *37*, (8), 1375-1379.

21. Mahadevappa, D. S., Paramagnetic resonance in gamma -irradiated Na dithionite. *Current Science* **1964,** *33*, (21), 647-648.

22. Getman, F. H., The ultra-violet absorption spectra of aqueous solutions of sulfur dioxide and some of its derivatives. *Journal of Physical and Chemical Reference Data* **1926,** *30*, 266-276.

23. Devonshire, R.; Weiss, J. J., Nature of the transient species in the photochemistry of negative ions in aqueous solution. *Journal of Physical and Chemical Reference Data* **1968,** *72*, (11), 3815-3820.

24. Dogliotti, L.; Hayon, E., Flash photolysis study of sulfite thiocyanate and thiosulfate ions in solution. *Journal of Physical and Chemical Reference Data* **1968,** *72*, (5), 1800-&.

25. Chawla, O. P.; Arthur, N. L.; Fessenden, R. W., Electron spin resonance study of the photolysis of aqueous sulfite solutions. *Journal of Physical and Chemical Reference Data* **1973,** *77*, (6), 772-776.

26. Buxton, G. V.; Greenstock, C. L.; Helman, W. P.; Ross, A. B., Critical review of rate constants for reactions of hydrated electrons, hydrogen atoms and hydroxyl radicals (.OH/.O-) in aqueous solution. *Journal of Physical and Chemical Reference Data* **1988,** *17*, (2), 513-886.

27. Jeevarajan, A. S.; Fessenden, R. W., ESR studies of solvated electron in liquid solution using photolytic production. *Journal of Physical and Chemical Reference Data* **1989,** *93*, (9), 3511-3514.

28. Ermakov, A. N.; Poskrebyshev, G. A.; Purmal, A. P., Sulfite oxidation: The state-of-the-art of the problem. *Kinet Catal+* **1997,** *38*, (3), 295-308.

29. Shchukin, G. L., Oxidation of sodium sulfide by oxygen in an aqueous solution. *Fotokhim. Radiats.-Khim. Protsessy Vod. Rastvorakh Tverd. Telakh* **1970**, 79-88.

30. Bronikowski, T.; Pasiuk-Bronikowska, W.; Ulejczyk, M., SO2 induced liberation of halide anions from organics. *Archiwum Ochrony Srodowiska* **1999,** *25*, (2), 9-16.

31. Shiroyama, H.; Totsupeizo, Y. Apparatus and method for organic chlorine compound containing wastewater treatment. 93-55033 06246263, 1993/02/19., **1994**.

32. Rassokhin, D. N.; Kovalev, G. V.; Bugaenko, L. T.; Rudnev, A. V., Catalytic oxidation of sulfur dioxide by oxygen in an aqueous solution of sulfuric acid in the

presence of bivalent manganese ions under ultrasound irradiation. *Mendeleev Communications* **1992**, (2), 71-72.

33. Dzhabiev, T. S.; Tarasov, B. B., Photochemical decomposition of an aqueous solution of sodium sulfide. *Journal of Photochemistry and Photobiology, A: Chemistry* **1993,** *72*, (1), 23-27.

34. Kotronarou, A.; Mills, G.; Hoffmann, M. R., Oxidation of hydrogen sulfide in aqueous solution by ultrasonic irradiation. *Environmental Science and Technology* **1992,** *26*, (12), 2420-2428.

35. Melsheimer, J.; Schlogl, R., Identification of reaction products of mild oxidation of H2S in solution and in solid state by UV-VIS spectroscopy. *Fresenius' Journal of Analytical Chemistry* **1997,** *357*, (4), 397-400.

36. Cauwet, G.; Coste, C. M.; Knoche, H.; Longuemard, J. P., Studies on the behavior of molecules under the influence of ultrasonics. I. Hydrogen formation by ultrasonic irradiation of an aqueous solution of hydrogen sulfide. *Bulletin de la Societe Chimique de France* **1976**, (1-2, Pt. 1), 45-48.

37. Potterill, R. H.; Walker, O. J.; Weiss, J., Electron affinity spectrum of ferrous ion in aqueous solution. *Proceedings of the Royal Society of London, Series A: Mathematical, Physical and Engineering Sciences* **1936,** *156*, 561-570.

38. Airey, P. L.; Dainton, F. S., The photochemistry of aqueous solutions of Fe(II). I. Photoelectron detachment from ferrous and ferrocyanide ions. *Proceedings of the Royal Society of London, Series A: Mathematical, Physical and Engineering Sciences* **1966,** *291*, (1426), 340-352.

39. ITRC. Perchlorate Team., Remediation technologies for perchlorate contamination in water and soil. PERC-2. Interstate Technology & Regulatory Council: Washington, DC, **2007**.

40. ITRC. Enhanced In Situ Biodenitrification Work Team., Emerging technologies for enhanced in situ biodenitrification (EISBD) of nitrate-contaminated ground water. Interstate Technology & Regulatory Council: United States, **2000**.

41. Fanning, J. C., The chemical reduction of nitrate in aqueous solution. *Coordin Chem Rev* **2000,** *199*, 159-179.

42. Hoffmann, M. R.; Vecitis, C. D.; Park, H.; Cheng, J.; Mader, B. T., Treatment technologies for aqueous perfluorooctanesulfonate (PFOS) and perfluorooctanoate (PFOA). *Front Environ Sci En* **2009,** *3*, (2), 129-151.

43. Exon, J. H.; Koller, L. D., Toxicity of 2-chlorophenol, 2,4-dichlorophenol, and 2,4,6-trichlorophenol. *Water Chlorination Chem., Environ. Impact Health Eff., Proc. Conf., 5th* **1985**, 307-330.

44. Gwinn, M. R.; Johns, D. O.; Bateson, T. F.; Guyton, K. Z., A review of the genotoxicity of 1,2-dichloroethane (EDC). *Mutat Res-Rev Mutat* **2011,** *727*, (1-2), 42-53.

45. Fischer, M.; Warneck, P., Photodecomposition and photooxidation of hydrogen sulfite in aqueous solution. *Journal of Physical and Chemical Reference Data* **1996,** *100*, (37), 15111-15117.

46. Tossell, J. A.; Zimmermann, M. D., Acidities of arsenic (III) and arsenic (V) thio- and oxyacids in aqueous solution using the CBS-QB3/CPCM method. *J Phys Chem A* **2009,** *113*, (17), 5105-5111.

47. Abu-Omar, M. M.; Appelman, E. H.; Espenson, J. H., Oxygen transfer reactions of methylrhenium oxides. *Inorganic Chemistry* **1996,** *35*, (26), 7751-7757.

48. Abu-Omar, M. M.; Espenson, J. H., Facile abstraction of successive oxygen atoms from perchlorate ions by methylrhenium dioxide. *Inorganic Chemistry* **1995,** *34*, (25), 6239-6240.

49. Lang, G.; Ujvari, M.; Horanyi, G., On the reduction of ClO4- ions in the course of metal dissolution in HClO4 solutions. *Corros. Sci.* **2002,** *45*, (Copyright (C) 2011 American Chemical Society (ACS). All Rights Reserved.), 1-5.

50. Kallen, T. W.; Earley, J. E., Reduction of perchlorate ion by aquoruthenium(ii). *Inorganic Chemistry* **1971,** *10*, (6), 1152-&.

51. Kallen, T. W.; Earley, J. E., Substitution as rate-determining step in reduction of perchlorate ion by ruthenium(ii). *J Chem Soc Chem Comm* **1970**, (14), 851-&.

52. Haight, G. P.; Sager, W. F., Evidence for preferential one-step divalent changes in the molybdate-catalyzed reduction of perchlorate by stannous ion in sulfuric acid solution. *J Am Chem Soc* **1952,** *74*, (23), 6056-6059.

53. Duke, F. R.; Quinney, P. R., The kinetics of the reduction of perchlorate ion by Ti(iii) in dilute solution. *J Am Chem Soc* **1954,** *76*, (14), 3800-3803.

54. Liu, B. Y.; Wagner, P. A.; Earley, J. E., Reduction of perchlorate ion by (N-(hydroxyethyl)ethylenediaminetriacetato)aquotitanium(iii). *Inorganic Chemistry* **1984,** *23*, (21), 3418-3420.

55. King, W. R.; Garner, C. S., Kinetics of the oxidation of vanadium(ii) and vanadium(iii) Ions by perchlorate ion. *Journal of Physical and Chemical Reference Data* **1954,** *58*, (1), 29-33.

56. Halperin, J.; Taube, H., Oxygen atom transfer in the reaction of chlorate with sulfite in aqueous solution. *J Am Chem Soc* **1950,** *72*, (7), 3319-3320.

57. Halperin, J.; Taube, H., The transfer of oxygen atoms in oxidation-reduction reactions-4. The reaction of hydrogen peroxide with sulfite and thiosulfate, and of oxygen, manganese dioxide and of permanganate with sulfite. *J Am Chem Soc* **1952,** *74*, (2), 380-382.

58. Taube, H., Observations on atom-transfer reactions. *ACS Symposium Series* **1982,** *198*, (Mech. Aspects Inorg. React.), 151-179.

59. Zuo, Y.; Zhan, J.; Wu, T., Effects of monochromatic UV-visible light and sunlight on Fe(III)-catalyzed oxidation of dissolved sulfur dioxide. *Journal of Atmospheric Chemistry* **2005,** *50*, (2), 195-210.

60. Haber, F.; Wansbrough-Jones, O. H., The impact of light on oxygen free and oxygen rich sulphite solutions. (VI. Announcement on auto oxydation.). *Z Phys Chem B-Chem E* **1932,** *18*, (2/3), 103-123.

61. Perchlorate: Overview of issues, status, and remedial Options. PERCHLORATE-1.; ITRC (Interstate Technology & Regulatory Council): Washington, D.C., **2005**.

62. Urbansky, E. T., Perchlorate as an environmental contaminant. *Environ Sci Pollut R* **2002,** *9*, (3), 187-192.

63. Remediation technologies for perchlorate contamination in water and soil. PERC-2.; ITRC (Interstate Technology & Regulatory Council): Washington, DC, **2007**.

64. Smith, R. M.; Martell, A. E.; Motekaitis, R. J., NIST critically selected stability constants of metal complexes database. In *NIST standard reference database 46*, 8.0. ed.; Standard Reference Data Program, National Institute of Standards and Technology: Gaithersburg, MD, **2004**.

65. Interstate Technology and Regulatory Cooperation Work Group. Enhanced In Situ Biodenitrification Work Team. Emerging technologies for enhanced in situ biodenitrification (EISBD) of nitrate-contaminated ground water; ITRC: United States, **2000**; p 1 v. (various pagings).

66. Pemberton, R. S.; Depew, M. C.; Heitner, C.; Wan, J. K. S., Some mechanistic insights into a model bleaching process of quinones by bisulfite and dithionite: an ESR-CIDEP study. *Journal of Wood Chemistry and Technology* **1995,** *15*, (1), 65-83.

APPENDIX A

Table A-1: Nitrate removal by various ARP.

	Nitrate Removal at 2/20 hr (%)					
	UVA-L			UVA-N		
No Reagent	0.4/20.9			3.2/-0.3		
	pH 2.2	*pH 7.2*	*pH 11.8*	*pH 2.2*	*pH 7.2*	*pH 11.8*
Ferrous Iron	18.3/18.1	7.0/89.8	21.2/55.5	11.5/-0.8	2.8/4.6	14.3/-1.8
Sulfite	1.6/55.8	100/100	100/100	7.2/-0.8	6.6/3.4	-0.7/4.4
Dithionite	0.3/30.9	50.9/91.6	57.0/100	-2.2/-8.1	-0.6/1.9	2.2/5.0

Table A-1: Nitrate removal by reductant/e-beam.

Reagent	pH	Dissolved oxygen	HCO_3^- (mM)	Nitrate Removal (%)
				Ebeam (10 kGy)
None	3	Saturated	0.005	0
None	7	Saturated	0.005	14
None	11	Saturated	0.005	36
None	3	Saturated	0.05	0
None	7	Saturated	0.05	14
None	11	Saturated	0.05	63
None	3	≅ 0	0.005	2
None	7	≅ 0	0.005	16
None	11	≅ 0	0.005	60
None	3	≅ 0	0.05	0
None	7	≅ 0	0.05	9
None	11	≅ 0	0.05	72
Dithionite	7	≅ 0	0.005	98
Sulfite	7	≅ 0	0.005	100
Ferrous iron	7	≅ 0	0.005	69
$Ti3^+$	n.a.	≅ 0	0.005	0

Table A-2: Perchlorate removal by various ARP.

	Perchlorate Removal (%)
	UVA-L (2/20 hr)
Sulfite	3/17

Table A-3: 2, 4 DCP removal by various ARP.

	2, 4 DCP Removal (%)				
	None	Microwave (7 min)	Ebeam (10 kGy)	Ultrasound (2 hr)	UV (ZooMed) (2/20 hr)
No Reagent	0	0	97		
Dithionite	1	9.0	17	87	4.2/61.3
Ferrous Iron			68		
Sulfite			72		

Table A-4: 2, 4 DCP reduction by reductants/UVA-L.

2, 4 DCP Removal at 0/2/20 hr (%)			
	pH 2.2	*pH 7.2*	*pH 11.8*
No Reagent		0.29/0.23/0.45	
Ferrous Iron	26.40/28.9/27.89	1.01/1.04/2.16	0.69/0.52/0.52
Sulfite		2.26/1.83/2.52	6.91/5.63/6.69
Dithionite		0/0/0	0/0/0
2, 4 DCP Removal at 2/20 hr (%)			
	UVA-L		
No Reagent	66.15/98.81		
	pH 2.2	*pH 7.2*	*pH 11.8*
Ferrous Iron	14.20/35.41	35.21/64.59	71.18/79.36
Sulfite		76.06/94.94	74.77/93.92
Dithionite		14.49/49.13	10.59/44.44

Table A-5: 2, 4 DCP reduction by reductants/UVA-N.

2, 4 DCP Removal at 0/2/20 hr (%)			
	pH 2.2	*pH 7.2*	*pH 11.8*
No Reagent	0/0.1/2.6	0.7/0.6/0.5	0.4/0.4/1.0
Ferrous Iron	1.3/1.4/1.6	1.4/0.9/0.8	1.5/2.0/2.3
Sulfite		0.9/0.0/0.0	0.2/1.1/0.1
Dithionite			
2, 4 DCP Removal at 2/20 hr (%)			
	UVA-N		
	pH 2.2	*pH 7.2*	*pH 11.8*
No Reagent	2.1/7.3	0.5/54.5	65.7/78.3
Ferrous Iron	1.7/88.6	25.5/44.2	52.0/64.7
Sulfite		55.5/66.05	69.9/73.88
Dithionite			

Table A-6: PFOA reduction by reductants/UVA-L.

PFOA Removal at 2/20 hr (%)			
	pH 2.2	*pH 7.2*	*pH 11.8*
No Reagent	2.8/2.9	2.6/2.8	2.5/2.6
Ferrous Iron	2.6/2.6	2.4/2.4	2.2/2.3
Sulfite	2.3/2.3	2.4/2.3	2.1/2.2
Dithionite	30.3/31.6	32.3/32.6	31.5/29.6
PFOA Removal at 2/20 hr (%)			
	UVA-L		
	pH 2.2	*pH 7.2*	*pH 11.8*
No Reagent	3.0/4.0	2.7/5.1	2.9/8.2
Ferrous Iron	4.0/4.3	3.4/6.3	2.3/5.2
Sulfite	2.3/3.5	3.1/25.4	2.1/40.8
Dithionite	31.1/27.9	34.2/14.9	30.5/32.7

Table A-7: PFOA reduction by reductants/UVA-N.

PFOA Removal at 2/20 hr (%)			
	pH 2.2	*pH 7.2*	*pH 11.8*
No Reagent	4.7/4.4	4.6/4.2	4.6/4.2
Ferrous Iron	0/5.0	0/0	0/0
Sulfite	0/0	0/0	0/0
Dithionite	14.3/NA	32.1/20.6	36.5/23.8
PFOA Removal at 2/20 hr (%)			
	UVA-N		
	pH 2.2	*pH 7.2*	*pH 11.8*
No Reagent	4.9/4.6	4.8/4.5	4.7/4.3
Ferrous Iron	6.5/0	0/0	0/0
Sulfite	0/0	0/0	0/0
Dithionite	31.3/20.0	35.9/16.2	34.7/21.7

Table A-8: 1,2 DCA reduction by reductants/UVA-L.

	Time in minutes	1,2 DCA removal (%)	Time in minutes	1,2 DCA removal (%)	Time in minutes	1,2 DCA removal (%)
UV, No reductant	pH 1.68		pH 6.86		pH 9	
	0	0	0	0	0	0
	82	0	94	0	100	9.2
	167	0	176	0	180	16.5
	pH 1.68		pH 6.86		pH 9	
UV, Ferrous iron	0	0	0	0	0	0
	29	0	50	73.3	29	96.5
	422	19.2	180	94.7	60	98.2
	pH 1.68		pH 6.86		pH 9	
No UV, Ferrous iron	0	0	0	0	0	0
	30	0	51	0.6	29	2.5
	420	2.2	129	0		
	pH 1.68		pH 6.86		pH 9	
UV, Sulfide	0	0	0	0	0	0
	54	0	62	61.8	32	97.5
	190	0	88	82.1	58	100
	pH 1.68		pH 6.86		pH 9	
No UV, Sulfide	0	0	0	0	0	0
	57	0	68	0	25	0
	190	0	98	0	53	1.8
	pH 2.4		pH 7.2		pH 11	
UV, Dithionite	0	0	0	0	0	0
	15	43	15	64	5	39
	120	52	120	96	285	96
	420	48	240	96		
	pH 2.4		pH 7.2		pH 11	
No UV, Dithionite	0	0	0	0	0	0
	15	0	15	0	5	0
	120	0	120	0	285	3
	420	5	240	0		
	pH 2.4		pH 7.2		pH 11	
UV, Sulfite	0	0	0	0	0	0
	17	45	15	74	15	100
	156	55	120	100		
	300	84				
	pH 2.4		pH 7.2		pH 11	
No UV, Sulfite	0	0	0	0	0	0
	17	0	15	0	15	0
	156	1.7	120	7		
	300	1.7				

Table A-9: UV-L/Nitrate kinetic control experiment

pH 3		pH 5		pH 7		pH 9	
Time (hours)	Nitrate concentration (mM)	Time (hours)	Nitrate concentration (mM)	Time (hours)	Nitrate concentration (mM)	Time (hours)	Nitrate concentration (mM)
0.00	0.16	0.00	0.16	0.00	0.18	0.00	0.16
1.97	0.15	1.25	0.16	0.53	0.15	0.60	0.15
4.38	0.15	2.85	0.15	1.03	0.15	1.14	0.14
5.90	0.14	4.15	0.15	1.53	0.14	1.73	0.13
7.98	0.14	5.62	0.15	2.12	0.14	2.01	0.13
9.92	0.14	7.25	0.14	2.70	0.14	2.58	0.12
18.57	0.13	8.78	0.14	3.17	0.14	2.99	0.12
19.82	0.13	11.25	0.14	3.72	0.13		

Table A-10: Sulfite/UV-L/Nitrate kinetic experiment, 2.8 mM sulfite concentration

pH 3		pH 5		pH 7		pH 9	
Time (hours)	Nitrate concentration (mM)	Time (hours)	Nitrate concentration (mM)	Time (hours)	Nitrate concentration (mM)	Time (hours)	Nitrate concentration (mM)
0.00	0.14	0.00	0.16	0.00	0.17	0.00	0.15
1.27	0.12	1.02	0.12	0.09	0.10	0.03	0.14
5.83	0.07	1.67	0.10	0.17	0.06	0.05	0.13
8.08	0.05	2.70	0.07	0.25	0.05	0.08	0.11
10.18	0.04	4.00	0.03	0.34	0.03	0.10	0.10
21.08	0.01	5.50	0.02	0.43	0.02	0.13	0.09
22.90	0.02	6.53	0.02	0.52	0.00	0.15	0.08
		8.70	0.00	0.60	0.00	0.18	0.07
						0.20	0.06

APPENDIX B

Table B-1: Experiment 1.

Time (hours)	Perchlorate concentration (mM)
0	0.099
1.4	0.098
2.9	0.099
5.4	0.098
7.3	0.097
9.2	0.095
20.8	0.094
23.6	0.094

Table B-2: Experiment 2.

Time (hours)	Perchlorate concentration (mM)
0	0.097
1.6	0.093
3.9	0.086
6.1	0.082
8.4	0.077
10.6	0.075
22.8	0.074

Table B-3: Experiment 3.

Time (hours)	Perchlorate concentration (mM)
0	0.098
1.93	0.079
4.08	0.062
5.92	0.052
7.93	0.046
10.08	0.036
21.92	0.023
27.07	0.023

Table B-4: Experiment 4.

Time (hours)	Perchlorate concentration (mM)	Sulfite Concentration (mM)
0	0.1	11.08
2	0.102	10.47
4	0.097	10.36
6.05	0.095	9.85
8	0.092	9.55
9.98	0.088	9.21
16.85	0.078	7.99
22	0.074	7.24

Table B-5: Experiment 5.

Time (hours)	Perchlorate concentration (mM)	Sulfite Concentration (mM)
0	0.115	11.08
1.983	0.107	10.36
3.667	0.102	9.29
5.883	0.102	8.93
8.167	0.099	7.67
13.933	0.086	5.34
15.75	0.085	5.1
24	0.077	2.71

Table B-6: Experiment 6.

Time (hours)	Perchlorate concentration (mM)	Sulfite Concentration (mM)
0	0.116	11.08
0.95	0.091	10.7
3.4	0.08	8.71
5.1	0.073	7.88
6.72	0.065	6.83
7.72	0.062	6.53
9.87	0.052	4.74
20.77	0.041	1.02

Table B-7: Experiment 7.

Time (hours)	Perchlorate concentration (mM)	Sulfite Concentration (mM)
0	0.111	11.08
0.95	0.099	10.08
2.23	0.08	8.68
3.65	0.072	7.17
5.2	0.068	5.74
6.7	0.058	4.61
8.42	0.051	3.27
10.68	0.05	1.86

Table B-8: Experiment 8.

Time (hours)	Perchlorate concentration (mM)	Sulfite Concentration (mM)
0	0.088	11.08
1.08	0.082	8.455
2.35	0.063	5.351
4.28	0.044	2.024
7.88	0.038	0.412
18.07	0.034	0.479

Table B-9: Experiment 9.

Time (hours)	Perchlorate concentration (mM)	Sulfite Concentration (mM)
0	0.103	11.08
2.1	0.104	8.79
3.9	0.104	6.98
6.1	0.104	5.01
7.3	0.105	4.15
8.4	0.105	3.44
9.9	0.106	3.20
16.8	0.105	0.73

Table B-10: Experiment 10.

Time (hours)	Perchlorate concentration (mM)	Sulfite Concentration (mM)
0	0.099	11.08
1.3	0.097	9.59
2.6	0.094	8.56
3.9	0.091	7.35
5.4	0.089	6.37
7	0.086	4.93
9.6	0.083	3.73
20.4	0.077	0.79

Table B-11: Experiment 11.

Time (hours)	Perchlorate concentration (mM)	Sulfite Concentration (mM)
0	0.108	11.08
0.9	0.104	10.81
2.1	0.100	10.17
3.3	0.095	9.63
4.6	0.092	9.27
6.3	0.086	8.24
9.4	0.077	6.98
17.5	0.064	3.98

Table B-12: Experiment 12.

Time (hours)	Perchlorate concentration (mM)	Sulfite Concentration (mM)
0	0.100	11.08
1	0.099	10.74
2	0.096	10.55
3	0.095	10.39
4	0.093	9.68
5.4	0.090	9.40
7.4	0.086	9.03
19.9	0.068	6.24

Table B-13: Experiment 13.

Time (hours)	Perchlorate concentration (mM)	Sulfite Concentration (mM)
0	0.100	11.08
0.7	0.096	10.41
1.5	0.092	9.78
2.4	0.087	9.29
3.7	0.082	8.43
5	0.077	7.48
6.5	0.073	6.54
8.4	0.067	5.26

Table B-14: Experiment 14.

Time (hours)	Perchlorate concentration (mM)	Sulfite Concentration (mM)
0.00	0.108	1.26
0.60	0.108	1.22
2.33	0.105	0.98
3.67	0.105	1.10
4.67	0.102	0.96
5.72	0.102	0.91
6.75	0.100	0.65
7.78	0.099	0.61

Table B-15: Experiment 15.

Time (hours)	Perchlorate concentration (mM)	Chlorate concentration (mM)	Chloride concentration (mM)	Sulfite Concentration (mM)
0.00	0.102	0.0000	0.0000	3.76
0.92	0.098	-0.0009	0.0034	3.44
2.33	0.094	0.0019	0.0013	2.96
3.83	0.090	0.0048	0.0044	2.54
5.32	0.086	0.0075	0.0039	2.43
6.77	0.083	0.0092	0.0023	2.14
8.18	0.081	0.0106	0.0027	1.66
9.63	0.078	0.0134	0.0046	1.30

Table B-16: Experiment 16.

Time (hours)	Perchlorate concentration (mM)	Sulfite Concentration (mM)
0	0.102	37.50
0.8	0.099	36.64
1.6	0.096	35.97
2.8	0.091	34.24
4.3	0.086	32.60
5.8	0.081	31.25
7.6	0.075	29.18
9.6	0.069	27.30

Table B-17: Experiment 17.

Time (hours)	Perchlorate concentration (mM)	Sulfite Concentration (mM)
0	0.099	113.70
0.8	0.095	111.44
1.5	0.092	107.07
2.5	0.089	106.00
3.9	0.086	103.93
5.3	0.082	101.09
7.2	0.079	98.70
9.3	0.073	94.16

Table B-18: Perchlorate no-circulation data.

Expt#	Initial ClO_4^- concentration (mM)	Initial SO_3^{2-} concentration (mM)	Light intensity (mW/cm^2)	pH	First-order rate constant ± 95% C.I. (hour-1)	Quantum yield ϕp	SSE	RMSE
1	9.90E-02	11.08	8	7	-3.50E-03±2.92E-03	1.71E-05±1.43E-05	2.63E-06	8.11E-04
2	9.70E-02	11.08	8	9	-2.53E-02±5.30E-03	1.09E-04±2.28E-05	8.36E-06	1.45E-03
3	9.80E-02	11.08	8	11	-1.00E-01±1.17E-02	4.20E-04±4.91E-05	1.61E-05	2.01E-03
4	1.02E-01	11.08	1.45	11	-1.51E-02±2.45E-03	3.64E-04±5.90E-05	1.67E-05	1.67E-03
5	1.15E-01	11.08	4	11	-1.65E-02±3.17E-03	1.62E-04±3.12E-05	3.61E-05	2.45E-03
6	1.16E-01	11.08	7	11	-7.58E-02±2.17E-02	4.30E-04±1.23E-04	1.52E-04	5.52E-03
7	1.11E-01	11.08	12	11	-9.45E-02±2.10E-02	2.99E-04±6.65E-05	9.10E-05	4.27E-03
8	8.80E-02	11.08	20	11	-1.59E-01±1.00E-01	2.39E-04±1.51E-04	4.06E-05	4.51E-03

Table B-19: Perchlorate circulation data.

Expt#	Initial ClO_4^- concentration (mM)	Initial SO_3^{2-} concentration (mM)	Light intensity (mW/cm^2)	pH	First-order rate constant ± 95% C.I. (hour-1)	Quantum yield ϕp	**SSE**	RMSE
9	1.03E-01	11	7	7	2.95E-03±9.24E-04	0.00E+00±0.00E+00	5.36E-07	3.27E-04
10	9.90E-02	11	7	9	-1.92E-02±2.35E-03	9.61E-05±2.35E-05	2.24E-06	6.69E-04
11	1.08E-01	11	7	11	-3.56E-02±1.89E-03	1.88E-04±2.00E-05	1.35E-06	5.20E-04
12	1.00E-01	11	2.1	11	-2.07E-02±1.85E-03	3.37E-04±3.02E-05	8.74E-07	4.18E-04
13	1.00E-01	11	9.8	11	-4.84E-02±3.35E-03	1.69E-04±1.17E-05	4.22E-06	8.39E-04
14	1.08E-01	1.26	7	11	-1.19E-02±1.51E-03	4.68E-04±5.93E-05	1.37E-06	4.78E-04
15	1.02E-01	3.76	7	11	-2.74E-02±2.80E-03	3.58E-04±3.67E-05	5.10E-06	9.22E-04
16	1.02E-01	37.5	7	11	-4.09E-02±1.16E-03	9.85E-05±2.79E-06	7.37E-07	3.51E-04
17	9.90E-02	110.8	7	11	-3.12E-02±2.99E-03	5.83E-05±5.59E-06	4.55E-06	8.71E-04

Table B-20: Sulfite no-circulation data.

Expt #	Initial ClO_4^- concentration (mM)	Initial SO_3^{2-} concentration (mM)	Light intensity (mW/cm^2)	pH	First-order rate constant ± 95% C.I. (hour-1)	Quantum yield ϕs	**SSE**	RMSE
4	1.02E-01	11.08	1.45	11	-1.91E-02±1.36E-03	4.95E-02±3.53E-03	4.35E+00	8.51E-01
5	1.15E-01	11.08	4	11	-5.29E-02±7.55E-03	4.98E-02±7.11E-03	6.48E+01	3.29E+00
6	1.16E-01	11.08	7	11	-8.48E-02±1.73E-02	4.56E-02±9.33E-03	1.41E+02	4.85E+00
7	1.11E-01	11.08	12	11	-1.41E-01±1.94E-02	4.43E-02±6.09E-03	7.65E+01	3.57E+00
8	8.80E-02	11.08	20	11	-3.48E-01±9.24E-02	6.55E-02±1.74E-02	9.24E+01	4.81E+00

Table B-21: Sulfite circulation data.

Expt #	Initial ClO_4^- concentration (mM)	Initial SO_3^{2-} concentration (mM)	Light intensity (mW/cm^2)	pH	First-order rate constant ± 95% C.I. (hour-1)	Quantum yield± 95% C.I. ϕ_S	SSE	RMSE
9	1.03E-01	11	7	7	-1.34E-01±1.29E-02	8.35E-02±8.01E-03	3.89E+01	2.55E+00
10	9.90E-02	11	7	9	-1.13E-01±1.00E-02	6.30E-02±5.58E-03	2.49E+01	2.04E+00
11	1.08E-01	11	7	11	-5.43E-02±7.54E-03	2.92E-02±4.06E-03	4.01E+01	2.58E+00
12	1.00E-01	11	2.1	11	-2.90E-02±2.77E-03	5.21E-02±4.97E-03	8.96E+00	1.22E+00
13	1.00E-01	11	9.8	11	-8.28E-02±7.94E-03	3.18E-02±3.05E-03	1.76E+01	1.71E+00
14	1.08E-01	1.26	7	11	-7.89E-02±3.38E-02	3.62E-02±1.55E-02	3.65E+02	7.80E+00
15	1.02E-01	3.76	7	11	-9.63E-02±1.57E-02	4.65E-02±7.60E-03	7.76E+01	3.60E+00
16	1.02E-01	37.5	7	11	-3.33E-02±1.18E-03	2.95E-02±1.05E-03	7.91E-01	3.63E-01
17	9.90E-02	110.8	7	11	-1.90E-02±3.43E-03	3.98E-02±7.18E-03	6.99E+00	1.08E+00

Perchlorate/sulfite/catalyst experiments:

- Perchlorate concentration ≅ 5 ppm ≅ 0.05 mM.
- Catalyst concentration ≅ 1.6 mM
- Sulfite concentration ≅ 8 mM
- No buffer

Catalyst Source:

- Ferrous Iron
  - $FeSO_4.7H_2O$
- Ferric Iron
  - $FeCl_3.6H_2O$
- Copper
  - $CuCl_2.2H_2O$
- Rubidium
  - RbCl
- Molybdenum
  - $(NH_4)_6Mo_7O_{24}.4H_2O$
- Nickel
  - $NiSO_4.6H_2O$
- Titanium
  - $TiCl_3$
- Vanadium
  - Vanadium (II) Oxide
- Osmium
  - Osmium (III) Chloride, trihydrate
- Tungsten
  - Tungsten (VI) Chloride

Table B-22: Summary of catalyst experiments at different pH.

Catalyst	Perchlorate: C_t/C_0*100			
	pH 3	pH 5	pH 7	pH 9
Ferrous Iron	99	104	104	111
Nickel	98	110	99	102
Titanium	108	95	231	119
Copper	95	107	101	100
Ferric Iron	110	101	100	98
Rubidium	105	92	103	105
Molybdenum	98	103	102	97

Perchlorate/ UV-L /Sulfite/Ferric iron/ experiments:

- Perchlorate concentration ≅ 10 ppm ≅ 0.1 mM.
- Ferric iron concentration ≅ 2.1 mM
- Sulfite concentration ≅ 11.5 mM
- No buffer

Table B-23: Ferric iron as catalyst, pH 4.4.

UV meter reading in $\mu W/cm^2$	Irradiation time in hours	Concentration in mM
	0.0	0.096
7980	4.5	0.094
8080	22.4	0.110

Table B-24: Ferric iron as catalyst, pH 6.9.

UV meter reading in $\mu W/cm^2$	Irradiation time in hours	Concentration in mM
	0.0	0.099
7850	4.5	0.097
9030	22.4	0.097

Table B-25: Ferric iron as catalyst, pH 9.1.

UV meter reading in $\mu W/cm^2$	Irradiation time in hours	Concentration in mM
	0.0	0.097
7730	4.5	0.093
9010	22.4	0.079

Perchlorate/ UV-L /Sulfite/Catalyst/ experiments:

- Perchlorate concentration ≅ 10 ppm ≅ 0.1 mM.
- Catalyst concentration ≥ 5 mM
- Sulfite concentration ≅ 11.5 mM
- No buffer

Table B-26: List of catalysts.

Catalyst set	Catalyst
Set 1	Ferrous iron Copper
Set 2	Rubidium Nickel Molybdenum
Set 3	Titanium Tungsten Vanadium Osmium

Table B-27: Set 1 catalyst experiment, pH 11.14.

UV meter reading in $\mu W/cm^2$	Irradiation time in hours	Concentration in mM
	0.0	0.094
8030	15.0	0.067
8750	24.8	0.056

Table B-28: Set 2 catalyst experiment, pH 11.

UV meter reading in $\mu W/cm^2$	Irradiation time in hours	Concentration in mM
	0.0	0.091
7800	15.0	0.092
8860	24.8	0.092

Table B-29: Set 3 catalyst experiment, pH 11.05.

UV meter reading in $\mu W/cm^2$	Irradiation time in hours	Concentration in mM
	0.0	0.098
7800	15.0	0.097
8790	24.8	0.102

APPENDIX C

Table C-1: Experiment 1.

Time (hours)	Nitrate concentration (mM)	Nitrite concentration (mM)	Sulfite concentration (mM)
0.00	0.164	0.000	2.80
1.00	0.148	0.007	2.66
2.00	0.136	0.013	2.58
3.00	0.124	0.008	2.38
4.00	0.114	0.007	2.35
5.00	0.116	0.008	2.18
6.00	0.101	0.006	2.15
7.00	0.091	0.006	2.06

Table C-2: Experiment 2.

Time (hours)	Nitrate concentration (mM)	Nitrite concentration (mM)	Sulfite concentration (mM)
0.00	0.161	0.000	2.80
0.07	0.130	0.027	2.82
0.13	0.103	0.053	2.82
0.20	0.088	0.066	2.81
0.27	0.062	0.082	2.80
0.33	0.041	0.090	2.73
0.40	0.033	0.094	2.72
0.47	0.034	0.097	2.75
0.53	0.012	0.083	2.62
0.60	0.004	0.066	2.56
0.70	0.003	0.061	2.47

Table C-3: Experiment 3.

Time (hours)	Nitrate concentration (mM)	Nitrite concentration (mM)	Sulfite concentration (mM)
0.00	0.163	0.000	2.80
0.08	0.154	0.007	2.76
0.13	0.154	0.015	2.75
0.21	0.146	0.022	2.74
0.27	0.138	0.030	2.78
0.33	0.130	0.037	2.72
0.40	0.125	0.043	2.80
0.47	0.115	0.050	2.76
0.53	0.112	0.052	2.73
0.60	0.100	0.062	2.71
0.67	0.101	0.063	2.84

Table C-4: Experiment 4.

Time (hours)	Nitrate concentration (mM)	Nitrite concentration (mM)	Sulfite concentration (mM)
0.00	0.165	0.000	2.80
0.07	0.123	0.039	2.90
0.13	0.087	0.066	2.88
0.20	0.070	0.075	2.88
0.27	0.039	0.086	2.76
0.33	0.026	0.084	2.67
0.40	0.015	0.078	2.63
0.47	0.011	0.071	2.54
0.53	0.001	0.037	2.34
0.60	0.000	0.019	2.24
0.70	0.000	0.013	2.22

Table C-5: Experiment 5.

Time (hours)	Nitrate concentration (mM)	Nitrite concentration (mM)	Sulfite concentration (mM)
0.00	0.165	0.000	0.94
0.07	0.158	0.002	0.98
0.13	0.153	0.012	0.98
0.20	0.145	0.016	0.98
0.27	0.139	0.022	0.98
0.33	0.135	0.025	0.96
0.40	0.128	0.034	0.99
0.47	0.117	0.045	1.03
0.63	0.105	0.051	0.99
0.80	0.094	0.063	1.00
1.00	0.072	0.070	0.96

Table C-6: Experiment 6.

Time (hours)	Nitrate concentration (mM)	Nitrite concentration (mM)	Sulfite concentration (mM)
0.00	0.180	0.000	2.80
0.07	0.155	0.015	2.82
0.13	0.137	0.032	2.83
0.20	0.128	0.036	2.85
0.27	0.106	0.050	2.87
0.33	0.091	0.058	2.82
0.40	0.083	0.062	2.84
0.47	0.064	0.084	2.85
0.53	0.050	0.088	2.85
0.60	0.049	0.089	2.83
0.70	0.040	0.091	2.85

Table C-7: Experiment 7.

Time (hours)	Nitrate concentration (mM)	Nitrite concentration (mM)	Sulfite concentration (mM)
0.00	0.161	0.000	8.50
0.07	0.129	0.032	8.54
0.13	0.100	0.053	8.55
0.20	0.071	0.069	8.56
0.27	0.049	0.078	8.49
0.33	0.049	0.079	8.47
0.40	0.036	0.083	8.42
0.47	0.022	0.080	8.38
0.53	0.015	0.071	8.51
0.60	0.010	0.056	8.25
0.67	0.004	0.037	8.08

Table C-8: Experiment 8.

Time (hours)	Nitrate concentration (mM)
0.00	0.146
0.93	0.132
1.77	0.120
3.09	0.104
4.60	0.098
6.12	0.090
7.93	0.074
10.42	0.053

Table C-9: Experiment 9.

Time (hours)	Nitrate concentration (mM)
0.00	0.154
0.50	0.140
0.98	0.123
1.50	0.109
1.99	0.098
2.48	0.085
3.27	0.069
4.08	0.053

Table C-10: Experiment 10.

Time (hours)	Nitrate concentration (mM)
0.00	0.182
0.02	0.159
0.03	0.149
0.05	0.140
0.07	0.131
0.08	0.123
0.11	0.110
0.13	0.099
0.17	0.080
0.21	0.067
0.26	0.040

Table C-11: Experiment 11.

Time (hours)	Nitrate concentration (mM)
0.00	0.142
0.01	0.137
0.02	0.130
0.03	0.123
0.03	0.113
0.04	0.104
0.05	0.092
0.06	0.085
0.07	0.077
0.08	0.081
0.08	0.063
0.09	0.058

Table C-12: Nitrate circulation data.

Expt#	Initial NO_3^- concentration (mM)	Initial SO_3^{2-} concentration (mM)	Light intensity (mW/cm^2)	pH	First-order rate constant ± 95% C.I. (hour-1)	Quantum yield ϕn	**SSE**	RMSE
1	1.64E-01	2.8	2.8	5	-7.91E-02±1.20E-02	1.27E-02±8.86E-03	8.94E-05	3.86E-03
2	1.61E-01	2.8	2.8	9	-3.90E+00±5.54E-01	2.77E-01±3.93E-02	5.26E-04	7.64E-03
3	1.63E-01	2.8	1	7	-7.59E-01±8.01E-02	1.74E-01±1.83E-02	8.91E-05	3.15E-03
4	1.65E-01	2.8	8	7	-5.34E+00±6.94E-01	1.55E-01±2.01E-02	3.92E-04	6.60E-03
5	1.65E-01	9.40E-01	2.8	7	-7.56E-01±7.31E-02	1.80E-01±1.74E-02	1.10E-04	3.49E-03
6	1.80E-01	2.80E+00	2.8	7	-2.12E+00±1.81E-01	1.91E-01±1.63E-02	2.14E-04	4.88E-03
7	1.61E-01	8.40E+00	2.8	7	-4.12E+00±3.82E-01	1.22E-01±1.13E-02	2.16E-04	4.90E-03

Table C-13: Nitrite circulation data.

Expt#	Initial NO_3^- concentration (mM)	Initial SO_3^{2-} concentration (mM)	Light intensity (mW/cm^2)	pH	First-order rate constant ± 95% C.I. (hour-1)	**SSE**	RMSE
1	1.64E-01	2.8	2.8	5	1.25E+00±2.64E-01	1.97E-05	1.68E-03
2	1.61E-01	2.8	2.8	9	1.66E+00±2.78E-01	5.83E-04	7.63E-03
3	1.63E-01	2.8	1	7	1.11E-02±9.25E-02	2.47E-05	1.57E-03
4	1.65E-01	2.8	8	7	3.37E+00±7.84E-01	1.76E-03	1.33E-02
5	1.65E-01	9.40E-01	2.8	7	4.86E-01±2.31E-01	2.57E-04	5.07E-03
6	1.80E-01	2.80E+00	2.8	7	1.32E+00±4.50E-01	1.30E-03	1.14E-02
7	1.61E-01	8.40E+00	2.8	7	2.34E+00±3.35E-01	5.31E-04	7.29E-03

Table C-14: Nitrate no-circulation data.

Expt #	Initial NO_3^- concentration (mM)	Initial SO_3^{2-} concentration (mM)	Light intensity (mW/cm^2)	pH	First-order rate constant ± 95% C.I. (hour-1)	Quantum yield ϕn	**SSE**	RMSE
8	1.46E-01	8.5	4	3	-8.70E-02±1.30E-02	1.21E-03±1.80E-04	1.14E-04	4.36E-03
9	1.54E-01	8.5	4	5	-2.49E-01±1.75E-02	9.84E-03±6.91E-04	3.41E-05	2.38E-03
10	1.82E-01	8.5	4	7	-4.83E+00±5.19E-01	1.24E-01±1.33E-02	2.54E-04	5.31E-03
11	1.42E-01	8.5	4	9	-9.41E+00±1.10E+00	1.70E-01±1.98E-02	2.18E-04	4.67E-03

APPENDIX D

COMPUTER PROGRAM (MATLAB) TO PREDICT PERCHLORATE/NITRATE DEGRADATION BY SULFITE/UV-L

This program calculates the sulfite quantum yield and reaction rate constant of the target contaminant with the $SO_3^{\bullet-}$ radical.

```
clear all
clc
tic;
%input kinetic experiment data
t_hr_exp= [0    0.066666667 0.133333333 0.2 0.266666667 0.333333333 0.4
0.466666667 0.633333333 0.8 1];
nitrate_exp=[0.164899215    0.157805372 0.152682325 0.144924984 0.139300167
0.135357529 0.127844451 0.117476712 0.104633487 0.094242231 0.07188243];
sulf_exp=[0.94  0.977933481 0.977099778 0.975015521 0.980851441 0.958341463
0.988771619 1.031707317 0.993773836 1.002527716 0.955423503];


q1 = 0.0:0.01:1;                %sulfite quantum yield
k1 = logspace(1,20,100);        %reaction rate constant of SO3•- with target
err_old = 10e10;
err_mat=zeros(length(q1),length(k1));

%calculate combination of quantum yield and reaction rate constant that gives least sum
of squared errors for the target and sulfite concentrations, normalized by the respective
initial concentrations

i=1;
for q1 = 0.0:0.01:1
   j=1;
   for k1 = logspace(1,20,100)

      arpsim254_input2(q1,k1);
      [t,c]=arpsim254_run;
      t_hr=t./3600;

      c_mod_nitrate=interp1(t_hr,c(:,21),t_hr_exp);
      c_mod_sulf=interp1(t_hr,c(:,26),t_hr_exp);
```

```
        err = sum(((nitrate_exp./1000-
        c_mod_nitrate)./(nitrate_exp(1)/1000)).^2)+sum(((sulf_exp./1000-
        c_mod_sulf)./(sulf_exp(1)/1000)).^2);

       if(err < err_old)

        err_old = err;
        min_values = [q1,k1];
        end;

      err_mat(i,j) = err;
      j=j+1;


   end
   i=i+1
end

toc;

min_values
```

```
function dummy=arpsim254_input(q1,k1)%(data_input)
% m-file to organize input for kinetic model that simulate radical
% reactions occurring in advanced reduction processes
% Variables:

% s = (n x m+1) matrix of stoichiometric coefficients
% c0 = (1 x m) matrix of initial concentrations of species
% k = (1 x n) matrix of rate coefficients

% Initialize matrices
n= 90;            % number of reactions
m= 33;             % number of species
c0=zeros(m,1); % initial concentrations, M
s=zeros(n,m);  % stoichiometric coefficients
k=zeros(1,n); % rate constants, can be second order (L/mol-s) or first-order (1/s)
mol_abs=zeros(1,m);

% Initialize Variables
tstop = 3600;    % time to stop simulation (s)
ph = 7 ;% pH of solution
r_vol =1.6e-5; % volume of reactor (m^3)
I0 = 0.596e-4; % light flux entering reactor (einstein/m^2-s)
r_area= 1.5e-3; % area of reactor perpindicular to light, m^2
h_nu_av= 4.715e5; % light energy = h*nu*Av =h c/lambda * Av, J/einstein (=4.715E5
J/E for 253.7 nm)
k1co3=10^-6.352; % first acid dissosciation constant for carbonic acid, VMinteq Ver. 3
k2co3=10^-10.329; % second acid dissosciation constant for carbonic acid,VMinteq
Ver. 3
k1so3=10^-1.85; %first acid dissosciation constant for sulfurous acid,VMinteq Ver. 3
k2so3=10^-7.19; %second acid dissosciation constant for sulfurous acid, VMinteq Ver.
3
kw=10^-13.997; % dissociation constant for water, VMinteq Ver. 3
abs_coef_water = 1.59; % absorption coefficient (ln based) for water (m-1)ref: Hale and
Querry, 1973.
q_yield_so3= q1;% quantum yield of reaction producing sulfite radical anion and e;
from
              % Fischer 1996
%specify options for ODE solver (Relative error tolerance, absolute error
%tolerance, and specify that all concentrations be non-negative)
options=odeset('RelTol', 1e-6, 'AbsTol', 1e-9, 'NonNegative', [1:m]);


% c0, initial concentations of all species, (M)
c0(1)=0;  % OH'
```

```
c0(2)=0;  % H2O2
c0(3)=0;  % eaq-
c0(4)=0;  % H'
c0(5)=0;  % H2
c0(6)=10^-ph;   % H+
c0(7)=kw/c0(6); % OH-
c0(8)=0;  % HO2'
c0(9)=0;  % HO2-'
c0(10)=0; % HO2-
c0(11)=0; % H2O2+
c0(12)=0; % OH-'
c0(13)=0; % O2
c0(14)=0; % O2-
c0(15)=0; % O2-'
c0(16)=0; % O22-
c0(17)=0; %O-'
c0(18)=0; % HCO3-
c0(19)=k2co3*c0(18)/c0(6); % CO32-
c0(20)=0; % CO3-'
c0(21)=0.000164899215; % NO3-
c0(22)=0; % NO32-'
c0(23)=0; % Cl-
c0(24)=0; % ClOH
c0(25)=c0(6)*c0(18)/k1co3; % H2CO3
c0(26)= 0.00094; % total sulfite (H2SO3+SO2, HSO3-, SO32-)
c0(27)=0; % sulfite radical anion, SO3-'
c0(28)=0; % unspecified target compound
c0(29)=0; %NO2'
c0(30)=0; %HNO2
c0(31)=0; %NO2-
c0(32)=0; %NO
c0(33)=0; %NO2-2

% Calculate variables that depend on others
alpha2_so3=k1so3*k2so3/(c0(6)^2+c0(6)*k1so3+k1so3*k2so3); % second ionization
fraction for SO3
mol_abs(26) = 4170*alpha2_so3; % molar abs for SO3 at 254 nm, ln-basis; source is
measurement (18.1 M^-1 cm^-1, decadic)
                        % made by Bhanu Prakash (11/4/2010)
                        % assumes HSO3 does not absorb at 254 nm
r_l = r_vol/r_area; % calculate depth of reactor in direction of light path
I0_l=I0/r_l; % ratio of incident light intensity to thickness of reactor (Einstein/m^3-s).
```

```
% Specify reactions, stoichiometric coefficients and rate equations
%(1) OH' + H2 --> H' + H2O     (k = 4.2*10^7 M-1 s-1)Ref: Buxton,  et al., 1988
%     1    5      4
   s(1,1)=-1;s(1,5)=-1;s(1,4)=1;
   k(1)=4.2e7;

%(2) OH' + H2O2 --> HO2' + H2O      (k = 2.7*10^7 M-1 s-1)Buxton,  et al., 1988
%     1      2       8
   s(2,1)=-1; s(2,2)=-1; s(2,8)=1;
   k(2)=2.7e7;

%(3) OH' + O2-' --> O2 + OH-     (k = 8.0*10^9 M-1 s-1)Ref: Buxton,  et al., 1988
%     1     15      13   7
   s(3,1)=-1; s(3,15)=-1; s(3,13)=1; s(3,7)=1;
   k(3)=8.0e9;

%(4) OH' + HO2' --> H2O + O2     (k = 6.0*10^9 M-1 s-1)Ref: Buxton,  et al., 1988
%      1     8              13
   s(4,1)=-1; s(4,8)=-1; s(4,13)=1;
   k(4)=6.0e9;

%(5) OH' + OH' --> H2O2     (k = 5.5 *10^9 M-1 s-1)Ref: Buxton,  et al., 1988
%     1     1       2
   s(5,1)=-2; s(5,2)=1;
   k(5)=5.5e9;

%(6) OH' + OH- --> O-' + H2O     (k = 1.3*10^10 M-1 s-1) Ref: Buxton,  et al., 1988
%     1     7       17
   s(6,1)=-1; s(6,7)=-1;
   k(6)=1.3e10;

%(7) OH' + H2O2+ --> H+ + H2O     (k = 1.2*10^10 M-1 s-1)Ref: Buxton,  et al., 1988
%     1     11       6
   s(7,1)=-1; s(7,11)=-1; s(7,6)=1;
   k(7)=1.2e10;

%(8) OH' + O-' --> HO2-     (k = 2.0*10^10 M-1 s-1)Ref: Buxton,  et al., 1988
%     1     17      10
   s(8,1)=-1; s(8,17)=-1; s(8,10)=1;
   k(8)=2.0e10;

%(9) OH' + HO2- --> HO2' + OH-     (k = 7.5*10^9 M-1 s-1) Ref: Buxton,  et al., 1988
%     1     10       8      7
   s(9,1)=-1; s(9,10)=-1; s(9,8)=1; s(9,7)=1;
```

```
   k(9)=7.5e9;

%(10) eaq- + H' + H2O --> H2 + OH-      (k = 2.5*10^10 M-1 s-1)Ref: Buxton,  et al.,
1988
%      3     4           5    7
   s(10,3)=-1; s(10,4)=-1; s(10,5)=1; s(10,7)=1;
   k(10)=2.5e10;

%(11) eaq- + eaq- + 2H2O --> 2 OH- + H2 (k = 5.5*10^9 M-1 s-1)Ref: Buxton,  et al.,
1988
%     3     3               7     5
   s(11,3)=-2; s(11,7)=2; s(11,5)=1;
   k(11)=5.5e9;

%(12) eaq- + H2O2 --> OH' + OH-     (k = 1.1*10^10 M-1 s-1)Ref: Buxton,  et al., 1988
%     3     2        1    7
   s(12,3)=-1; s(12,2)=-1; s(12,1)=1; s(12,7)=1;
   k(12)=1.1e10;

%(13) eaq- + O2 --> O2-'     (K = 1.9*10^10 M-1 s-1)Ref: Buxton,  et al., 1988
%     3     13     15
   s(13,3)=-1; s(13,13)=-1; s(13,15)=1;
   k(13)=1.9e10;

%(14) eaq- + O2-' --> O22-     (k = 1.3*10^10 M-1 s-1)Ref: Buxton,  et al., 1988
%     3     15       16
   s(14,3)=-1; s(14,15)=-1; s(14,16)=1;
   k(14)=1.3e10;

%(15) eaq- + H+ --> H'    (k = 2.3*10^10 M-1 s-1)Ref: Buxton,  et al., 1988
%     3     6     4
   s(15,3)=-1; s(15,6)=-1; s(15,4)=1;
   k(15)=2.3e10;

%(16) eaq- + H2O  --> H' + OH- (k = 1.9*10^1 s-1)Ref: Buxton,  et al., 1988
%     3            4     7
   s(16,3)=-1; s(16,4)=1; s(16,7)=1;
   k(16)=1.9e1;

%(17) eaq- + HO2- --> products     (k = 3.5*10^9 M-1 s-1)Ref: Buxton,  et
%al., 1988; Buxton does not show products, but Zele uses OH' and 2OH-
%although it is not balanced
%     3     10
   s(17,3)=-1; s(17,10)=-1;
```

```
   k(17)=3.5e9;

%(18) eaq- + OH' --> OH-    (k = 3.0*10^10 M-1 s-1) Ref: Buxton,  et al., 1988
%     3     1       7
   s(18,3)=-1; s(18,1)=-1; s(18,7)=1;
   k(18)=3.0e10;

%(19) eaq- + O'- + H2O --> 2OH-     (k = 2.2*10^10 M-1 s-1)Ref: Buxton,  et
%al., 1988; water not in Buxton, but needed for balance
%     3    17             7
   s(19,3)=-1; s(19,17)=-1; s(19,7)=2;
   k(19)=2.2e10;

%(20) H' + O2 --> HO2'     (k = 2.1*10^10 M-1 s-1)Ref: Buxton,  et al., 1988
%     4    13      8
   s(20,4)=-1; s(20,13)=-1; s(20,8)=1;
   k(20)=2.1e10;

%(21) H' + O2-' --> HO2-'     (k = 2.0*10^10 M-1 s-1, Ref?)
%     4     15       9
   s(21,4)=-1; s(21,15)=-1; s(21,9)=1;
   k(21)=2.0e10;

%(22) H' + H' --> H2     (k = 7.8*10^9 M-1 s-1)Ref: Buxton,  et al., 1988
%     4    4      5
   s(22,4)=-2; s(22,5)=1;
   k(22)=7.8e9;

%(23) H' + OH' --> H2O     (k = 7.0*10^9 M-1 s-1)Ref: Buxton,  et al., 1988
%     4     1
   s(23,4)=-1; s(23,1)=-1;
   k(23)=7.0e9;

%(24) H' + HO2' --> H2O2     (k = 1.0*10^10 M-1 s-1)Ref: Buxton,  et al., 1988
%     4     8        2
   s(24,4)=-1; s(24,8)=-1; s(24,2)=1;
   k(24)=1.0e10;

%(25) H' + H2O2 --> H2O + OH'    (k = 9.0*10^7 M-1 s-1)Ref: Buxton,  et al., 1988
%     4     2              1
   s(25,4)=-1; s(25,2)=-1; s(25,1)=1;
   k(25)=9.0e7;

%(26) H' + OH- --> eaq- + H2O     (k = 2.2*10^7 M-1 s-1)Ref: Buxton,  et al., 1988
```

```
%     4     7       3
   s(26,4)=-1; s(26,7)=-1; s(26,3)=1;
   k(26)=2.2e7;

%(27) H' + H2O -->  H2 + OH'  (k = 1.0*10^1 s-1)Ref: Buxton,  et al., 1988 (assume
first-order, unrecomended value, too low to measure accurately)
%     4             5     1
   s(27,4)=-1; s(27,5)=1; s(27,1)=1;
   k(27)=1.0e1;

%(28) O-' + H2O --> OH' + OH- (k = 1.8*10^6 s-1)Ref:Buxton,  et al., 1988 (assume
first-order)
%     17            1     7
   s(28,17)=-1; s(28,1)=1; s(28,7)=1;
   k(28)=1.8e6;

%(29) O-' + HO2- --> O2-' + OH-      (k = 4.0*10^8 M-1 s-1)Ref: Buxton,  et al., 1988
%      17    10       15     7
   s(29,17)=-1; s(29,10)=-1; s(29,15)=1; s(29,7)=1;
   k(29)=4.0e8;

%(30) O-' + H2 --> H' + OH-      (k = 8.0*10^7 M-1 s-1)Ref: Buxton,  et al., 1988
%     17    5      4     7
   s(30,17)=-1; s(30,5)=-1; s(30,4)=1; s(30,7)=1;
   k(30)=8.0e7;

%(31) O-' + H2O2 --> O2-' + H2O      (k = 5.0*10^8 M-1 s-1)Ref: Buxton,  et al., 1988
%     17     2        15
   s(31,17)=-1; s(31,2)=-1; s(31,15)=1;
   k(31)=5.0e8;

%(32) O-' + O2-' --> 2OH- + O2      (k = 6.0*10^8 M-1 s-1)Ref: Buxton,  et al., 1988
%     17     15       7      13
   s(32,17)=-1; s(32,15)=-1; s(32,7)=2; s(32,13)=1;
   k(32)=6.0e8;

%(33) HO2' + O2-' --> O2 + H2O2 + OH-      (k = 9.7*10^7 M-1 s-1) Ref: Zele et al.,
1998
%      8      15       13   2      7
   s(33,8)=-1; s(33,15)=-1; s(33,13)=1; s(33,2)=1; s(33,7)=1;
   k(33)=9.7e7;

%(34) HO2' + HO2' --> H2O2 + O2      (k = 8.3*10^5 M-1 s-1)Ref: Zele et al., 1998
%      8      8        2     13
```

```
   s(34,8)=-2; s(34,2)=1; s(34,13)=1;
   k(34)=8.3e5;

%(35) HO2' --> H+ + O2-'     (k = 8.0*10^5 M-1 s-1)Ref: Zele et al., 1998
%     8       6    15
   s(35,8)=-1; s(35,6)=1; s(35,15)=1;
   k(35)=8.0e5;

%(36) H+ + O2-' --> HO2'     (k = 4.5*10^10 M-1 s-1)Ref: Zele et al., 1998
%     6    15       8
   s(36,6)=-1; s(36,15)=-1; s(36,8)=1;
   k(36)=4.5e10;

%(37) H+ + OH- --> H2O     (k = 1.4*10^11 M-1 s-1) Ref: from Laidler 1965 in Stumm
and Morgan, p. 71
%     6    7
   s(37,6)=-1; s(37,7)=-1;
   k(37)=1.4e11;

%(38) H+ + HO2-' --> H2O2     (k = 2.0*10^10 M-1 s-1)Ref: Zele et al., 1998
%     6    9        2
   s(38,6)=-1; s(38,9)=-1; s(38,2)=1;
   k(38)=2.0e10;

%(39) H2O2 --> H+ + HO2-'     (k = 3.6*10^-2 M-1 s-1)Ref: Zele et al., 1998
%     2       6    9
   s(39,2)=-1; s(39,6)=1; s(39,9)=1;
   k(39)=3.6e-2;

%(40) hold for future addition

%(41) HCO3- + eaq- --> products     (k = 1.0*10^6 M-1 s-1) Ref: Buxton et al. 1988
(give value as maximum)
%     18     3
   s(41,18)=-1; s(41,3)=-1;
   k(41)=1.0e6;

%(42) HCO3- + H' --> products     (k = 4.4*10^4 M-1 s-1)Ref: Buxton et al. 1988
%     18    4
   s(42,18)=-1; s(42,4)=-1;
   k(42)=4.4e4;

%(43) HCO3- + OH' --> CO3-' + H2O     (k = 8.5*10^6 M-1 s-1) Ref: Buxton et al.,
1988
```

```
%       18    1        20
   s(43,18)=-1; s(43,1)=-1; s(43,20)=1;
   k(43)=8.5e6;

%(44) CO32- + eaq- --> products     (k = 3.9*10^5 M-1 s-1)Ref: Buxton et al., 1988
%      19      3
   s(44,19)=-1; s(44,3)=-1;
   k(44)=3.9e5;

%(45) CO32- + OH' --> CO3-' + OH-     (k = 3.9*10^8 M-1 s-1)Ref: Buxton et al., 1988
%     19       1       20      7
   s(45,19)=-1; s(45,1)=-1; s(45,20)=1; s(45,7)=1;
   k(45)=3.9e8;

%(46) CO3-' + OH' --> products     (k = 3.0*10^9 M-1 s-1)Ref: Zele et al., 1998
%      20      1
   s(46,20)=-1; s(46,1)=-1;
   k(46)=3.0e9;

%(47) NO3- + eaq- --> NO32-'     (k = 9.7*10^9 M-1 s-1)Ref: Buxton et al., 1988
%      21     3         22
   s(47,21)=-1; s(47,3)=-1; s(47,22)=1;
     k(47)=9.7e9;

%(48) NO3- + H' --> products     (k = 1.4*10^6 M-1 s-1)Ref: Buxton et al., 1988
%      21    4
   s(48,21)=-1; s(48,4)=-1;
      k(48)= 1.4e6;

%(49) NO32-' + O2 --> O2-' + NO3-     (k = 2*10^8 M-1 s-1) Neta et al. 1988
%      22     13      15    21
   s(49,22)=-1; s(49,13)=-1; s(49,15)=1; s(49,21)=1;
   k(49)=2e8;

%(50) Cl- + eaq- --> products     (k = 1.0*10^6 M-1 s-1)Ref: Buxton et al. 1988 (give
value as maximum)
%      23    3
   s(50,23)=-1; s(50,3)=-1;
   k(50)=1.0e6;

%(51) Cl- + OH' --> ClOH-     (k = 4.3*10^9 M-1 s-1)Ref: Buxton et al. 1988
%     23     1       24
   s(51,23)=-1; s(51,1)=-1; s(51,24)=1;
   k(51)=4.3e9;
```

```
%(52) ClOH- --> Cl- + OH'     (k = 6.1*10^9 M-1 s-1) Zele et al., 1998
%      24       23    1
   s(52, 24)=-1; s(52,23)=1; s(52,1)=1;
   k(52)=6.1e9;

%(53) H20 --> H+ + OH-   (k = 1.4 * 10^-3 M s-1 (zeroth order); to match rxn (37) with
equilibrium constant 1e-14
%             6     7
   s(53,6)=1; s(53,7)=1;
   k(53)=1.4e-3;

%(54) H+ + HCO3- --> H2CO3 (k = 4.7*10^10 M-1 s-1; from Laidler 1965 in Stumm
and Morgan, p. 71
%     6     18        25
   s(54,6)=-1; s(54,18)=-1; s(54,25)=1;
   k(54)=4.7e10;

%(55) H2CO3 --> H+ + HCO3-     (k= 2.1 E4 s-1, calculated with equilibrium constant
and rate constant for reaction (55)
%      25       6     18
   s(55,25)=-1; s(55,6)=1; s(55,18)=1;
   k(55)=2.1e4;

%(56) H+ + CO32- --> HCO3-     (k=5*10^10 M-1 s-1; assumed value near that for
reaction (55))
%      6     19       18
   s(56,6)=-1; s(56,19)=-1; s(56,18)=1;
   k(56)=5e10;

%(57) HCO3- --> H+ + CO32-     (k = 2.4, calculated with equilibrium constant and
value of rate constant for rxn (57)
%      18       6     19
   s(57,18)=-1; s(57,6)=1; s(57,19)=1;
   k(57)=2.4;

%(58) SO32- + light --> SO3-' + eaq-  (rate calculated using quantum yield, absorbtivity
and light intensity
%      26              27     3      note: species 26 is TotSO3
   s(58,26)=-1; s(58,27)=1; s(58,3)=1;

%(59) SO32- + eaq- --> products    (k<1.5e6) Buxton et al., 1988
%      26     3                  note: species 26 is TotSO3
   s(59,26)=-1; s(59, 3)=-1;
```

```
   k(59)=1.5e6*alpha2_so3;  % modify rate constant for pH (alpha2_so3=SO32-
/TotSO3)

%(60)  SO32- + OH' = SO3-' + OH-  k=5.5e9, Buxton et al., 1988
%       26     1      27      7         note: species 26 is TotSO3
   s(60,26)=-1; s(60,1)=-1; s(60,27)=1; s(60,7)=1;
   k(60)=5.5e9*alpha2_so3; % modify rate constant for pH (alpha2_so3=SO32-
/TotSO3)

%(61)  HSO3- + OH' = SO3-' + H2O  k=4.5e9, Buxton et al., 1988
%       26      1      27      7   note: species 26 is TotSO3
   s(60,26)=-1; s(60,1)=-1; s(60,27)=1; s(60,7)=1;
   k(60)=4.5e9*(1-alpha2_so3);% modify rate constant for pH (1-alpha2_so3=HSO32-
/TotSO3)

%(62)  SO32- + O-' + H2O = SO3-' + 2OH-   k=3e8 Buxton et al., 1988 Note
%Buxton does not show OH- and water, but is needed for balance (do not add
%H+ on left hand side to avoid having it affect kinetics)
%       26     17         27      7   note: species 26 is TotSO3
   s(62,26)=-1; s(62, 17)=-1; s(62,27)=1; s(62,7)=2;
   k(62)=3e8*alpha2_so3;% modify rate constant for pH (alpha2_so3=SO32-/TotSO3)

%(63) SO3-' + eaq- --> SO32-  (k=2.1e9; Buxton et al., 1988 and 1982HOR in
NRDL/NIST Soln. Chem. database; Buxton has OH- as additional product, even though
it is not balanced
%      27      3        26
   s(63,27)=-1; s(63,3)=-1; s(63,26)=1;
   k(63)=2.1e9;

%(64) SO3-' + SO3-' --> S2O62-   k=1.8e8; 1992WAY/MCE1525-1530 in NTIS online
database
%      27      27
   s(64,27)=-2;
   k(64)=1.8e8;

%(65) SO3-' + SO3-' + H2O --> SO42- + SO32- + 2 H+   k=2.3e8;
1992WAY/MCE1525-1530 in NTIS online database
%      27      27                    26       6
   s(65,27)=-2; s(65,26)=1; s(65,6)=2;
   k(65)=2.3e8;

%(66) SO3-' + CO3-' --> CO2 + SO42-  k = 5.5 e8; 1978LIL/HAN225-227,NRDL/NIST
%       27      20
   s(66,27)=-1; s(66,20)=-1;
```

```
   k(66)=5.5e8;

%(67) SO3-' + O2 --> SO5-'    k = 1.5e9 1984HUI/NET566505669, =2.3E9
1990BUX/SAL245-250B, =1.1E9 1989HUI/CLI361-370 NRDL/NIST, avg=1.6E9
Neta et al., 1988
%      27      13
   s(67,27)=-1; s(67,13)=-1;
   k(67)=1.6e9;

%(68) SO3-' + NO3- --> products
%      27      28
   %s(68,27)=0; s(68,21)=0;
   s(68,27)=-1; s(68,21)=-1;
   k(68)=k1;

%(69) H2O + NO32-' --> OH- +  NO2'   k=1e5 1987BEN/KRI1435-1439,NRDL/NIST
%            28
   s(69,22)=-1; s(69,7)=1; s(69,29)=1;
   k(69)=1e5;

%(70) OH' + NO32-'  --> NO3- + OH-    k=3e9        1993LOG/SEH6664-
6669,NRDL/NIST
%      1     22           21    7
   s(70,1)=-1; s(70,22)=-1; s(70,21)=1; s(70,7)=1;
   k(70)=3e9;

%(71) H+ + NO32-' --> OH- + NO2'       k=2e10          1987BEN/KRI1435-
1439,NRDL/NIST
%      6     22       7     29
   s(71,6)=-1; s(71,22)=-1; s(71,7)=1; s(71,29)=1;
   k(71)=2e10;

%(72) H2O + ·NO2 + ·NO2 --> HNO2 + NO3- + H+       k=1.5e8
1988PAR/LEE6294-6302,NRDL/NIST
%            29      29     30       21    6
   s(72,29)=-2; s(72,30)=1; s(72,21)=1; s(72,6)=1;
   k(72)=1.5e8;

%(73)H2O + ·NO2 + ·NO2 --> NO2- + NO3- + H+ + H+      k=1e8
1981LEE/SCH840-848,NRDL/NIST
%            29     29     31      21    6    6
   s(73,29)=-2; s(73,31)=1; s(73,21)=1; s(73,6)=2;
   k(73)=1e8;
```

```
%(74)H2O + ·NO2 + NO --> HNO2 + HNO2      k=2e8          1988PAR/LEE6294-
6302,NRDL/NIST
%           29   32     30      30
   s(74,29)=-1; s(74,32)=-1; s(74,30)=2;
   k(74)=2e8;

%(75)·OH + ·NO2 --> HO2NO      k=4.5e9          1993LOG/SEH6664-
6669,NRDL/NIST
%     1      29
   s(75,1)=-1; s(75,29)=-1;
   k(75)=4.5e9;

%(76) HO2· + ·NO2 --> HO2NO2      k=1.8e9          1993LOG/SEH10047-
10052,NRDL/NIST
%     8      29
   s(76,8)=-1; s(76,29)=-1;
   k(76)=1.8e9;

%(77) HSO3- + ·NO2 --> products     k=1.2e7          1988CLI/ALT586-
589,NRDL/NIST
%     26      29
   s(77,26)=-1; s(77,29)=-1;
   k(77)=1.2e7*(1-alpha2_so3);

%(78) SO32- + ·NO2 --> products     k=2.1e7          1988CLI/ALT586-589,NRDL/NIST
%     26      29
   s(78,26)=-1; s(78,29)=-1;
   k(78)=2.1e7*alpha2_so3;

 %(79) H· + ·NO2 --> HNO2     k=1e10          1993LOG/SEH6664-6669,NRDL/NIST
%     4      29       30
   s(79,4)=-1; s(79,29)=-1; s(79,30)=1;
   k(79)=1e10;

 %(80) NO3· + ·NO2 --> N2O5    k=1.7e9          1991KAT/JIA4435-4439,NRDL/NIST
%             29
   s(80,29)=0;
   k(80)=1.7e9 ;

 %(81) O2·- + ·NO2 --> O2NO2-    k=4.5e9          1993LOG/SEH10047-
10052,NRDL/NIST
%     15      29
   s(81,15)=-1; s(81,29)=-1;
   k(81)=4.5e9 ;
```

```
 %(82) O2·- + ·NO2 --> O2 + NO2-    k=1e8          1988WAR/WUR6278-
6283,NRDL/NIST
%       15      29      13   31
   s(82,15)=-1; s(82,29)=-1; s(82,13)=1; s(82,31)=1;
   k(82)=1e8;

 %(83) ·NO2 + ·NO2 --> N2O4    k=4.6e8          1976BRO221-229,NRDL/NIST
%       29      29
   s(83,29)=-2;
   k(83)=1e8;

%(84) ·NO2 + ·NO2 --> products    k=6e6          1993CAP/STO2613-2621,NRDL/NIST
%       29      29
   s(84,29)=-2;
   k(84)=6e6;

%(85) ·NO2 + NO --> N2O3    k=1.1e9          1970GRA/TAN488-492,NRDL/NIST
%       29    32
   s(85,29)=-1; s(85,32)=-1;
   k(85)=1.1e9;

%(86) HNO2 + H· --> H2O + NO    k=4.5e8          1966HAL/RAB699-704,NRDL/NIST
%       30   4             32
   s(86,30)=-1; s(86,4)=-1; s(86,32)=1;
   k(86)=4.5e8;

%(87) eaq- + NO2- --> NO22-    k=3.5e9          1990ELL/MCC1539-1547,NRDL/NIST
%       3     31      33
   s(87,3)=-1; s(87,31)=-1; s(87,33)=1;
   k(87)=3.5e9;


%(88) ·OH + NO2- --> OH- + ·NO2   k=6e9          1993LOG/SEH6664-
6669,NRDL/NIST
%       1     31      7      29
   s(88,1)=-1; s(88,31)=-1; s(88,7)=1; s(88,29)=1;
   k(88)=6e9;

%(89) NO2- + O·- --> OH- + ·NO2   k=3.1e8          1988BUX/GRE513-
886,NRDL/NIST
%       31   17      7      29
   s(89,31)=-1; s(89,17)=-1; s(89,7)=1; s(89,29)=1;
   k(89)=3.1e8;
```

```
%(90) NO2- + H· --> OH- + NO   k=7.1e8         1971SMA/AVE2414-
2418,NRDL/NIST
%       31   4       7    32
   s(90,31)=-1; s(90,4)=-1; s(90,7)=1; s(90,32)=1;
   k(90)=7.1e8;


% Note: when new reactions are added, value of n (number of reactions) must be
changed



% Model Notes
% 1. Coefficients in the "s" matrix are obtained from the above equations.  They are used
to determine the second-order rate equations and to determine the material balance
equations, with one exception.  That exception is water. Water is shown in reactions to
provide balanced stoichiometry, but does not play role in reactions.
% 2. pH is assumed constant, but stoichiometric coefficients are included for production
and loss of H+ and OH-, so that changes in pH can be modeled more easily in the future.

  save('data_input', 'n', 'm', 'c0', 's', 'k', 'tstop', 'ph', 'r_vol', 'I0', 'r_area', ...
     'h_nu_av', 'r_l', 'mol_abs', 'abs_coef_water', ...
     'I0_l', 'q_yield_so3', 'options');
```

```
function [t,c]=arpsim254_run%(data_input)
% function to simulate reactions resulting from reaction of radicals
% load values for n,m,c0,s,k,tstop,ph,r_vol,I0,r_area,h_nu_av,r_l,mol_abs,
%                 abs_coef_water,I0_l,q_yield_so3, options
load data_input;

tspan = [0:tstop/100:tstop];

% call ODE solver
[t, c]=ode15s(@arpsim254_deriv_constant_ph, tspan, c0, options,n, m, k, s, mol_abs, ...
    abs_coef_water, I0_l, q_yield_so3, r_l);
```

```
function dcdt=arpsim254_deriv_constant_ph(t,c,n,m,k,s,mol_abs,abs_coef_water, I0_l,
q_yield_so3, r_l)
% This function calculates the deriviatives of concentration with respect to time for a
model that describes reactions of radicals in water.
% initialize matrices
r=zeros(1,n); % rates of reactions

% Calculate variables
% calculate total absorption coefficinet using molar absorptivities and molar
concentrations
abs_coef=mol_abs*c+abs_coef_water;
% calculate first-order rate constant for rxn 58 (form radicals from SO32-)
% assumes well mixed reactor
k(58)= q_yield_so3*mol_abs(26)*I0_l/abs_coef*(1-exp(-abs_coef*r_l))*0.001; % 0.001
m^3/L

% calculate rates of reactions
i=zeros(1, n);
j=zeros(1, m);
r=k;

for i=1:1:n;
  for j=1:1:m;
    if s(i, j) < 0;
      r(i) = r(i)*c(j)^-s(i, j);
    end
  end
end

% calculate derivative from rates of reactions and stoichiometry
dcdt = r*s;
dcdt(6)=0; %to keep pH(H+) constant
dcdt(7)=0; %to keep OH- constant
dcdt = dcdt'; % transpose to obtain required column vector

end
```

VITA

Name:	Bhanu Prakash Vellanki
Address:	Department of Civil Engineering, Texas A&M University, 3136 TAMU, WERC 212 A College Station, Texas 77843-3136 c/o Bill Batchelor
Email Address:	bhanuprakashvellanki@gmail.com
Education:	B.Tech., Civil Engineering, 2006 Acharya Nagarjuna University, India M.En., Civil Engineering, 2007 Texas A&M University, College Station, Texas Ph.D., Civil Engineering, 2012 Texas A&M University, College Station, Texas